Therapeutic anti-PD-L1 antibody affects ESCRT-mediated functions in cells expressing oncogenic EGFR.

Anudari Letian[1,2], Eyoel Yemanaberhan[1,3], Paola Cavaliere[1], Noah Dephoure[1,4], Nasser K. Altorki[3,4,5] and Timothy E. McGraw[1,3,4,5]*

*corresponding author.

Affiliations

[1] Department of Biochemistry, Weill Cornell Medicine, New York, NY 10065

[2] Biochemistry, Cell & Molecular Biology Graduate Program, Weill Cornell Medicine, New York, NY 10065

[3] Department of Cardiothoracic Surgery, Weill Cornell Medicine and NY Presbyterian Hospital, New York, NY 10065

[4] Sandra and Edward Meyer Cancer Center, Weill Cornell Medicine and NY Presbyterian Hospital, New York, NY 10065

[5] Neuberger Berman Foundation Lung Cancer Research Center, Weill Cornell Medicine, New York, NY 10065

Word count: 7051 (main text and figure legends)

Disclosures: NKA has equity in Angiocrine Bioscience. TEM receives research funding from Janssen and from Pfizer, Inc. The other authors have nothing to disclose.

Summary

PD-L1 is a ligand for immune checkpoint receptor PD1. Anti-PD-L1 antibody is an effective therapy for a variety of solid tumors, although a durable response is only achieved in a subset of patients. For unknown reasons, EGFR-mutant tumors respond poorly to checkpoint blockade. Applying quantitative cell biological methods to study PD-L1 biology in lung cancer cells, we establish that growth factors acutely regulate PD-L1 trafficking between the plasma membrane and the interior of cells. Changes in plasma membrane PD-L1 levels will impact PD1 engagement on T cells, thereby influencing PD-L1's immune suppressive activity. To discover potential cell-intrinsic functions of PD-L1, we used APEX2 biotinylation to generate a high-resolution map of the PD-L1 proximal proteome. ESCRT pathway proteins were enriched in PD-L1's proximal proteome, and two ESCRT-dependent functions, turnover of mutant EGFR and biogenesis of extracellular vesicles, were affected by anti-PD-L1 treatment, suggesting a link between PD-L1 and ESCRT function. Proteins that control cytoskeletal dynamics were also enriched in the PD-L1 proteome, and anti-PD-L1 treatment reduced cell migration, identifying migration as a PD-L1 associated function. PD-L1 knockout mimics the effects of the antibody treatment, suggesting anti-PD-L1 antibody effects are loss of function(s). The effects of anti-PD-L1 on the ESCRT-dependent functions and cell migration were restricted to cells harboring oncogenic EGFR mutations. Wildtype and KRAS mutant cells lines were unaffected. Our study reveals new cell-intrinsic roles for PD-L1 in EGFR mutant cells, activities that might contribute to the resistance of EGFR mutant tumors to PD-L1 checkpoint blockade.

Introduction

Therapies targeting the PD1/PD-L1 checkpoint axis are effective in many cancers, including non-small-cell lung carcinoma (NSCLC)[1,2]. However, only a limited subset of patients shows durable response to anti-PD-L1 antibody (α-PD-L1) therapy. Expression of PD-L1 by cancer cells does not predict response to α-PD-L1 therapy, and some molecular subtypes, most notably EGFR mutant tumors, respond poorly to α-PD-L1 therapy, regardless of PD-L1 expression [3-5]. Thus, despite the well-described role of PD-L1 as a PD1 ligand and the remarkable clinical successes of α-PD-L1 therapies, there is still much to be learned about PD-L1 biology, particularly its cell intrinsic functions and behavior, information that will provide a context for better understanding response and resistance to α-PD-L1 therapy.

PD-L1 is a single pass type I transmembrane protein widely expressed on immune cells as well as many non-lymphoid cells, including epithelial cells [6]. Because PD-L1 functions to blunt immune response by binding PD1 on target T cells, regulation of the amount of PD-L1 on the plasma membrane is key for controlling its immune checkpoint activity. A number of transcriptional and post-translational regulatory mechanisms impacting PD-L1 expression have been identified. Numerous cytokines, cell stress stimuli and oncogenes stimulate PD-L1 transcription downstream of several signaling pathways [7-9]. Several modes of post translational regulation have also been identified that impact PD-L1 protein turnover, including regulation of glycosylation, palmitoylation and phosphorylation [10-13], and proteins specifically involved in determining whether PD-L1 is degraded or not have also been identified (e.g. CMTM6 and HIP1R) [14-16].

Although PD-L1 as a ligand for PD1 has been the predominant focus of its role in cancers, there is mounting evidence for cell intrinsic functions of PD-L1 that might affect tumor progression independent of PD-L1 binding PD1[17,18]. Along these lines, PD-L1 has been implicated in the regulation of epithelial mesenchymal transition, resistance to chemotherapeutic agents as well as interferon-mediated cell toxicity[17,19-21]. Some of the non-PD1 ligand activities of PD-L1 might be more reflective of PD-L1's role outside of cancer. For example, in a non-cancer setting, PD-L1 expression by non-immune cells might have a major function in protecting healthy cells/tissue from collateral damage at sites of active immune response and these cell-intrinsic PD-L1 activities might be vital for cell survival and tissue healing.

Here we report on the interrogation of PD-L1 biology using quantitative cell biological methods. We report that growth factors, via AKT activation, acutely regulate the distribution of PD-L1 between the plasma membrane and the interior of cells. Growth factor regulation of PD-L1 trafficking is independent of previously described transcriptional upregulation by IFNγ and of the control of PD-L1 protein turnover by the CKFL-like MARVEL transmembrane protein 6 (CMTM6)[14,15]. Thus, growth factor modulation of PD-L1 cycling to and from the plasma membrane provides a mechanism for rapid modulation of cell surface levels that augments previously described regulatory mechanisms that control the total amount of PD-L1. We used APEX2 biotinylation mapping to define the proteome in proximity to PD-L1. Proteins

of the ESCRT pathway were enriched in the PD-L1 proximal proteome. αPD-L1 treatment of cells affected two ESCRT-dependent activities: biogenesis of extracellular vesicles (EVs) and turnover of mutant EGFR. Proteins that control cytoskeleton dynamics were also enriched in the PD-L1 proximal proteome and the cytoskeletal dependent activities of cell-migration were affected by α-PD-L1 antibody treatment. The effects of α-PD-L1 treatment were restricted to cells harboring oncogenic EGFR. PD-L1 knockout phenocopied the effects of α-PD-L1 treatment of EGFR mutant cells, establishing the effects of α-PD-L1 are due to a loss of PD-L1 function. These data reveal a heretofore undescribed interplay between constitutively active mutant EGFR and α-PD-L1 treatment. Thus, in EGFR mutant tumors, α-PD-L1 therapy not only disrupts PD-L1/PD1 interaction but potentially affects cancer cell migration as well as the broader tumor microenvironment downstream of changes in EVs that could impact response to the immune checkpoint therapy.

Results

Intracellular and plasma membrane PD-L1 are in rapid equilibrium regulated by growth factors.

We used fluorescence microcopy to interrogate the subcellular distribution of PD-L1 in primary human NSCLC cells (Fig 1A). In addition to PD-L1 localized to the plasma membrane detected by staining intact cells, staining of permeabilized primary cells revealed a significant intracellular accumulation of PD-L1. Quantification of the fluorescence revealed that the majority of PD-L1 expressed in primary lung cancer cells was intracellular. Mutant KRAS or EGFR, the two most common driver oncogenes in lung cancer[22], did not affect this PD-L1 distribution. (Fig 1B). Similarly, in established NSCLC cell lines and a non-transformed human lung epithelial cell line (BEAS-2B), there was a significant intracellular accumulation of PD-L1 that was predominantly concentrated in the peri-nuclear region of cells (Fig 1C). Quantification revealed a nearly equal distribution of PD-L1 between the plasma membrane and the interior of cells, independent of whether the cells were KRAS or EGF receptor (EGFR) mutants (Fig 1D).

Interferon gamma (IFNγ), a potent transcriptional regulator of PD-L1, increased total PD-L1 protein levels in a non-transformed human lung epithelial line (BEAS-2B), an EGFR mutant (H1650) cell line and a KRAS mutant (A549) cell line by approximately 3 fold, without affecting either the distribution of PD-L1 between the interior and surface of cells or the punctate plasma membrane distribution of PD-L1 (Fig 1C, E & F). Immunostaining with Durvalumab, a therapeutic α-PD-L1 antibody[23,24], revealed a similar PD-L1 distribution between the plasma membrane and cell interior as the laboratory grade α-PD-L1 antibody (clone #130021, Novus Biologicals) (Fig 1G).

Plasma membrane localized PD-L1 mediates its immune suppressive function as a ligand for PD1 on target T cells, thereby raising the question of the biological function of the large intracellular accumulation of PD-L1. To explore this question, we first investigated the relationship between plasma membrane and intracellular PD-L1. We used a quantitative fluorescence microscopy assay adapted from our previous studies of membrane trafficking to interrogate the relationship between the plasma membrane and intracellular pools of PD-L1[25]. If these pools are in equilibrium, then when live cells are incubated with a saturating concentration of an antibody that binds to the extracellular domain of PD-L1, the total amount of cell-associated α-PD-L1 antibody will increase as a function of incubation time. This is observed because the antibody-bound PD-L1 on the plasma membrane is internalized and replaced by recycling of intracellular PD-L1 that is not occupied by the antibody. The cell-associated α-PD-L1 plateaus when all the PD-L1 in equilibrium with the plasma membrane has been bound by antibody (that is, transited to the plasma membrane). Our analyses demonstrate that intracellular PD-L1 constitutively traffics to the cell surface with a halftime of approximately 10 min, establishing that PD-L1 plasma membrane levels are dynamically maintained by constitutive internalization and recycling back to the plasma membrane (Fig 2A). Furthermore, the maximum amount of cell-associated α-PD-L1 that is labeled by incubation with antibody in the medium (i.e., the plateau amount) is greater than 90% of the total amount of PD-L1

expressed in cells, demonstrating that greater than 90% of intracellular PD-L1 is in rapid equilibrium with the plasma membrane (Fig 2A). Together these data suggest one function of the intracellular PD-L1 pool is to serve as a reservoir for the plasma membrane pool of PD-L1.

We next determined if the amount of PD-L1 in the plasma membrane can be acutely regulated. Incubation of cells in serum-free medium for 4 hrs resulted in a near 50% depletion of plasma membrane PD-L1 (Fig 2B). This depletion of plasma membrane PD-L1 reflected a redistribution of PD-L1 from the cell surface to intracellular compartments without a significant reduction in total PD-L1 protein (Fig S1A). Replacing the serum with different growth factors (EGF, IGF and insulin) restored plasma membrane PD-L1 levels without affecting the total amount of PD-L1, establishing that growth factors acutely control PD-L1 trafficking to and/or from the plasma membrane and consequently the distribution of PD-L1 between the plasma membrane and the interior of cells (Fig 2B). There were, however, no differences among the 3 growth factors in promoting PD-L1 accumulation on the plasma membrane.

Growth factors are known to regulate membrane protein trafficking downstream of AKT activation[26,27]. We used pharmacologic inhibition of AKT (MK2206) to determine its role in controlling PD-L1 trafficking. Within 4 hours of pharmacologic inhibition of AKT, plasma membrane PD-L1 was reduced by the same degree as induced by serum withdrawal, demonstrating the amount of PD-L1 on the cell surface is dynamically maintained and acutely regulated by AKT activity (Fig 2B).

The effects of serum and AKT on the expression of PD-L1 in the plasma membrane were not due to global changes in membrane protein traffic because the plasma membrane expression of transferrin receptor, a cargo protein of general endocytic recycling, was not affected by either treatment (Fig 2C). Inhibition of AKT induced downregulation of plasma membrane PD-L1 in all NSCLC cell lines examined (Fig 2D, Fig S1B). Thus, the plasma membrane level of PD-L1 is dynamically maintained and regulated by AKT, irrespective of driver oncogene.

Importantly, inhibition of AKT reduced the amount of PD-L1 in the plasma membrane of IFNγ-treated cells, demonstrating that the increased total amount of PD-L1 induced by IFNγ stimulation remained under the control of AKT regulation (Fig 2E). Consequently, the effects of IFNγ and AKT on the amount of PD-L1 in the plasma membrane are independent and additive.

Previous studies have defined a role for CMTM6 in determining the fate of internalized PD-L1[14,15]. In agreement with those studies, transient knockdown of CMTM6 resulted in a 30% reduction of total PD-L1 amounts (Fig 2F, Fig S1C). However, the distribution of the remaining PD-L1 between the plasma membrane and interior of cells was unchanged (Fig 2F). These data establish that the amount of PD-L1 recycled back to the plasma membrane, but not the rate at which it is recycled, is controlled by CMTM6. Furthermore, AKT regulation of PD-L1 recycling is unaffected by depletion of CMTM6, providing

additional evidence that regulation of PD-L1 downstream of CMTM6 is distinct and independent from regulation downstream of AKT (Fig 2G).

PD-L1 proximal proteome.

In addition to PD-L1's function as a PD1 ligand, there is an emerging literature on cell-intrinsic functions of PD-L1[17,18,28]. To provide a context for the further investigation of potential cell-intrinsic roles of PD-L1, we used APEX2 mapping to define the PD-L1 proximal proteome. APEX2 is a peroxidase that specifically oxidizes biotin-phenol to the short-lived phenoxyl radical that reacts with nearby proteins (within a radius of ~20 nm) resulting in their biotinylation[29,30]. The biotinylated proteins are isolated and identified in mass spectrometry to generate an accounting of proteins in the proximity of APEX2. We linked APEX2 enzyme to the cytoplasmic carboxyl-terminus of human PD-L1. Linkage of APEX2 to PD-L1 did not alter PD-L1's distribution between the plasma membrane and the interior of cells or affect AKT regulation of PD-L1 expression in the plasma membrane, data that support the use of the PD-L1-APEX2 for proximity mapping studies (Fig 3A-C).

We generated a proximity map for PD-L1-APEX2 stably expressed in a non-transformed human lung epithelial cell line, BEAS-2B. We identified an overlapping set of 399 proteins biotinylated in 5 independent experiments (Fig 3D, Fig S2A, Table S1). PD-L1 proximal proteins reflect many biological pathways, as anticipated for a protein distributed among several cellular compartments as it constitutively cycles to and from the plasma membrane. Here we focus on 4 of the pathways as discussed below (Fig 3E).

Proteins of the MHC I antigen presentation pathway were enriched among the PD-L1 proximity map proteins, including the MHC I receptor proteins HLA-A, HLA-B and HLA-C (Table S1). We confirmed the proximity of PD-L1 to HLA I by immunofluorescence (Fig 3F, Fig S2B). The specificity of the identified proteins to those in proximity to PD-L1 was supported by the fact that the transferrin receptor was neither enriched in the proximity map nor highly colocalized with PD-L1 by immunofluorescence (Table S1, Fig 3F, Fig S2B). The proximity of PD-L1 and MHC I localizes PD-L1 adjacent to the TCR-MHC I complex formed between T cells and target cells, an organization that would enhance the efficiency of PD-L1 to engage PD1 and blunt T cell activation.

There was also an enrichment of proteins that function in various aspects of membrane protein trafficking, a finding in line with constitutive trafficking of PD-L1 to and from the plasma membrane. More unexpected was the finding that 29% of the PD-L1 proximity map proteins are annotated to cytoskeleton organization, covering a broad range of both actin and microtubule biology (Fig 3E). These results infer a close association of PD-L1 or PD-L1-containing compartments with the actin cytoskeleton, which might have implications for PD-L1 function.

Most notably, APEX2 proximity mapping revealed a highly significant enrichment of proteins involved in EGF receptor signaling and trafficking, including the EGFR and several ESCRT proteins, that controls the turnover of activated EGFR. Supporting these findings EGFR and HGS (a subunit of ESCRT-0 complex) overlap with PD-L1 in immunofluorescence (Fig 3E & F, Fig S2B, Table S2).

αPD-L1 antibody induces an increase of mutant EGFR

EGFR and 12 proteins involved in EGFR trafficking and degradation were part of the PD-L1 proximity map (Table S2). As noted above, EGFR activation promotes PD-L1 accumulation on the plasma membrane. However, the other growth factor receptors (insulin receptor and IGF receptor) that can also regulate PD-L1 distribution between the plasma membrane and interior of cells, were not identified in PD-L1 proximity mapping. These findings suggest the possibility of a more direct connection between PD-L1 and EGFR. Finding EGFR and proteins associated with its signaling and trafficking was intriguing because EGFR mutant tumors respond poorly to α-PD-L1 therapy, despite expressing PD-L1[3-5]. Perhaps the reduced response of EGFR mutant tumors is related to a physical or functional interaction between PD-L1 and activated EGFR. To further probe the relationship between EGFR and PD-L1 in the context of PD-L1 therapy, we first determined the effect of α-PD-L1 antibody treatment on EGFR (Fig 4A). Incubation of three different EGFR mutant human NSCLC cell lines for 7 hours with α-PD-L1 antibody caused a significant increase of EGFR protein, whereas similar treatment of two KRAS mutant lines and non-transformed BEAS-2B cells did not affect EGFR protein levels. Of note, the EGFR mutant lines harbor different activating mutations, demonstrating the effect is not linked to a specific EGFR mutation. Additionally, despite differences in PD-L1 expression among the lines, the effect of α-PD-L1 was restricted to cells with oncogenic EGFR. (Fig S3A).

Two α-PD-L1 antibodies, Durvalumab and reagent grade PD-L1 antibody (clone# 130021, Novus Biologicals), which bind different extracellular epitopes of PD-L1, had a similar effect on mutant EGFR levels, demonstrating the effect is not dependent on antibody binding to a specific region/epitope of PD-L1 (Fig 4B). Neither an anti-transferrin receptor antibody, which binds to the extracellular domain of the transferrin receptor, nor a control human IgG antibody, when incubated with cells for 7 hrs, affected the amount of EGFR protein, demonstrating the effect on mutant EGFR is specific for antibodies that bind PD-L1 (Fig 4B & C, Fig S3B). Finally, treatment with an α-PD-L1 Fab (monovalent) caused an increase in EGFR protein, thus proving that the effect of the antibody is not through forced dimerization of PD-L1 (Fig 4D, Fig S3C).

α-PD-L1 antibody treatment did not alter the total amount of PD-L1 nor its cellular distribution in either non-transformed or EGFR mutant human lung epithelial cell lines (Fig 4E&F). In addition, α-PD-L1 treatment did not affect the distribution of the transferrin receptor, demonstrating the treatment did not affect clathrin-mediated endocytosis or constitutive recycling back to the plasma membranes (Fig 4G).

αPD-L1 antibody reduces degradation of mutant EGFR

We next knocked-out PD-L1 in an EGFR mutant cell line using CRISPR/CAS9. We focused on EGFR mutant cells because these are the cells that upregulated EGFR in response to α-PD-L1 treatment. PD-L1 knockout resulted in an increase in mutant EGFR that was reduced to control levels by re-expression of PD-L1 (Fig 4H & I, Fig S3D). These data support the hypothesis that the effect of α-PD-L1 is not a gain of function induced by antibody binding, but rather that antibody binding disrupts a cell-intrinsic function of PD-L1.

α-PD-L1 treatment did not affect EGFR or PD-L1 mRNA levels, demonstrating a post-transcriptional mechanism is responsible for the increase in mutant EGFR protein levels (Fig 4J & K). Inhibition of translation via cycloheximide (CHX) did not alter the effect of α-PD-L1 on mutant EGFR levels, supporting the conclusion that α-PD-L1 inhibits EGFR degradation rather than increases translation of EGFR mRNA (Fig 4L). Accordingly, α-PD-L1 treatment approximately doubled the half-life of mutant EGFR without an appreciable effect on the half-life of the wildtype EGFR (Fig 4M-O). Consistent with the effect of α-PD-L1 on mutant EGFR being independent of kinase activity, α-PD-L1 did not affect the half-life of wildtype EGFR stimulated with EGF or TGF-α (Fig S3E & F). These data indicate that some feature of mutant EGFR biology or the cellular context of EGFR mutant cells is not recapitulated by acute activation of EGFR and is responsible for the effect of α-PD-L1. However, α-PD-L1 treatment did not lead to significant differences in AKT or ERK phosphorylation or an increase in transcription of immediate EGFR response genes, providing additional evidence that the α-PD-L1 effect was not a consequence of altered EGFR signaling (Fig S3G & H).

Prior studies have shown that ligand activated wildtype EGFR and constitutively active mutant EGFR have different intracellular trafficking patterns[31]. One prominent difference between trafficking of wildtype and mutant EGFR is that activated wildtype EGFR is sorted to luminal vesicles of multivesicular late endosomes, followed by degradation in mature lysosomes[32]. Mutant EGFR, despite being active, is poorly trafficked to late endosomes and rather is recycled back to the plasma membrane, thereby avoiding efficient degradation[31,33]. Although unstimulated wildtype EGFR co-localized with PD-L1, this colocalization was significantly decreased upon EGF activation of the wildtype EGFR, presumably because activated wildtype EGFR is targeted for degradation. Mutant EGFR, however, remained co-localized with PD-L1 regardless of ligand stimulation (Fig S3I). Thus, the different effect of α-PD-L1 on the half-lives of wildtype and mutant EGFR may be due to differences in the trafficking of wildtype and mutant EGFR.

Ubiquitination of activated wildtype EGFR targets it for degradation by a mechanism involving the ESCRT pathway, and although mutant EGFR is ubiquitylated following binding of EGF, ubiquitination is not required for internalization of mutant EGFR[32,34-37]. α-PD-L1 antibody treatment of cells reduced ubiquitination of both wildtype and mutant EGFR, suggesting differences in EGFR ubiquitination do not

account for the difference in turnover of wildtype and EGFR mutants in cells treated with α-PD-L1 (Fig 4P & Q).

αPD-L1 antibody treatment effect on the whole cell proteome

ESCRT proteins were identified in the PD-L1 proximity map (Fig 3E, Table S2). Because α-PD-L1 affects mutant EGFR turnover and ESCRTs are involved in controlling the turnover of a number of proteins[38], not just EGFR, we next explored the possibility that α-PD-L1 treatment has a global effect on protein turnover. To test this hypothesis, we performed whole cell proteomic analysis on wildtype, KRAS and EGFR mutant cells 48 hrs after treatment with therapeutic α-PD-L1 Durvalumab antibody (Fig 5A). Remarkably, in the EGFR mutant cell line there was an overall increase in the post-to-pre α-PD-L1 treatment ratios of individual proteins, whereas in wildtype and KRAS mutant cells lines there was a small overall decrease in post to pretreatment ratios (Fig 5A). Mutant EGFR was increased 1.3-fold in whole cell mass spec, whereas wildtype EGFR was unchanged (Table S3). These data demonstrate that α-PD-L1 treatment does not just affect mutant EGFR but that it has broader effects that are limited to cells with mutant EGFR, revealing the effect is in the context of a cell expressing constitutively active EGFR.

To explore specific biology that might be most affected by α-PD-L1 treatment we queried the proteins most consistently increased by α-PD-L1 by applying thresholds of greater than 1.2-fold increase and a coefficient of variance less than 0.1 (lowest quartile of variation between the experiments). Among these proteins, there was an enrichment of proteins involved in immune responses such as cellular response to interferon-beta, regulation of innate immune responses as well as viral release from host cells, suggesting the possibility that PD-L1, in addition to its function as an immune checkpoint ligand, has cell-intrinsic immune-related function intersecting with ESCRT-dependent functions (Fig 5B, Fig S4A). We also detected an enrichment of proteins annotated to cell adhesion and cell polarity, suggesting a role for PD-L1 in regulating cytoskeletal organization (Fig 5C, Fig S4A). Notably, these proteins were unchanged in KRAS and non-transformed cells with α-PD-L1 antibody treatment (Fig 5B & C, Table S3).

αPD-L1 antibody treatment affects extracellular vesicles

ESCRTs, in addition to having a key role in targeting EGFR (and other proteins) for lysosomal degradation, are also involved in the formation and secretion of extracellular vesicles (EVs)[39]. To determine the impact of α-PD-L1 treatment on EVs, we performed proteomic analysis on EVs isolated from the media of non-transformed, KRAS and EGFR mutant lung cell lines with and without α-PD-L1 treatment. α-PD-L1 treatment had a pronounced effect on EV biogenesis in EGFR mutant cells compared to KRAS and wildtype cells (Fig 5D & E). There was an increase in a set of 6 canonical EV proteins in EVs isolated from the medium of EGFR mutant cells treated with α-PD-L1. There was no similar increase of these proteins in EVs isolated from the media of wildtype or KRAS mutant cells incubated with α-PD-L1 (Fig 5D). The increase of these EV proteins in the extracellular space was higher

than the increase-in the whole cell extracts, supporting the hypothesis that α-PD-L1 treatment enhances EV biogenesis and/or release from EGFR mutant cells (Fig 5D). In addition, there was a striking overall increase of EV cargo proteins from EGFR mutant α-PD-L1 treated cells, suggesting either enhanced biogenesis of EVs or increased protein packaging into EVs (Fig 5E). Thus, our data establish that α-PD-L1 treatment affects protein turnover and EV biogenesis, two ESCRT dependent functions.

The proper maturation and acidification of late endosomes is critical for EV biogenesis as well as lysosomal activity[40,41]. We determined that the acidification and maturation of late endosomes/lysosomes in EGFR mutant cells were not affected by α-PD-L1 treatment, demonstrating that the global effects of α-PD-L1 treatment on the proteome of EGFR mutant cells was not due to perturbations in lysosomal acidification (Fig S4B-D).

PD-L1 controls cell migration in EGFR mutant cells

Our APEX2 mapping (Fig 3D), in addition to revealing proximity of PD-L1 to EGFR, also identified an enrichment of proteins that function in cytoskeletal biology. We also identified proteins involved in cell polarity and cell adhesion processes among the ones increased with α-PD-L1 treatment in EGFR mutant cells. Thus, we next determined whether PD-L1 impacts cytoskeleton-dependent processes. α-PD-L1 treatment of an EGFR mutant cell line reduced migration measured in a scratch assay and reduced migration assayed in a transwell migration assay (Fig 6A-B, Fig S5A). Treatment with a control IgG antibody did not impact cell migration (Fig 6C). Furthermore, prolonged α-PD-L1 treatment did not affect total cell levels of PD-L1, demonstrating the effect of antibody is not through induced degradation and loss of PD-L1 protein (Fig S5B). α-PD-L1 treatment inhibited migration of a second EGFR mutant harboring a different EGFR mutation, whereas α-PD-L1 treatment of a KRAS mutant cell line had no effect (Fig 6D &E). In line with those results, PD-L1 knockout blunted cell migration, mimicking the effect of the α-PD-L1 antibody (Fig 6F &G, Fig S5C). Migration was restored when full length PD-L1 was re-expressed in PD-L1 knockout cells, but not when a mutant PD-L1, which lacks the cytoplasmic domain (CDΔ) was expressed. This suggests a role for PD-L1's cytoplasmic domain in the regulation of migration (Fig 6F & G, Fig S5C). Neither α-PD-L1 treatment nor PD-L1 knockout impacted cell viability or proliferation, demonstrating the difference in migration is not confounded by changes in cell proliferation (Fig S5D & E).

Discussion

In this study, we show that PD-L1, beyond its function as ligand for the immune checkpoint receptor PD1, is spatially linked with key protein pathways involved in EGFR/ESCRT biology and actin-dependent motility. We demonstrate that α-PD-L1 treatment, including the use of the therapeutic α-PD-L1 Durvalumab antibody, has a global effect on the whole cell proteome and leads to increased biogenesis of extracellular vesicles, specifically in EGFR mutant cells. In addition, α-PD-L1 treatment leads to decreased cell migration in EGFR mutant cells. Mechanistically, α-PD-L1 treatment results in loss of function of PD-L1, suggesting that the clinical effects of α-PD-L1 may, by affecting tumor cell-intrinsic functions of PD-L1, extend beyond the disruption of PD1 engagement.

EGFR mutant tumors are generally resistant to α-PD-L1 therapy as compared to EGFR WT tumors[3-5]. While the mechanism behind this therapeutic disparity is not clear, there is emerging evidence suggesting that EGFR activity and PD-L1 may be functionally linked. We have shown here that surface PD-L1 levels are acutely increased by AKT signaling downstream of EGFR without affecting total protein abundance and independently of CMTM6. We found that the majority of PD-L1 at steady state is located in a dynamic intracellular storage pool, which allows cells to rapidly modulate PD-L1 expression on the plasma membrane in response to EGF. This EGFR:PD-L1 link is further supported by our finding that PD-L1 is located in close proximity to not only EGFR, but 12 other proteins known to be involved in EGFR endocytosis, signaling and protein degradation including members of the ESCRT complexes. This suggests that PD-L1 which can be regulated by EGFR may in turn directly affect EGFR protein biology. Indeed, we show that α-PD-L1 treatment reduces EGFR degradation and results in an increase of EGFR protein in EGFR mutant cells. In our in vitro experiments we did not observe a significant difference in downstream EGFR signaling accompanying the α-PD-L1 stimulated increase of total EGFR protein; however, it is possible that the 50% increase in total EGFR might result in increased tumor growth *in vivo* by providing essential signals that support survival in the nutrient-deprived tumor microenvironment.

The effect of Durvalumab or other antibody binding to PD-L1 has not been extensively studied in the context of PD-L1 reverse signaling. We find that antibody binding results in a loss of function of PD-L1 as it phenocopies the effect of PD-L1 KO on EGFR expression. Although, PD-L1 antibody binding can trigger antibody-dependent cell cytotoxcity[42,43], Durvalumab lacks a functional Fc domain, and anti-transferrin receptor antibody treatment suggests the changes are not associated with cell response to antibody binding but is specific to PD-L1 function. It is possible that antibody binding causes transmembrane signaling or disrupts PD-L1 binding with partner proteins, which are responsible for signaling changes. Recent studies have identified PD-L1 signaling motifs and binding partners that result in broad transcriptional and signaling changes within the cells[17,18,28] .

PD-L1 protein is reported to be degraded both through proteasomal and lysosomal pathways[9,12,16], and our APEX2 mapping data are consistent with PD-L1 being in proximity to the ESCRT machinery. ESCRT

proteins drive the formation of multi vesicular bodies (MVBs), which either fuse with lysosomes, resulting in degradation of contents or fuse with the plasma membrane releasing into the extracellular space the luminal vesicles as EVs[38,39,44,45]. The global increase in total cell protein and EV biogenesis that we observe in Durvalumab treated mutant EGFR cells suggests that PD-L1 is not merely a client of the ESCRT machinery but is involved in its regulation. Finding reduced turnover of EGFR (a client of ESCRT-dependent degradation)[32] and an increased biogenesis of EVs is consistent with α-PD-L1 biasing MVB maturation towards EV biogenesis. This is in line with previous reports implicating PD-L1 in the ESCRT-dependent process of autophagy[46]. The oncogenic EGFR-specific whole cell proteome and EV changes may explain why only cells with mutant EGFR were susceptible to antibody-induced change in migration. EVs are known to have broad roles in regulating cell migration, ranging from autocrine signaling in directed migration to recruitment and infiltration of immune cells in the microenvironment[47]. However, at this time we cannot distinguish between a direct effect of anti-PD-L1 on cell migration or if it is secondary to changes in ESCRT function. Additionally, EGFR signaling regulates cell migration and invasion[48,49], and, although we did not find differences in EGF-stimulated EGFR signaling, we cannot rule out the possibility of increased mutant EGFR protein directly impacting cell migration in oncogenic EGFR cells.

Although PD-L1 has been reported to affect cell migration in cell lines with non-EGFR driver oncogenes[50], most of these studies rely on PD-L1 ablation and do not employ α-PD-L1 treatment. We propose that α-PD-L1 treatment does not result in a complete loss of function of PD-L1 and requires, in vitro at least, the enhanced signaling of EGFR mutant cells to display a change in phenotype. A recent study showed such a scenario where in PD-L1 induces phospholipase C-γ1 (PLC-γ1) activation only in the presence of activated EGFR[18]. Wildtype and mutant EGFR have been described to have largely dissimilar downstream signaling[51,52], and our data with non-transformed, KRAS and EGFR mutant cells suggests that the cellular context created by oncogenic EGFR signaling may make EGFR mutant cells more susceptible to α-PD-L1 antibody mediated signaling changes. Among the proteins that increased the most in EGFR mutant cells upon Durvalumab treatment, were those involved in immune regulatory processes, which closely relate to PD-L1's role as an immune checkpoint protein[53]. Most notably, these proteins were unchanged in non-transformed and KRAS mutant cells highlighting the distinct response of EGFR mutant cells to α-PD-L1 antibody. This finding may at least partially explain why EGFR mutant tumors respond poorly to PD-L1 checkpoint blockade and suggest that PD-L1 checkpoint monotherapy should be carefully reconsidered for patients with mutant EGFR tumors.

Besides tumor cells, PD-L1 expression on immune cells has been shown to be important for regulation of migration. Specifically, PD-L1 on dendritic cells (DCs) was shown to be necessary for efficient homing of dermal DCs to the lymph nodes through modulation of chemokine receptor signaling and actin remodeling[28]. Our data suggests that in addition to anti-PD-L1 effect on PD-L1 blockade on DCs, shown

to be crucial for tumor control[54,55], it is important to follow up on the cell intrinsic effects of anti-PD-L1 treatment on immune cell migration and proliferation.

In line with literature suggesting that PD-L1 traffics through endosomes[16,56], we find that PD-L1 is localized on the plasma membrane of cells as well as in intracellular storage pools. Unlike, previous reports of PD-L1 transiting through endosomes for degradation, we find that majority of PD-L1 at steady state is located in intracellular compartments and this pool is maintained to dynamically modulate PD-L1 expression on the plasma membrane. This change is achieved within hours, and perhaps represents the fastest mode of modulating plasma membrane PD-L1, which could be crucial to limit collateral damage and promote cell survival in an immune inflamed environment.

Through APEX proximity labeling and confocal microscopy we establish the proximity of PD-L1 with MHC I, in agreement with recent results[57]. This organization suggest that PD-L1 is part of the immune synapse, which would contribute to its efficiency as an immune checkpoint upon engagement of MHC-I and the T cell receptor. In accordance with PD-L1 localization to specialized domains of the plasma membrane, caveolin 1 and flotillin, both of which have roles in establishing specialized membranes within a membrane[58,59], are constituents of the PD-L1 proximal proteome (Table S1). Additional studies are required to determine how the clusters form and what role they have PD-L1 engagement of PD1 receptor[60-62].

In conclusion, we describe a novel aspect of PD-L1 biology whereby α-PD-L1 treatment results in a loss of function of cell intrinsic PD-L1 function leading to profound changes in whole cell proteome and EV secretion, upregulation of mutant EGFR protein and reduced cell migration specifically in EGFR mutant lung cancer cells. The signaling mechanism behind the changes in EGFR mutant cells with α-PD-L1 treatment remain to be elucidated. Our study highlights the importance of tumor intrinsic role of PD-L1 in EGFR mutant cells and stress the need for further studies of PD-L1 antibody-based therapies beyond the immune cell regulatory context.

Materials and Methods:

Cell lines and culture:

A549, BEAS-2B and H23 were purchased from ATCC. H1650, HCC827, HCC4006 and PC9 were a gift from Dr. Rafaella Sordella (Cold Spring Harbor Laboratory). H1975 were a gift from Dr. Brandon Stiles (Weill Cornell Medicine). All primary human samples were obtained and used in accordance with an approved IRB protocol. Primary tumor cells were processed to obtain single cell suspensions as described previously[63] and plated onto glass-bottom dishes and analyzed 3-5 days later. All cells were cultured in DMEM media supplemented with 10% FBS and 1% penicillin-streptomycin at 37°C and 5% CO_2. Where indicated, cells were treated with serum-free DMEM media supplemented with 0.02M HEPES and 0.03M $NAHCO_3$. Stable cell lines were generated via lentiviral infection using Lenti-X packaging system. Cells were either antibiotic selected via blasticidin (5 µg/mL) or puromycin (3 µg/mL), or sorted for expression of protein of interest via FACS. PD-L1 KO cells were generated via CRISPR/CAS9 with both targeting sequences (guide1: 5'-CGGGAAGCTGCGCAGAACTG-3'; guide2: 5' -TCTTTATATTCATGACCTAC-3'). Live cells were stained with PD-L1 antibody and KO cells were sorted by FACS. Bulk population of KO cells was verified for PD-L1 KO via Western Blot. CMTM6 stable inducible shRNA knockdown cells were generated with one shRNA targeting sequence (5'-TTCAAAGAAGTAGAGGCCTCCA-3') and mRNA knock-down was confirmed via qRT-PCR.

Cell treatments:

For PD-L1 PM to total measurements, cells were plated on glass bottom dishes in full growth media and assayed the next day. Cells were switched to either serum-free media, serum free media supplemented with growth factors or fresh full growth media for 4 hours. EGF was used at 8nM, IGF at 10nM and insulin at 10nM. For Akt inhibition experiments, cells were incubated in full growth media with 5 µM MK2206 or DMSO for 4 hours. Interferon gamma treatment was performed at 40 ng/mL for 24 hrs, and CMTM6 shRNA knock-down was induced by doxycycline at 1 µg/mL for 48hrs. For antibody treatment experiments, cells were treated with specified antibody or Fab for 7 hr at a final concentration of 10 µg/mL in serum free DMEM media. For protein turn-over experiments cycloheximide was used at 10 µg/mL. For stimulated EGFR degradation, cells were serum starved for 4 hr and 5 hr and treated with EGF or TGFα at 50ng/mL for indicated timepoints respectively, while antibody was used at 10 µg/mL and maintained for the duration of the experiment. For EGFR signaling experiments, cells were incubated with antibody in serum free media for 7 hr and stimulated with 0.5 ng/mL EGF for specified timepoints. For migration assays, cells were pre-incubated with Durvalumab or IgG control antibody for 5 days before being plated for experiment.

Microscopy:

Cells were plated on glass-bottom dishes prior to all experiments. After corresponding experimental treatments, cells were washed and fixed in 3.7% formaldehyde for 5 minutes. Cells were stained with primary and fluorescent secondary antibodies for proteins of interest on the plasma membrane without permeabilization. Saponin (0.25 mg/mL) was used to permeabilize the cells for total protein stain. Cell nuclei were labeled with Hoechst stain. For quantifications, images were acquired on an inverted microscope with a 20× air objective or a 40x oil objective (Leica Biosystems DMI6000-B). Images were analyzed on MetaMorph image processing software and the background corrected average intensity under each cell's area was used to quantify protein amount. The values were normalized to the average of replicate coverslip dishes in control condition in each experiment to allow for comparison across experiments. Unpaired two tailed Student's t test or paired ratio t-test were performed on unnormalized raw data, and one sample t test was used on normalized data respectively as indicated. For comparison of three and more groups, one-way ANOVA was performed on raw data with post-hoc Tuckey test where indicated. For PD-L1 stain images, Z stack of the cells was acquired using Zeiss Confocal microscope (LSM880) with Airyscan on a 40x oil objective.

Exocytosis assay:

Live cells were incubated with a saturating concentration of PD-L1 antibody (50 µg/mL) for indicated times, washed extensively with PBS, and then fixed. All cells were permeabilized and stained with a secondary antibody to visualize all antibody bound to the cells. Separate set of dishes was used to quantify total PD-L1 stain in fixed cells in each experiment. Cells were imaged and quantified as described above. All values were normalized to the plateau, which is defined as the average of values at 60 and 120min in each experiment.

Colocalization analysis:

For co-localization analysis cells were fixed and stained for total PD-L1 and the protein of interest with primary antibody followed by Cy3 and Alexa488-labeled secondary antibodies. Cells were imaged on Zeiss Confocal microscope (LSM880) with Airyscan on a 40x oil objective. Images were analyzed in MetaMorph software. Intensity threshold was manually determined for each colocalization marker and kept constant for a binary mask of the marker. The binary mask was overlayed with PD-L1 staining resulting in PD-L1 stain only in pixels positive for the marker proteins. For each cell, integrated intensity of PD-L1 staining in the original images as well as the overlayed images were calculated. Ratio of overlayed intensity over original intensity was used as "fraction under mask". Unpaired t-test was performed on raw data.

Quantitative RT-PCR:

Cells were lysed after indicated treatments in each experiments and RNA was extracted using RNeasy kit, and cDNA was prepared from extracted RNA using the RNA to cDNA EcoDry Premix. Quantitative

RT-PCR was performed using appropriate primer pairs indicated in Supplementary Table 4. 2(-Delta Delta C(T)) method was used to quantify gene expression.

Western blotting:

Cells were lysed in laemmli buffer with protease/phosphatase inhibitors and the lysate was boiled at 95°C for 7 minutes. Lysates were run on 8% or 10% SDS gels and transferred onto nitrocellulose membranes. The membrane was blocked with 5% milk or Licor blocking buffer for 1 hr at room temperature, then incubated with primary antibody overnight at 4°C followed by secondary antibody for 1 hr at room temperature. Blots were visualized using Licor Odyssey Fc Imager for two color or Thermofisher MyECL Imager for single color assays and analyzed on ImageStudio or ImageJ software respectively. Actin or GAPDH expression was used as loading control where indicated. One sample t-test was performed on normalized data for comparison of two groups. One-way ANOVA and post-hoc paired ratio t-test was performed on raw data for three or more groups. For degradation assays, K rate constant for the non-linear regression and slopes for linear regression were used to calculate statistical difference.

EGFR Immunoprecipitation:

Cells were grown to confluency and treated with anti-PD-L1 Ab (clone #130021, Novus Biologicals) for 7 hr in serum free media, followed by addition of EGF (50ng/mL) for specified times. Cells were lysed in lysis buffer (150 mM NaCl, 50 mM Tris-HCl pH 7.5, 1% Triton X-100) with protease/phosphatase inhibitors at given timepoints. Protein concentration was measured using BCA assay and lysates were incubated with anti-EGFR antibody (4 µg/mL) for 1 hr at 4°C on a rotator. Lysates were then added to pre-washed protein A/G agarose beads and rotated overnight at 4°C. Beads were washed four times with lysis buffer and boiled in 1.5x Laemmli buffer for 5 minutes at 95°C to elute the proteins. Resulting IP fraction was analyzed via Western blot along with whole cell extract.

Extracellular vesicle, whole cell extract mass spectrometry:

Cells were adjusted to media supplemented with 10% exosome free FBS for 1 passage and plated at 60% confluency in exosome free media. After 48 hours of Durvalumab treatment (10 µg/mL), cell media was collected for extracellular vesicle isolation and cells were lysed in 1x RIPA buffer with protease/phosphatase inhibitors. Extracellular vesicles were isolated by sequential ultracentrifugation (12000g for 10 min to discard cell debris, 20000 g for 20 min to discard microvesicles, 100000 g for 70 min twice to isolate and wash the EVs) and resuspended in a final volume of 100 µL of RIPA buffer with protease/phosphatase inhibitors. Cell extract and EV lysates were quantified for protein concentration. A final amount of 100 µg of WCE, and equi-volume of EVs approximating 10 µg of protein in each sample was submitted for mass spectrometry analysis.

The samples were digested in solution with trypsin overnight at 37C following reduction with 5mM DTT and 14mM alkylation with iodoacetamide. The digests were vacuum centrifuged to near dryness and desalted by Sep-Pak column.

A Thermo Fisher Scientific EASY-nLC 1000 coupled on-line to a Fusion Lumos mass spectrometer (Thermo Fisher Scientific) was used. Buffer A (0.1% FA in water) and buffer B (0.1% FA in ACN) were used as mobile phases for gradient separation (1). A 75 µm x 15 cm chromatography column (ReproSil-Pur C18-AQ, 3 µm, Dr. Maisch GmbH, German) was packed in-house for peptides separation. Peptides were separated with a gradient of 3–28% buffer B over 110 min, 28%-80% B over 10 min at a flow rate of 300 nL/min. The Fusion Lumos mass spectrometer was operated in data dependent mode. Full MS scans were acquired in the Orbitrap mass analyzer over a range of 300-1500 m/z with resolution 120,000 at m/z 200. The top 15 most abundant precursors with charge states between 2 and 5 were selected with an isolation window of 1.4 Thomsons by the quadrupole and fragmented by higher-energy collisional dissociation with normalized collision energy of 35. MS/MS scans were acquired in the Orbitrap mass analyzer with resolution 15,000 at m/z 200. The automatic gain control target value was 1e6 for full scans and 5e4 for MS/MS scans respectively, and the maximum ion injection time is 60 ms for both.

The raw files were processed using the MaxQuant computational proteomics platform version 1.5.5.1 (Max Planck Institute, Munich, Germany) for protein identification. The fragmentation spectra were used to search the UniProt human protein database (downloaded on 01/16/2021). Oxidation of methionine and protein N-terminal acetylation were used as variable modifications for database searching. The precursor and fragment mass tolerances were set to 7 and 20 ppm, respectively. Both peptide and protein identifications were filtered at 1% false discovery rate based on decoy search using a database with the protein sequences reversed.

PD-L1-APEX2 labeling and mass spectrometry:

APEX2 proximity assay was performed as described previously[64]. Briefly, BEAS-2B cells stably expressing PD-L1 APEX2 were grown until confluency. Cells were preincubated with biotin phenol in full growth media for 30 minutes and hydrogen peroxide was added for 1 minute (except in negative control). Cells were washed three times with ice cold quenching solution (10 mM sodium ascorbate, 5 mM Trolox and 10 mM sodium azide solution in PBS) and cells were lysed in 1x RIPA lysis buffer with protease/phosphatase inhibitors. Protein concentration was measured, and biotinylated proteins were pulled down using streptavidin-agarose beads overnight at 4°C. Beads were washed (twice with RIPA lysis buffer, once with 1 M KCl, once with 0.1 M Na2CO3, once with 2 M urea in 10 mM Tris-HCl,pH 8.0, and twice with RIPA lysis buffer) and pull-down proteins were submitted for mass spectrometry.

Peptides from streptavidin purified proteins were released via on-bead digestion using trypsin (Promega) and desalted on C18 STAGE Tips [PMID: 12585499]. Eluted peptides were dried and re-suspended in 5% formic acid (FA). Mass Spectrometric analysis was performed on a Thermo Orbitrap Fusion mass spectrometer equipped with an Easy nLC-1000 UHPLC. Peptides were separated with a 115 min gradient of 5–25% acetonitrile in 0.1 % FA at 350 nl/min and introduced into the mass spectrometer by electrospray ionization as they eluted off a self-packed 40 cm, 100 µm (ID) column packed with 1.8 µm, 120 Å pore size, C18 resin (Sepax Technologies, Newark, DE). The column was heated to 60°C. Peptides were detected using a data-dependent method. For each 3 sec cycle, high resolution MS1 scans performed in the orbitrap and the most abundant ions per were isolated, fragmented by CID, and scanned in the ion trap. Ions selected for MS2 analysis were excluded from reanalysis for 60 sec. Ions with +1 or unassigned charge were also excluded from analysis. MS/MS spectra were matched to peptide sequences using COMET (version 2019.01 rev. 5) (PMID: 23148064) and a composite database containing the 20,415 Uniprot reviewed canonical predicted human protein sequences (http://uniprot.org, downloaded 5/1/2019) and its reversed complement. Search parameters allowed for two missed cleavages, a mass tolerance of 25 ppm, a static modification of 57.02146 Da (carboxyamidomethylation) on cysteine, and a dynamic modification of 15.99491 Da (oxidation) on methionine. Peptide spectral matches (PSMs) were filtered to 1% FDR using the target-decoy strategy[65] and then to 1% protein FDR. Label-free quantification was performed using peptide intensities from the integrated areas under each corresponding extracted-ion-chromatogram peak. Intensities for all peptides mapping to each protein were summed for each sample.

Mass spectrometry data analysis:

PD-L1APEX2 data were analyzed in two different ways. In one, proteins that satisfied the following criteria were identified to be in the proximity of PD-L1: proteins with peptides in the experimental sample without peptides in the negative control ($-H_2O_2$) samples, or proteins in which peptides in the experimental sample were two-fold or greater than in the control sample. Data from 5 independent experiments were analyzed individually and the final PD-L1 proximity map was determined as those proteins satisfying the criteria for PD-L1 proximity in each of the five experiments, yielding 399 PD-L1 proximity proteins. This set of proteins was used for further analyses, including biological processes pathway analysis via geneontology.org (GO database released 7-2-2021)[66] (as shown in Fig. 3D). The data were also analyzed by performing a t-test on Log_{10} transformed spectral intensity values between labeled and negative control samples ($-H_2O_2$) on the set of 1647 proteins common to all five experiments. Significant differences between the experimental and control were determined using Benjamini-Hochberg correction for multiple testing. Fold change was calculated as ratio of average spectral intensity in labeled samples over average in negative control samples (as shown in Fig S2A). The two different methods yielded essentially the same group of proteins.

For whole cell extract mass spectrometry analysis, sum intensity in each sample was confirmed to be similar across all samples in each experiment. For each protein, average ratio of +/- Durvalumab between two biological replicate experiments was calculated. Proteins with an average +/- Durvalumab ratio >1.2 (top 25th percentile of ratios across three cell lines) and coefficient of variance below 0.1 (bottom 25th percentile) in H1650 whole cells extract were analyzed for function across biological processes using geneontology.org (GO database released 7-2-2021)[66]. For EV mass spectrometry analysis, ratio of +/- Durvalumab between two biological replicate experiments was calculated for each protein and plotted as a frequency distribution.

Migration and proliferation:

For scratch assays 35K cells were plated on each side of the Ibidi 2-well scratch assay chambers. Cells were allowed to attach for 24 hrs and wound healing was assayed in complete or serum-free media for KO/rescue cells and Durvalumab treated cells respectively at specified timepoints. Cell were imaged in bright-field on Leica Microscope. 9 images of each sample were taken at each timepoint, and three distances were measured in each image using Image J. For migration assay, 30k cells were plated on the top chamber of transwell-migration plates with 8 micron pore size in serum free media. Bottom chamber was filled with DMEM with 10% FBS and cells were allowed to migrate for 24 hrs. Cells were then fixed in 3.7% formaldehyde for 15 minutes, washed and then stained in Crystal Violet for 20 minutes. Unmigrated cells were scraped off with damp cotton swab and membrane was cut out and mounted on slides. Migrated cells were imaged on upright microscope (Zeiss Axioplan) with 10x objective and analyzed via ImageJ. For proliferation assay, 5k cells were plated in triplicate 96 wells (day 0) and MTT was used to quantify viable cells on days 1-5. Paired t test was performed on raw transwell migration data, and slopes of nonlinear regression lines were used to calculate significance for scratch and MTT assays.

Acknowledgements:
We are grateful to Dr. Raffaella Sordella (Cold Spring Harbor Laboratories) for generously sharing EGFR mutant cell lines with us. We thank Astra Zeneca for the gift of Durvalumab antibody. We thank Dr. Alberto Benito and Dr. Kristy Brown for help with EV purification. We thank Rosemary Leahey for assistance with imaging studies. We thank the Optical Microscopy & Image Analysis Core at Weill Cornell Medicine for assistance with confocal microscopy. We thank Guoan Zhang and the Weill Cornell Medicine Proteomics and Metabolomics Core for assistance with whole cell and EV proteomics. We thank Dr. Jeremy Dittman, Dr. Geoffrey Markowitz, Dr. Lucie Yammine, Dr. Anuttoma Ray, Jennifer Wen, and Emma Johnson for helpful discussions and critical reading of the manuscript. The project was supported in part by NCI UG3 CA244697 (NKA, TEM), the Yoram Cohen family foundation (NKA), Vicky and Jay Furhman family fund (NKA) and a WCM Meyer Cancer Center pilot grant (NKA,TEM). TEM is also supported by DOD LC180227. EY is supported by a diversity supplement to CA244697.

Author contributions:

AL designed and performed the experiments, analyzed the data, and wrote the manuscript.

EY designed experiments, generated the KO cells, and wrote the manuscript.

PC and ND performed and assisted with APEX2 mass spectrometry experiments and analysis

NKA conceptualized the project, contributed to experimental design and interpretations, and edited the manuscript.

TEM conceptualized the project, contributed to experimental design, performed analysis and interpretation, and wrote the manuscript.

References

1 Hamanishi, J. *et al.* PD-1/PD-L1 blockade in cancer treatment: perspectives and issues. *Int J Clin Oncol* **21**, 462-473, doi:10.1007/s10147-016-0959-z (2016).

2 Jiang, Y., Zhao, X., Fu, J. & Wang, H. Progress and Challenges in Precise Treatment of Tumors With PD-1/PD-L1 Blockade. *Front Immunol* **11**, 339, doi:10.3389/fimmu.2020.00339 (2020).

3 Gainor, J. F. *et al.* EGFR Mutations and ALK Rearrangements Are Associated with Low Response Rates to PD-1 Pathway Blockade in Non-Small Cell Lung Cancer: A Retrospective Analysis. *Clin Cancer Res* **22**, 4585-4593, doi:10.1158/1078-0432.CCR-15-3101 (2016).

4 Lee, C. K. *et al.* Checkpoint Inhibitors in Metastatic EGFR-Mutated Non-Small Cell Lung Cancer-A Meta-Analysis. *J Thorac Oncol* **12**, 403-407, doi:10.1016/j.jtho.2016.10.007 (2017).

5 Mazieres, J. *et al.* Immune checkpoint inhibitors for patients with advanced lung cancer and oncogenic driver alterations: results from the IMMUNOTARGET registry. *Ann Oncol*, doi:10.1093/annonc/mdz167 (2019).

6 Pardoll, D. M. The blockade of immune checkpoints in cancer immunotherapy. *Nat Rev Cancer* **12**, 252-264, doi:10.1038/nrc3239 (2012).

7 Fang, W. *et al.* EBV-driven LMP1 and IFN-gamma up-regulate PD-L1 in nasopharyngeal carcinoma: Implications for oncotargeted therapy. *Oncotarget* **5**, 12189-12202, doi:10.18632/oncotarget.2608 (2014).

8 Gowrishankar, K. *et al.* Inducible but not constitutive expression of PD-L1 in human melanoma cells is dependent on activation of NF-kappaB. *PLoS One* **10**, e0123410, doi:10.1371/journal.pone.0123410 (2015).

9 Shen, X. *et al.* Recent Findings in the Regulation of Programmed Death Ligand 1 Expression. *Front Immunol* **10**, 1337, doi:10.3389/fimmu.2019.01337 (2019).

10 Hsu, J. M. *et al.* STT3-dependent PD-L1 accumulation on cancer stem cells promotes immune evasion. *Nat Commun* **9**, 1908, doi:10.1038/s41467-018-04313-6 (2018).

11 Huang, X. *et al.* USP22 Deubiquitinates CD274 to Suppress Anticancer Immunity. *Cancer Immunol Res* **7**, 1580-1590, doi:10.1158/2326-6066.CIR-18-0910 (2019).

12 Li, C. W. *et al.* Glycosylation and stabilization of programmed death ligand-1 suppresses T-cell activity. *Nat Commun* **7**, 12632, doi:10.1038/ncomms12632 (2016).

13 Yang, Y. *et al.* Palmitoylation stabilizes PD-L1 to promote breast tumor growth. *Cell Res* **29**, 83-86, doi:10.1038/s41422-018-0124-5 (2019).

14 Burr, M. L. *et al.* CMTM6 maintains the expression of PD-L1 and regulates anti-tumour immunity. *Nature*, doi:10.1038/nature23643 (2017).

15 Mezzadra, R. *et al.* Identification of CMTM6 and CMTM4 as PD-L1 protein regulators. *Nature*, doi:10.1038/nature23669 (2017).

16 Wang, H. *et al.* HIP1R targets PD-L1 to lysosomal degradation to alter T cell-mediated cytotoxicity. *Nat Chem Biol* **15**, 42-50, doi:10.1038/s41589-018-0161-x (2019).

17 Gato-Canas, M. *et al.* PDL1 Signals through Conserved Sequence Motifs to Overcome Interferon-Mediated Cytotoxicity. *Cell Rep* **20**, 1818-1829, doi:10.1016/j.celrep.2017.07.075 (2017).

18 Ghosh, S. *et al.* PD-L1 recruits phospholipase C and enhances tumorigenicity of lung tumors harboring mutant forms of EGFR. *Cell Rep* **35**, 109181, doi:10.1016/j.celrep.2021.109181 (2021).

19 Chen, L. *et al.* PD-L1 Expression Promotes Epithelial to Mesenchymal Transition in Human Esophageal Cancer. *Cell Physiol Biochem* **42**, 2267-2280, doi:10.1159/000480000 (2017).

20 Wang, Y. *et al.* PD-L1 induces epithelial-to-mesenchymal transition via activating SREBP-1c in renal cell carcinoma. *Med Oncol* **32**, 212, doi:10.1007/s12032-015-0655-2 (2015).

21 Zhang, P. *et al.* The up-regulation of PD-L1 promotes the resistant response in non-small cell lung cancer patients with neo-adjuvant chemotherapy. *Cancer Sci*, doi:10.1111/cas.13072 (2016).

22 Sholl, L. M. *et al.* Multi-institutional Oncogenic Driver Mutation Analysis in Lung Adenocarcinoma: The Lung Cancer Mutation Consortium Experience. *J Thorac Oncol* **10**, 768-777, doi:10.1097/JTO.0000000000000516 (2015).

23 Ibrahim, R., Stewart, R. & Shalabi, A. PD-L1 blockade for cancer treatment: MEDI4736. *Semin Oncol* **42**, 474-483, doi:10.1053/j.seminoncol.2015.02.007 (2015).

24 Stewart, R. *et al.* Identification and Characterization of MEDI4736, an Antagonistic Anti-PD-L1 Monoclonal Antibody. *Cancer Immunol Res* **3**, 1052-1062, doi:10.1158/2326-6066.CIR-14-0191 (2015).

25 Blot, V. & McGraw, T. E. Use of quantitative immunofluorescence microscopy to study intracellular trafficking: studies of the GLUT4 glucose transporter. *Methods Mol Biol* **457**, 347-366 (2008).

26 Gonzalez, E. & McGraw, T. E. The Akt kinases: isoform specificity in metabolism and cancer. *Cell Cycle* **8**, 2502-2508, doi:10.4161/cc.8.16.9335 (2009).

27 Chen, B. S. & Roche, K. W. Growth factor-dependent trafficking of cerebellar NMDA receptors via protein kinase B/Akt phosphorylation of NR2C. *Neuron* **62**, 471-478, doi:10.1016/j.neuron.2009.04.015 (2009).

28 Lucas, E. D. *et al.* PD-L1 Reverse Signaling in Dermal Dendritic Cells Promotes Dendritic Cell Migration Required for Skin Immunity. *Cell Rep* **33**, 108258, doi:10.1016/j.celrep.2020.108258 (2020).

29 Lobingier, B. T. *et al.* An Approach to Spatiotemporally Resolve Protein Interaction Networks in Living Cells. *Cell* **169**, 350-360 e312, doi:10.1016/j.cell.2017.03.022 (2017).

30 Lam, S. S. *et al.* Directed evolution of APEX2 for electron microscopy and proximity labeling. *Nat Methods* **12**, 51-54, doi:10.1038/nmeth.3179 (2015).

31 Chung, B. M. *et al.* Aberrant trafficking of NSCLC-associated EGFR mutants through the endocytic recycling pathway promotes interaction with Src. *BMC Cell Biol* **10**, 84, doi:10.1186/1471-2121-10-84 (2009).

32 Katzmann, D. J., Babst, M. & Emr, S. D. Ubiquitin-dependent sorting into the multivesicular body pathway requires the function of a conserved endosomal protein sorting complex, ESCRT-I. *Cell* **106**, 145-155, doi:10.1016/s0092-8674(01)00434-2 (2001).

33 Sigismund, S. *et al.* Clathrin-mediated internalization is essential for sustained EGFR signaling but dispensable for degradation. *Dev Cell* **15**, 209-219, doi:10.1016/j.devcel.2008.06.012 (2008).

34 Huang, F., Kirkpatrick, D., Jiang, X., Gygi, S. & Sorkin, A. Differential regulation of EGF receptor internalization and degradation by multiubiquitination within the kinase domain. *Mol Cell* **21**, 737-748, doi:10.1016/j.molcel.2006.02.018 (2006).

35 Hosaka, T. *et al.* Mutant epidermal growth factor receptor undergoes less protein degradation due to diminished binding to c-Cbl. *Anticancer Res* **27**, 2253-2263 (2007).

36 Huang, F., Goh, L. K. & Sorkin, A. EGF receptor ubiquitination is not necessary for its internalization. *Proc Natl Acad Sci U S A* **104**, 16904-16909, doi:10.1073/pnas.0707416104 (2007).

37 Shtiegman, K. *et al.* Defective ubiquitinylation of EGFR mutants of lung cancer confers prolonged signaling. *Oncogene* **26**, 6968-6978, doi:10.1038/sj.onc.1210503 (2007).

38 Raiborg, C. & Stenmark, H. The ESCRT machinery in endosomal sorting of ubiquitylated membrane proteins. *Nature* **458**, 445-452, doi:10.1038/nature07961 (2009).

39 McAndrews, K. M. & Kalluri, R. Mechanisms associated with biogenesis of exosomes in cancer. *Mol Cancer* **18**, 52, doi:10.1186/s12943-019-0963-9 (2019).

40 Eitan, E., Suire, C., Zhang, S. & Mattson, M. P. Impact of lysosome status on extracellular vesicle content and release. *Ageing Res Rev* **32**, 65-74, doi:10.1016/j.arr.2016.05.001 (2016).

41 Latifkar, A. *et al.* Loss of Sirtuin 1 Alters the Secretome of Breast Cancer Cells by Impairing Lysosomal Integrity. *Dev Cell* **49**, 393-408 e397, doi:10.1016/j.devcel.2019.03.011 (2019).

42 Saleh, R., Taha, R. Z., Sasidharan Nair, V., Alajez, N. M. & Elkord, E. PD-L1 Blockade by Atezolizumab Downregulates Signaling Pathways Associated with Tumor Growth, Metastasis, and Hypoxia in Human Triple Negative Breast Cancer. *Cancers (Basel)* **11**, doi:10.3390/cancers11081050 (2019).

43 Chew, H. Y. *et al.* Endocytosis Inhibition in Humans to Improve Responses to ADCC-Mediating Antibodies. *Cell* **180**, 895-914 e827, doi:10.1016/j.cell.2020.02.019 (2020).

44 Henne, W. M., Buchkovich, N. J. & Emr, S. D. The ESCRT pathway. *Dev Cell* **21**, 77-91, doi:10.1016/j.devcel.2011.05.015 (2011).

45 Juan, T. & Furthauer, M. Biogenesis and function of ESCRT-dependent extracellular vesicles. *Semin Cell Dev Biol* **74**, 66-77, doi:10.1016/j.semcdb.2017.08.022 (2018).

46 Clark, C. A. *et al.* Tumor-Intrinsic PD-L1 Signals Regulate Cell Growth, Pathogenesis, and Autophagy in Ovarian Cancer and Melanoma. *Cancer Res* **76**, 6964-6974, doi:10.1158/0008-5472.CAN-16-0258 (2016).

47 Sung, B. H., Parent, C. A. & Weaver, A. M. Extracellular vesicles: Critical players during cell migration. *Dev Cell*, doi:10.1016/j.devcel.2021.03.020 (2021).

48 Mittal, S., Kamath, A., Joseph, A. M. & Rajala, M. S. PLCgamma1dependent invasion and migration of cells expressing NSCLCassociated EGFR mutants. *Int J Oncol* **57**, 989-1000, doi:10.3892/ijo.2020.5112 (2020).

49 Holsken, A. *et al.* EGFR signaling regulates tumor cell migration in craniopharyngiomas. *Clin Cancer Res* **17**, 4367-4377, doi:10.1158/1078-0432.CCR-10-2811 (2011).

50 Yu, W. *et al.* PD-L1 promotes tumor growth and progression by activating WIP and beta-catenin signaling pathways and predicts poor prognosis in lung cancer. *Cell Death Dis* **11**, 506, doi:10.1038/s41419-020-2701-z (2020).

51 Guo, A. *et al.* Signaling networks assembled by oncogenic EGFR and c-Met. *Proc Natl Acad Sci U S A* **105**, 692-697, doi:10.1073/pnas.0707270105 (2008).

52 Pines, G., Kostler, W. J. & Yarden, Y. Oncogenic mutant forms of EGFR: lessons in signal transduction and targets for cancer therapy. *FEBS Lett* **584**, 2699-2706, doi:10.1016/j.febslet.2010.04.019 (2010).

53 Chen, L. & Han, X. Anti-PD-1/PD-L1 therapy of human cancer: past, present, and future. *J Clin Invest* **125**, 3384-3391, doi:10.1172/JCI80011 (2015).

54 Oh, S. A. *et al.* PD-L1 expression by dendritic cells is a key regulator of T-cell immunity in cancer. *Nature Cancer* **1**, 681-691, doi:10.1038/s43018-020-0075-x (2020).

55 Peng, Q. *et al.* PD-L1 on dendritic cells attenuates T cell activation and regulates response to immune checkpoint blockade. *Nat Commun* **11**, 4835, doi:10.1038/s41467-020-18570-x (2020).

56 Yao, H. *et al.* Inhibiting PD-L1 palmitoylation enhances T-cell immune responses against tumours. *Nat Biomed Eng* **3**, 306-317, doi:10.1038/s41551-019-0375-6 (2019).

57 Geri, J. B. *et al.* Microenvironment mapping via Dexter energy transfer on immune cells. *Science* **367**, 1091-1097, doi:10.1126/science.aay4106 (2020).

58 Head, B. P., Patel, H. H. & Insel, P. A. Interaction of membrane/lipid rafts with the cytoskeleton: impact on signaling and function: membrane/lipid rafts, mediators of cytoskeletal arrangement and cell signaling. *Biochim Biophys Acta* **1838**, 532-545, doi:10.1016/j.bbamem.2013.07.018 (2014).

59 Staubach, S. & Hanisch, F. G. Lipid rafts: signaling and sorting platforms of cells and their roles in cancer. *Expert Rev Proteomics* **8**, 263-277, doi:10.1586/epr.11.2 (2011).

60 Yokosuka, T. *et al.* Programmed cell death 1 forms negative costimulatory microclusters that directly inhibit T cell receptor signaling by recruiting phosphatase SHP2. *J Exp Med* **209**, 1201-1217, doi:10.1084/jem.20112741 (2012).

61 Arasanz, H. *et al.* PD1 signal transduction pathways in T cells. *Oncotarget* **8**, 51936-51945, doi:10.18632/oncotarget.17232 (2017).

62 Fooksman, D. R., Gronvall, G. K., Tang, Q. & Edidin, M. Clustering class I MHC modulates sensitivity of T cell recognition. *J Immunol* **176**, 6673-6680 (2006).

63 Chaudhri, V. K. *et al.* Metabolic alterations in lung cancer-associated fibroblasts correlated with increased glycolytic metabolism of the tumor. *Mol Cancer Res* **11**, 579-592, doi:10.1158/1541-7786.MCR-12-0437-T (2013).

64 Hung, V. *et al.* Spatially resolved proteomic mapping in living cells with the engineered peroxidase APEX2. *Nat Protoc* **11**, 456-475, doi:10.1038/nprot.2016.018 (2016).

65 Elias, J. E. & Gygi, S. P. Target-decoy search strategy for increased confidence in large-scale protein identifications by mass spectrometry. *Nat Methods* **4**, 207-214, doi:10.1038/nmeth1019 (2007).

66 Ashburner, M. *et al.* Gene ontology: tool for the unification of biology. The Gene Ontology Consortium. *Nat Genet* **25**, 25-29, doi:10.1038/75556 (2000).

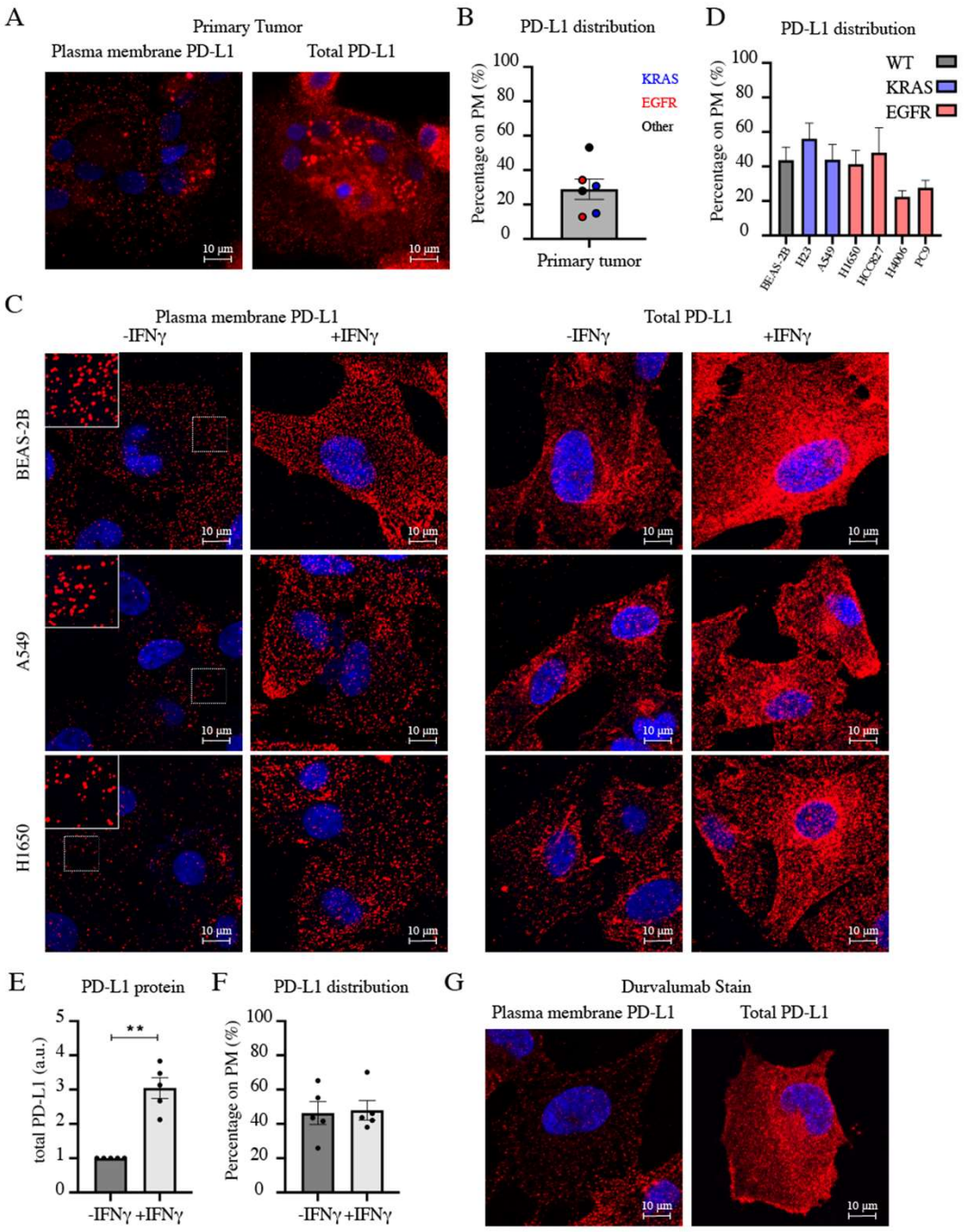

Figure 1. **PD-L1 is localized to the plasma membrane and intracellular compartments.**

A. Representative confocal images of primary human tumor cells immunostained for plasma membrane (PM) and total PD-L1. Red: PD-L1. Blue: Hoechst
B. Quantification of percentage of PM PD-L1 in primary human tumors. Each data point is a patient sample color coded for known oncogenes.
C. Representative confocal images of human lung cell lines with or without IFNγ treatment (40ng/mL, 24 hr) and immunostained for PM and total PD-L1. Red: PD-L1. Blue: Hoechst. Sum intensity of z-stacks is projected. Fluoresence intensity is equally scaled across panels for each cell line. Insets in -IFNγ PM are enhanced for better visualization.
D. Quantification of percentage of PM PD-L1 in human lung cell lines.
E. Total PD-L1 protein level in BEAS-2B cells treated with IFNγ (40ng/mL, 24 hr). Each data point is an experiment. One sample t-test.
F. Quantification of PM localization of PD-L1 in BEAS-2B cells treated with IFNγ (40ng/mL, 24 hr). Each data point is an experiment. Unpaired student's t-test.
G. Representative confocal images BEAS-2B cells stained for PM and total PD-L1 using clinical Durvalumab antibody. Red: PD-L1. Blue: Hoechst

All quantifications are calculated from average immunofluorescence staining intensity on epifluorescence images. All error bars = SEM. * ≤ 0.05, ** ≤ 0.01, *** ≤0.001

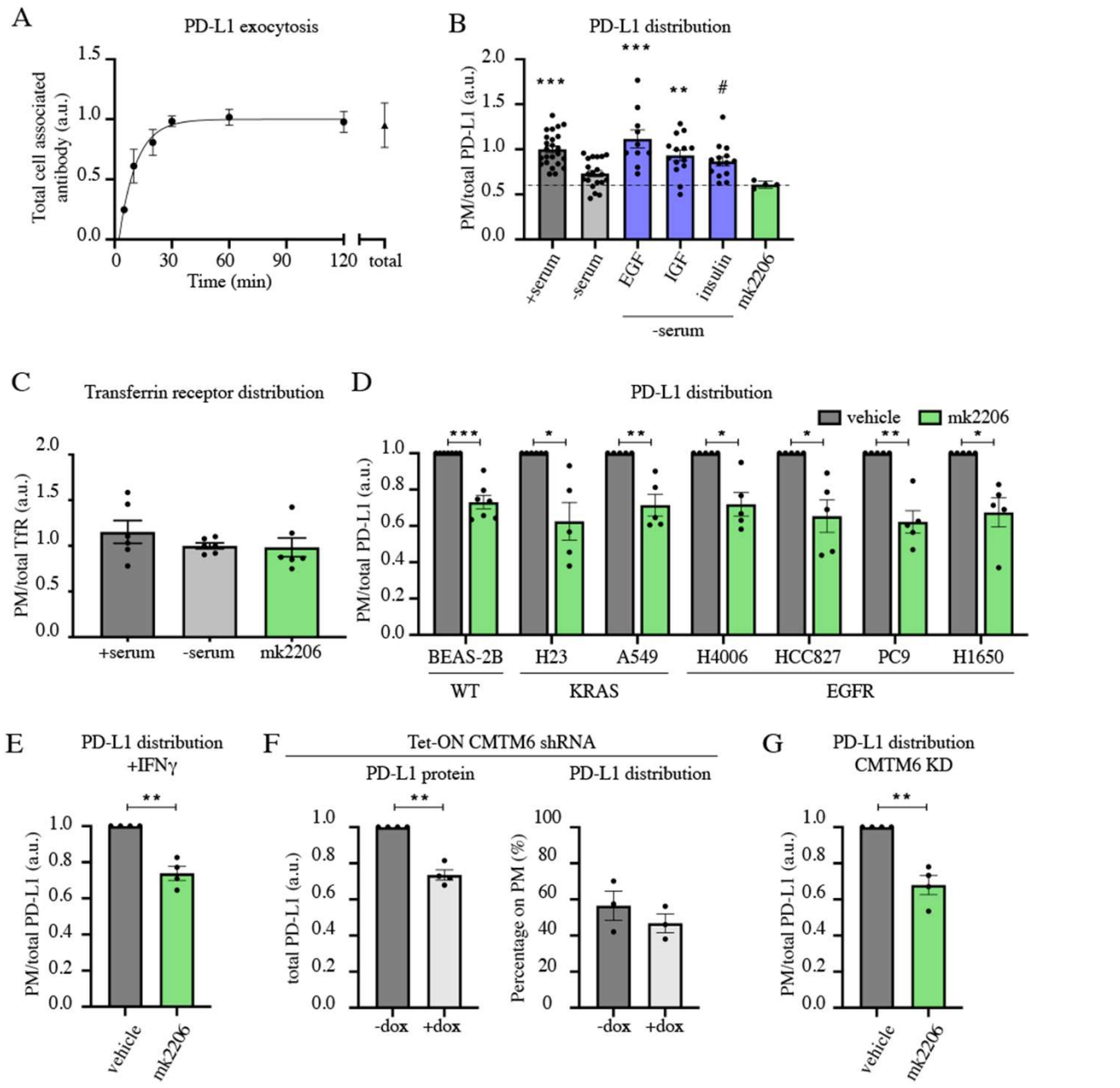

Figure 2. **PD-L1 plasma membrane localization is controlled by growth factor and Akt signaling.**

A. PD-L1 steady state exocytosis in BEAS-2B cells. The line is a fit of the data to one-phase association exponential equation. Total PD-L1 stain normalized to exocytosis plateau is shown on the right. N=3

B. PD-L1 PM to total ratio with growth factors treatment or Akt inhibition in BEAS-2B cells. Cells were subjected to 4 hr of corresponding treatment prior to fixation and immunostain. Growth factors were added to serum-free media (EGF 8nM, IGF 10nM, insulin 10nM), MK2206 was added to serum complete media (MK2206 5μM). One-way ANOVA and post-hoc Tukey test.

C. Transferrin receptor (TfR) PM to total ratio in BEAS-2B cells. Cells were treated for 4 hrs. MK2206 was added to serum complete media (MK2206 5μM). One-way ANOVA.

D. PD-L1 PM to total ratio in cell lines treated with vehicle (DMSO) or Akt inhibitor for 4 hrs (MK2206 5μM). One sample t-test.

E. PD-L1 PM to total ratio in IFNγ (40 ng/mL, 24 hr) treated BEAS-2B cells incubated with vehicle (DMSO) or Akt inhibitor (MK2206 5μM) for 4 hrs. One sample t-test.

F. PD-L1 protein expression and distribution in BEAS-2B expressing doxycycline inducible CMTM6 shRNA (doxycycline 48 hr, 1 μg/mL; all cells in IFNγ 24 hr, 40 ng/mL). Left: Total PD-L1 protein. Right: PM localization of PD-L1. One sample and unpaired t-tests.

G. PD-L1 PM to total ratio in CMTM6 knocked-down (KD) BEAS-2B cells (doxycycline 48 hr, 1 μg/mL; all cells in IFNγ 24 hr, 40 ng/mL) treated with vehicle (DMSO) or Akt inhibitor (MK2206 5μM) for 4 hrs. One sample t-test.

All quantifications are calculated from average immunofluorescence staining intensity on epifluorescence images. Except panel A, each data point is an experiment. All error bars = SEM. * ≤ 0.05, ** ≤ 0.01, *** ≤0.001, # = 0.058

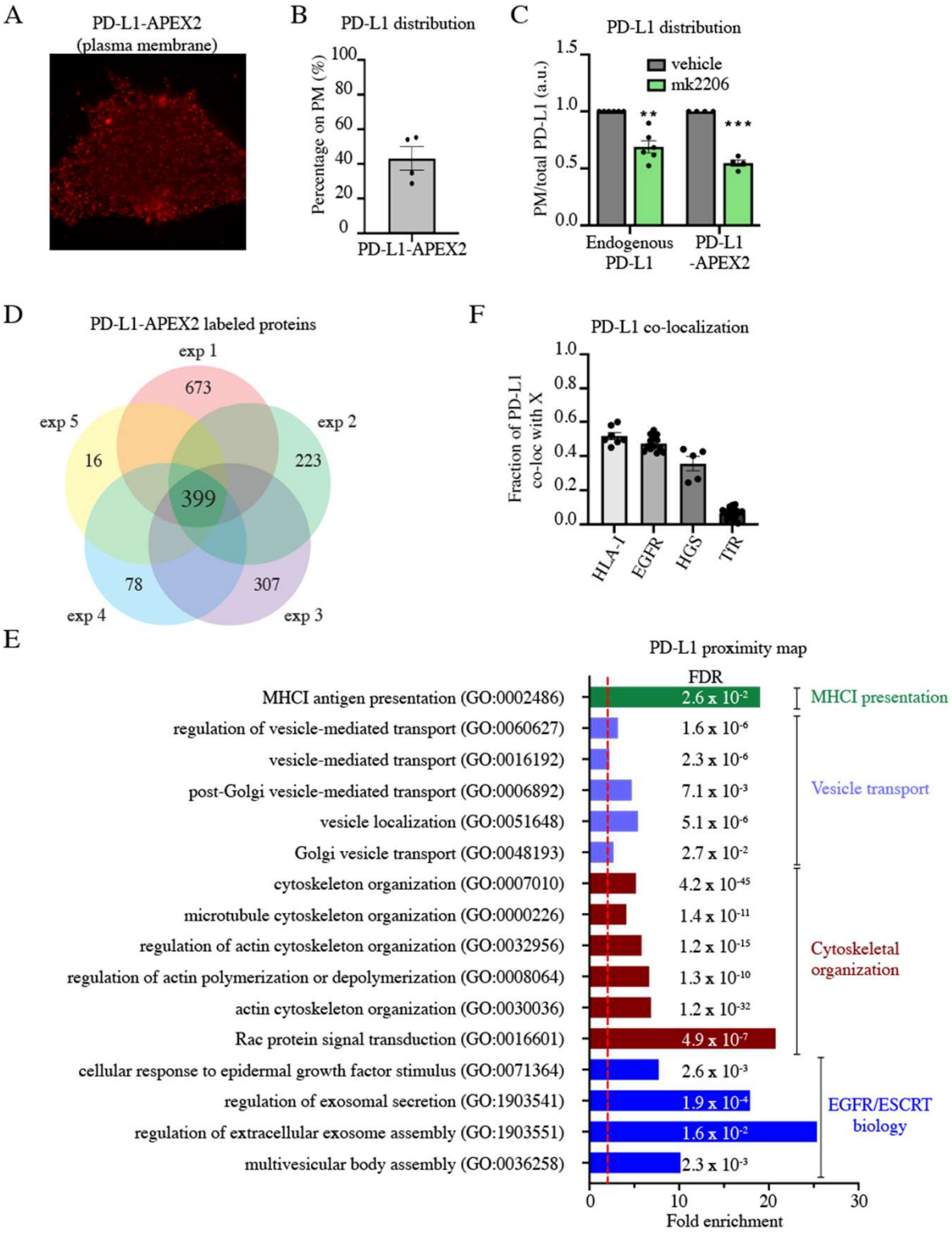

Figure 3. PD-L1 proximal proteome

A. Representative epifluorescence image of PD-L1-APEX2 plasma membrane stain in BEAS-2B cells.
B. PM to total distribution of PD-L1-APEX2 in BEAS-2B cells. Each data point is an experiment.
C. PM to total ratio of endogenous PD-L1 and PD-L1-APEX2 construct in BEAS-2B cells treated with vehicle (DMSO) or Akt inhibitor (MK2206 5 μM) for 4 hrs. One-sample t -test. Each data point is an experiment.
D. Venn diagram of PD-L1-APEX2 proximal proteins identified in 5 biological replicate experiments.
E. Biological processes pathways enriched in PD-L1-APEX2 labeling in BEAS-2B. Enrichment fold change and FDR are shown for each pathway. N=5
F. PD-L1 co-localization with specified proteins quantified by fraction of PD-L1 intensity co-localized with each target protein. Each point is a collected from single plane images of individual cells under confocal microscopy.

All error bars = SEM. * ≤ 0.05, ** ≤ 0.01, *** ≤0.001

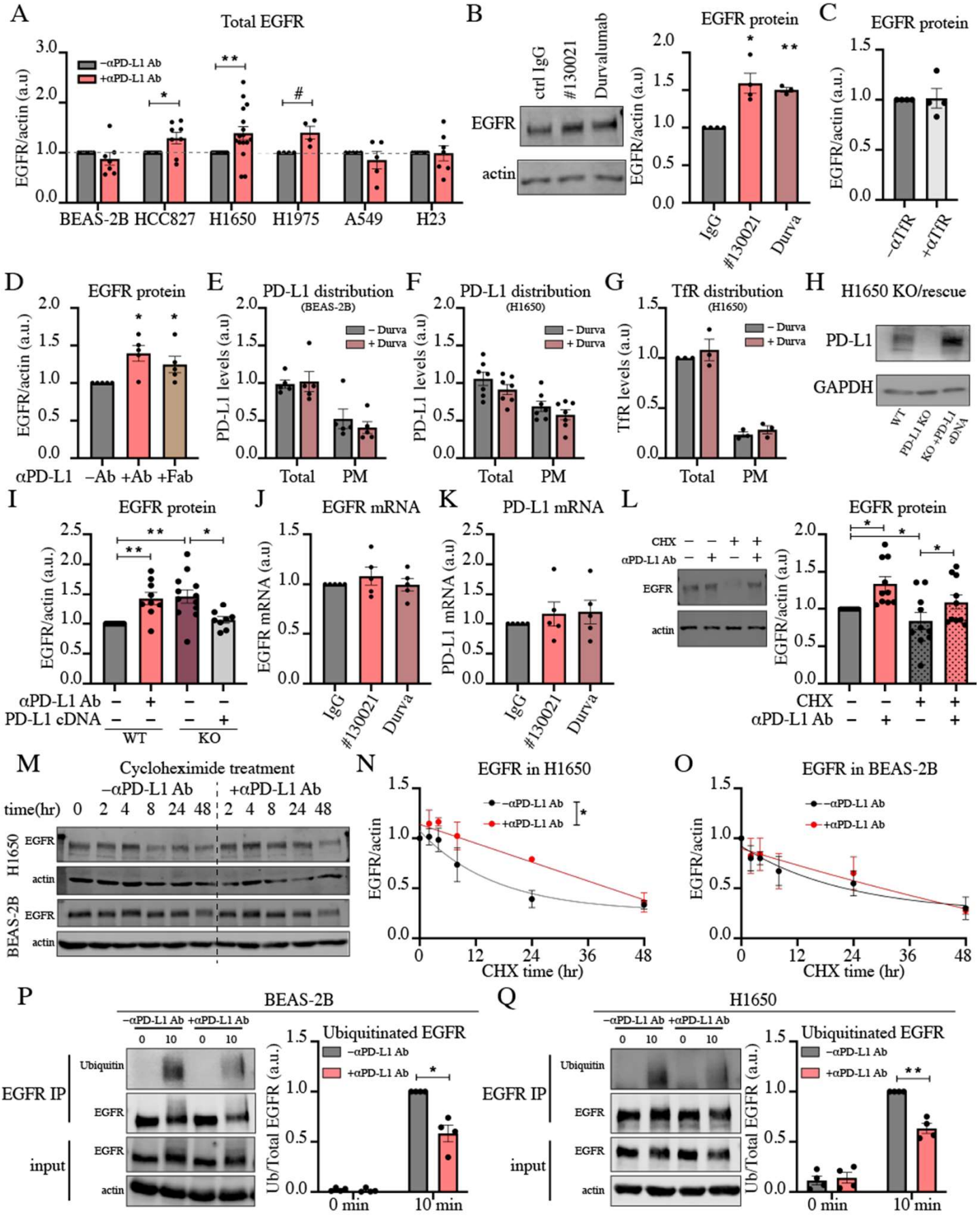

Figure 4. αPD-L1 antibody increases mutant but not wildtype EGFR protein

Legends on next page

Figure 4. αPD-L1 antibody increases mutant but not wildtype EGFR protein

A. EGFR protein expression in cell lines treated with αPD-L1 antibody (10μg/mL, 7 hr). Western blot quantifications of EGFR protein normalized to actin expression are shown. One sample t-test.
B. Immunoblot of EGFR protein expression in H1650 cells treated with reagent grade αPD-L1 antibody (clone # 130021, Novus Biologicals) and clinical Durvalumab as compared to isotype IgG control antibody (all antibodies at 10μg/mL, 7 hr). Western blot quantifications of EGFR protein normalized to actin expression are shown. One-way ANOVA and post-hoc Tukey test.
C. EGFR protein in H1650 cells with αTfR antibody treatment (10μg/mL, 7 hr). One sample t-test.
D. EGFR protein in H1650 cells with αPD-L1 antibody and αPD-L1 Fab treatment (10μg/mL). One way ANOVA and post-hoc Tukey test.
E. PD-L1 protein levels and distribution in BEAS-2B cells treated with Durvalumab (10μg/mL, 7 hr). Unpaired multiple t-tests.
F. PD-L1 protein levels and distribution in H1650 cells treated with Durvalumab (10μg/mL, 7 hr). Unpaired multiple t-tests.
G. TfR protein levels and distribution in H1650 cells treated with Durvalumab (10μg/mL, 7 hr). Unpaired multiple t-tests.
H. Immunoblot of PD-L1 protein expression in WT, PD-L1 KO and PD-L1-reexpressing H1650 cells. Cells were pretreated with IFNγ (40ng/mL, 24 hr)
I. EGFR protein in WT, PD-L1 KO and PD-L1-reexpressing H1650 cells. One way ANOVA and post-hoc Tukey test.
J. EGFR mRNA in H1650 cells treated with αPD-L1 antibodies (10μg/mL, 7 hr). One sample t-test.
K. PD-L1 mRNA in H1650 cells treated with αPD-L1 antibodies (10μg/mL, 7 hr). One sample t-test.
L. Immunoblot of EGFR protein expression in H1650 cells treated with αPD-L1 antibody (10μg/mL, 7 hr) and cycloheximide (10μg/mL, 7 hr). Western blot quantifications of EGFR protein normalized to actin expression are shown. One-way ANOVA and post-hoc Tukey test.
M. Immunoblots of EGFR degradation in H1650 and BEAS-2B cells treated with cycloheximide (10 μg/mL) in serum complete media. Actin is used as loading control.
N. Quantification of EGFR degradation in H1650 cells. N=3 Tested for change in rate constants.
O. Quantification of EGFR degradation in H1650 cells. N=3 Tested for change in rate constants.
P. Ubiquitinated EGFR protein in BEAS-2B cells treated with αPD-L1 (10μg/mL, 7 hr) followed by EGF for specified time (50 ng/mL). Immunoblots of whole cell extract and EGFR IP fraction are shown. Ubiquitinated/total EGFR in IP fraction was quantified. Paired ratio t-test.
Q. Ubiquitinated EGFR protein in H1650 cells treated with antibody (10μg/mL, 7 hr) followed by EGF for specified time (50 ng/mL). Immunoblots of whole cell extract and EGFR IP fraction are shown. Ubiquitinated/total EGFR in IP fraction was quantified. Paired ratio t-test.

Except panel N &O, each data point is an experiment. All error bars = SEM. * ≤ 0.05, ** ≤ 0.01, *** ≤0.001, # = 0.051

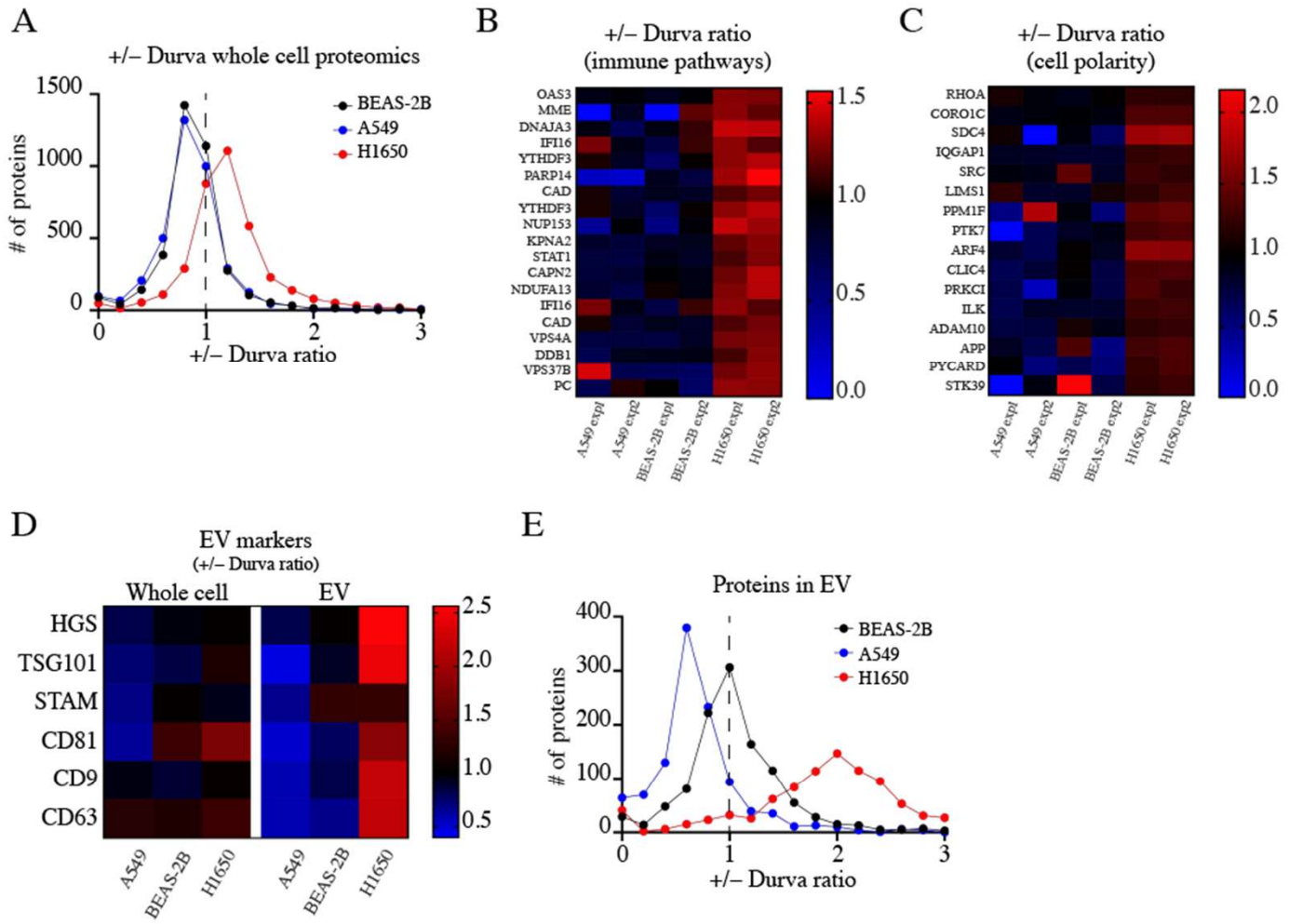

Figure 5. Durvalumab affects whole cell proteomics and EV secretion in EGFR mutant cells

A. Ratio of mass spectrometry intensity of proteins in extracts from cells treated with Durvalumab (10μg/mL, 48 hr) to those from untreated cells. Frequency distribution of +/− Durvalumab ratios of whole cell proteins identified is plotted. Average value for N=2 is shown.

B. Heatmap of proteins enriched in H1650 cells with Durvalumab treatment that were identified in immune related processes. +/− Durvalumab ratio for each of the two experiments is shown.

C. Heatmap of proteins enriched in H1650 cells with Durvalumab treatment that were identified in cell polarity related processes. +/− Durvalumab ratio for each of the two experiments is shown.

D. Heatmap of extracellular vesicle marker proteins expression in whole cell and EV fraction across cell lines treated with Durvalumab (10μg/mL, 48 hr). Average +/ − Durvalumab value for N=2 is shown.

E. Ratio of mass spectrometry intensity of proteins identified in extracellular vesicles from cells treated with Durvalumab (10μg/mL, 48 hr) to those from untreated cells. Frequency distribution of +/− Durvalumab ratios of extracellular vesicle proteins is plotted. Average value for N=2 is shown.

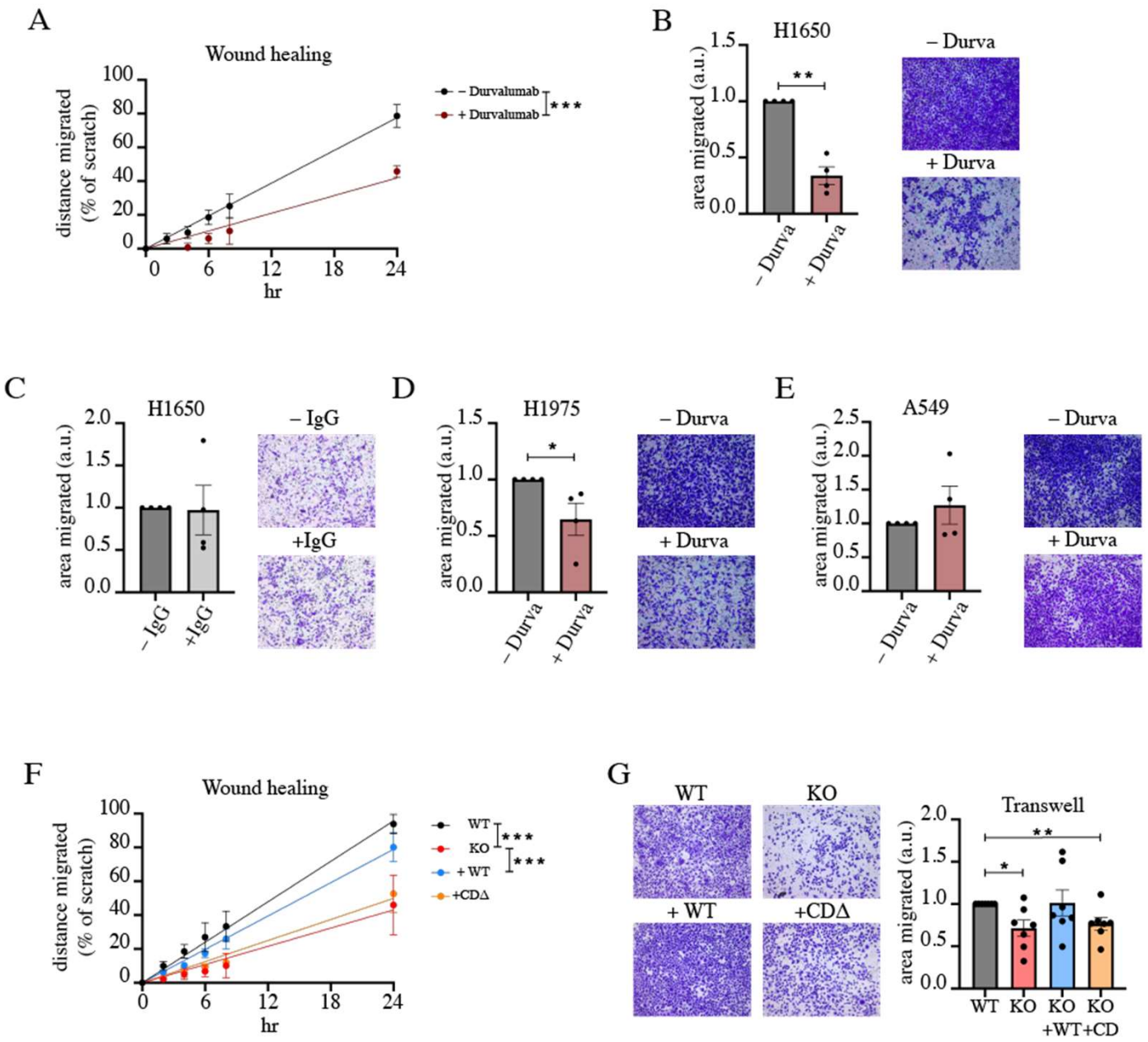

Figure 6. PD-L1 affects cell migration in EGFR mutant cells

A. Quantification of scratch assay in H1650 cells treated with Durvalumab (10μg/mL). Cells were in serum-free media for the duration of the assay. N=3 Difference in slope values is calculated.
B. Transwell migration of H1650 cells treated with Durvalumab (10μg/mL). Paired t-test
C. Transwell migration of H1650 cells treated with control IgG (10μg/mL). Paired t-test
D. Transwell migration of H1975 cells treated with Durvalumab (10μg/mL). Paired t-test.
E. Transwell migration of A549 cells treated with Durvalumab (10μg/mL). Paired t-test
F. Quantification of scratch assay in H1650 KO/rescue cells. Cells were in serum complete media for the duration of the assay. N=3-4 Difference in slope values is calculated.
G. Transwell migration in H1650 KO/rescue cells. One-way ANOVA and post-hoc Tuckey test.

For all experiments with antibody treatments, cells were pretreated with specified antibody (10μg/mL) for 5 days prior to the start of experiment. Except panels A & F, each data point is an experiment. All error bars = SEM. * ≤ 0.05, ** ≤ 0.01, *** ≤0.001

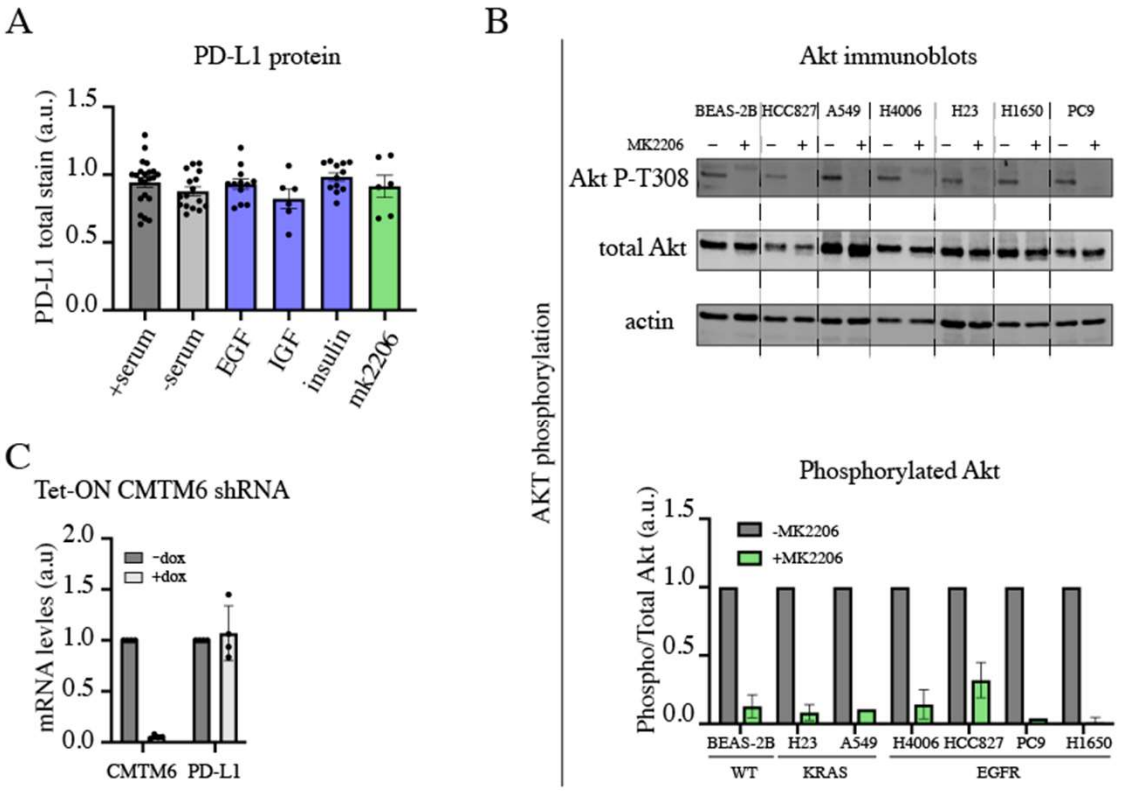

Figure Supplemental 1. PD-L1 plasma membrane localization is controlled by growth factor and Akt signaling.

A. Total PD-L1 protein expression in BEAS-2B cells. Cells were subjected to 4 hr of corresponding treatment prior to fixation and immunostain. Growth factors were added to serum-free media (EGF 8nM, IGF 10nM, insulin 10nM), MK2206 was added to serum complete media (MK2206 5μM). One-way ANOVA.

B. Immunoblots showing Akt T308 phosphorylation in cells treated with vehicle (DMSO) or Akt inhibitior (MK2206 5 μM) for 4 hrs. Corresponding quantification of phospho-T308/total Akt is shown in the graph.

C. CMTM6 and PD-L1 mRNA expression in doxycycline inducible CMTM6 shRNA BEAS-2B cells. (48 hr doxycycline, 1 μg/mL)

Each data point is an experiment All error bars = SEM. * ≤ 0.05, ** ≤ 0.01, *** ≤0.001

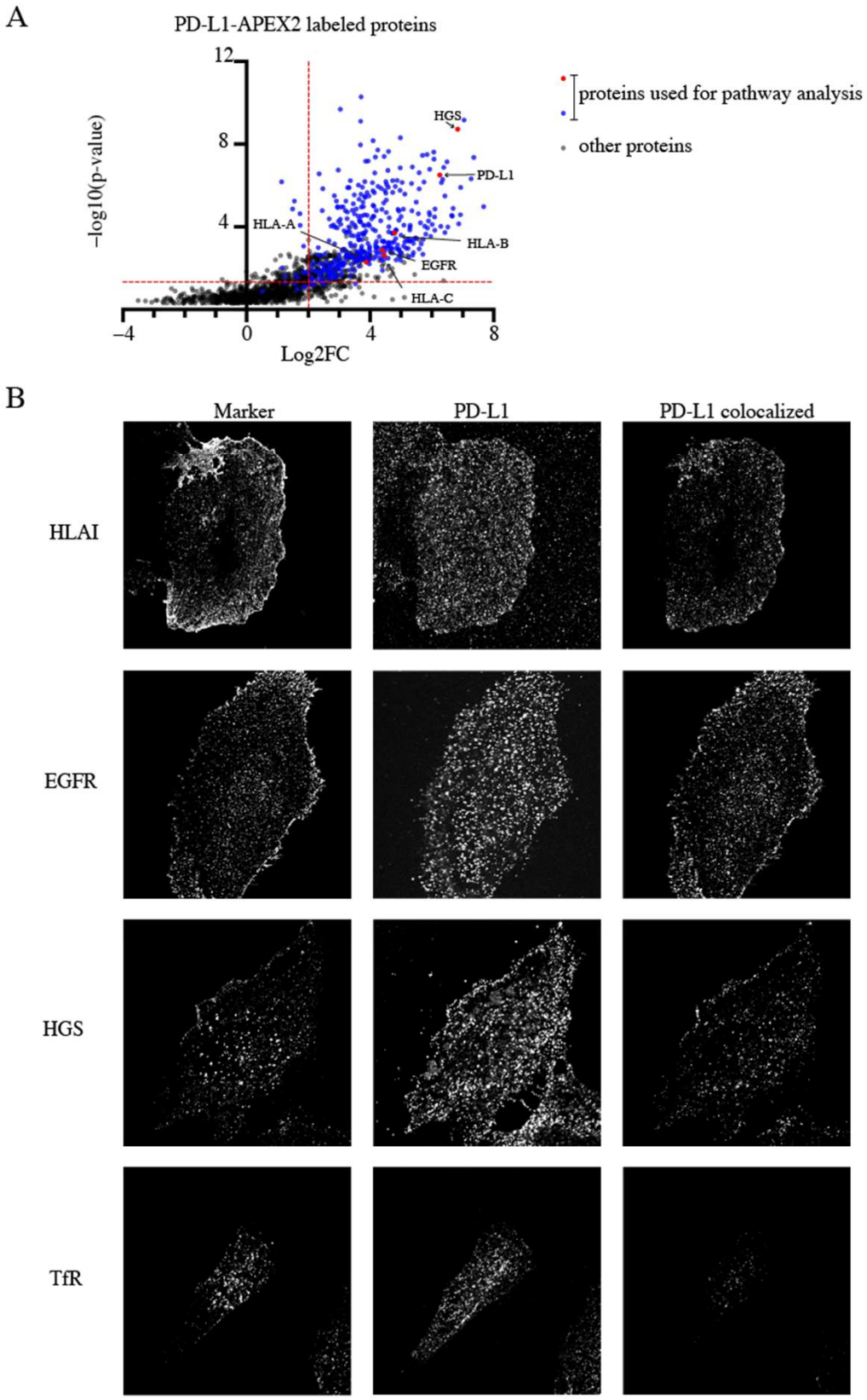

Figure Supplemental 2. PD-L1 proximal proteome

A. Volcano plot of PD-L1-APEX2 labeled proteins. FC = fold change of (labeled/−ctrl) spectral intensity. Dashed red lines represent 4-fold change on the x-axis, and p-value corresponding to FDR=0.1 after Benjamini-Hochberg correction on the y-axis respectively.

B. Representative confocal images of PD-L1 colocalization with marked proteins. PD-L1 staining intensity co-localized with marker protein staining was calculated and shown in rightmost panel. Ratio of PD-L1 intensity in colocalized image over original PD-L1 staining was used for quantifications.

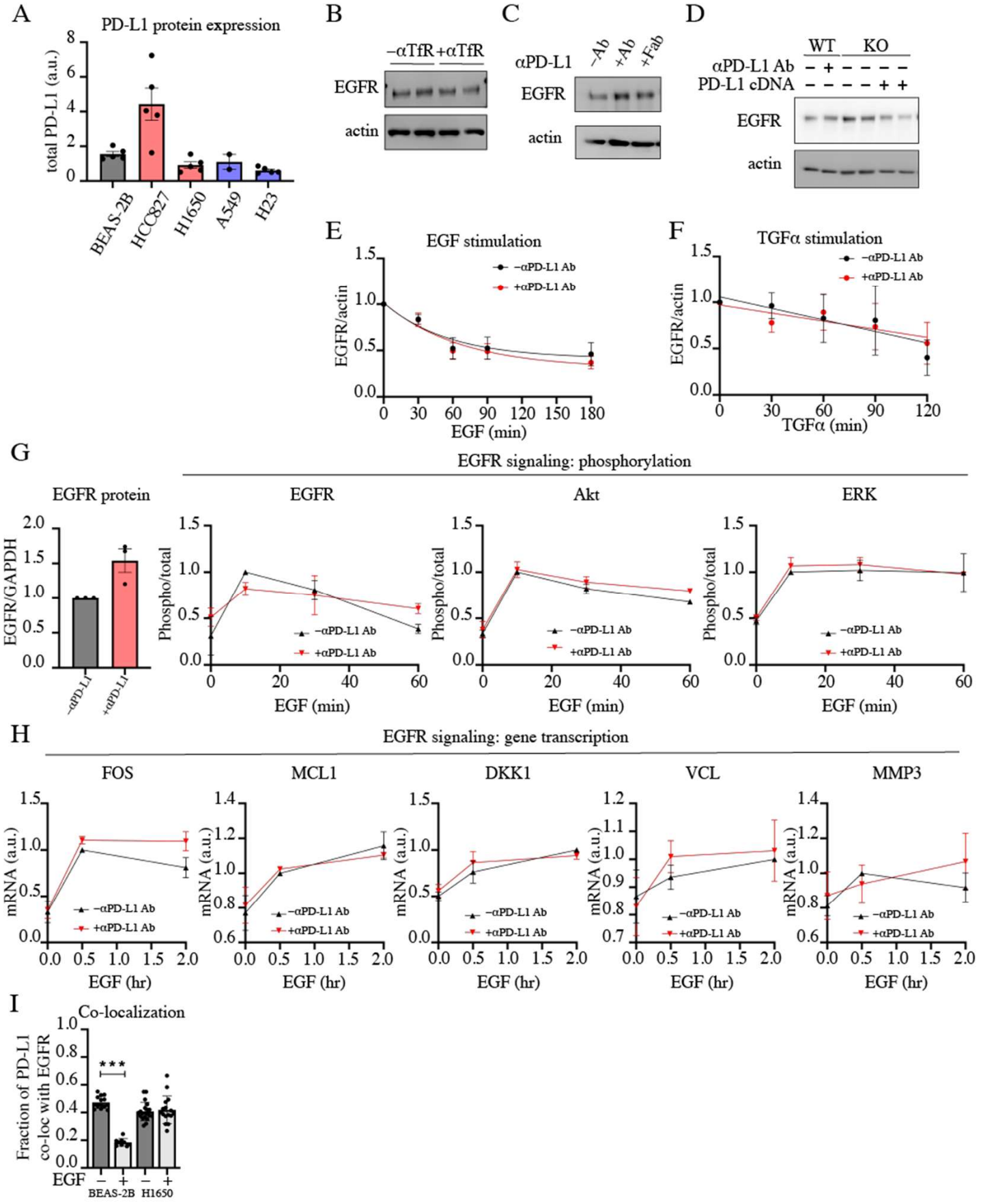

Figure Supplemental 3. αPD-L1 antibody increases mutant but not wildtype EGFR protein

Legends on next page

Figure Supplemental 3. αPD-L1 antibody increases mutant but not wildtype EGFR protein

A. PD-L1 total protein expression in cell lines. Quantification of immunofluoresncence staining is shown. Each data point is an experiment.
B. Representative immunoblot of EGFR and actin in H1650 cells treated with αTfR antibody
C. Representative immunoblot of EGFR and actin in WT, PD-L1 KO and PD-L1-reexpressing H1650 cells.
D. Representative immunoblot of EGFR and actin in H1650 cells treated with αPD-L1 antibody and αPD-L1 Fab.
E. EGF (50ng/mL) stimulated EGFR degradation in BEAS-2B cells treated with αPD-L1 antibody (10μg/mL, 7 hr). N=4. Tested for change in rate constants.
F. TGFα (50ng/mL) stimulated EGFR degradation in BEAS-2B cells treated with αPD-L1 antibody (10μg/mL, 7 hr). N=3. Tested for change in slope values.
G. EGF (0.5 ng/mL) stimulated EGFR, Akt and ERK phosphorylation in H1650 cells treated with αPD-L1 antibody (10μg/mL, 7 hr). Immunoblot quantification of EGFR protein (left) and phospho/total EGFR, Akt and ERK is shown respectively (right three panels) . N=3
H. EGF (0.5 ng/mL) stimulated gene transcription in H1650 cells treated with αPD-L1 antibody (10μg/mL,7 hr). qRT-PCR mRNA quantification of EGFR target genes is shown. N=3
I. PD-L1 colocalization with EGFR quantified by fraction of PD-L1 intensity co-localizing with EGFR via confocal microscopy. Each point is collected from single plane images of individual cells under confocal microscopy. Unpaired t-test.

All error bars = SEM. * ≤ 0.05, ** ≤ 0.01, *** ≤0.001

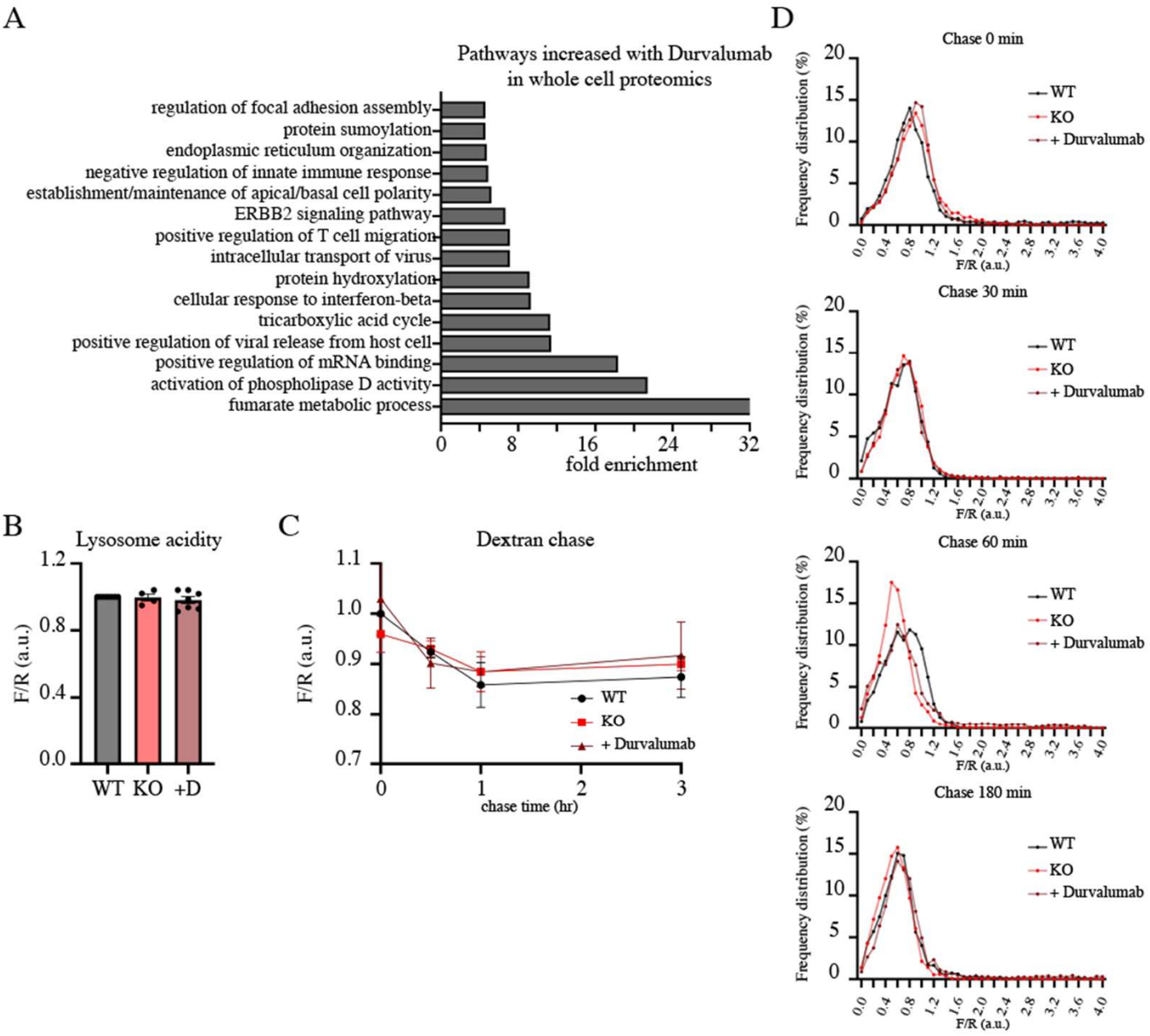

Figure Supplemental 4. Durvalumab affects whole cell proteomics and EV secretion in EGFR mutant cells

A. Biological processes representing proteins that are increased in whole cell extract of H1650 cells treated with Durvalumab (10μg/mL, 48 hr) over untreated cells.

B. Lysosomal acidity in H1650 cells with PD-L1 KO or treated with αPD-L1 antibody. Fluorescein and rhodamine labeled dextran was pulsed into cell growth media at 1mg/mL for 16 hours and chased for 0-3 hr. Cells were imaged live and fluorescein/rhodamine (F/R) ratio was calculated for regions automatically determined by rhodamine threshold. Fluorescein/rhodamine ratio in H1650 following 16 hr pulse and 3 hr chase of labeled dextran is shown. αPD-L1 antibody (10μg/mL) was added during the pulse and maintained in the chase. Each data point is an experiment. One sample t-test.

C. Lysosomal maturation as shown by average fluorescein/rhodamine ratio during 3 hr dextran chase in αPD-L1 antibody treated or PD-L1 KO H1650 cells. αPD-L1 antibody (10μg/mL) was added during the 16 hr pulse and maintained in the chase. N=3

D. Lysosomal maturation as shown by fluorescein/rhodamine frequency distribution of dextran labeled compartments during 3 hr chase. Representative experiment

All error bars = SEM. * ≤ 0.05, ** ≤ 0.01, *** ≤0.001

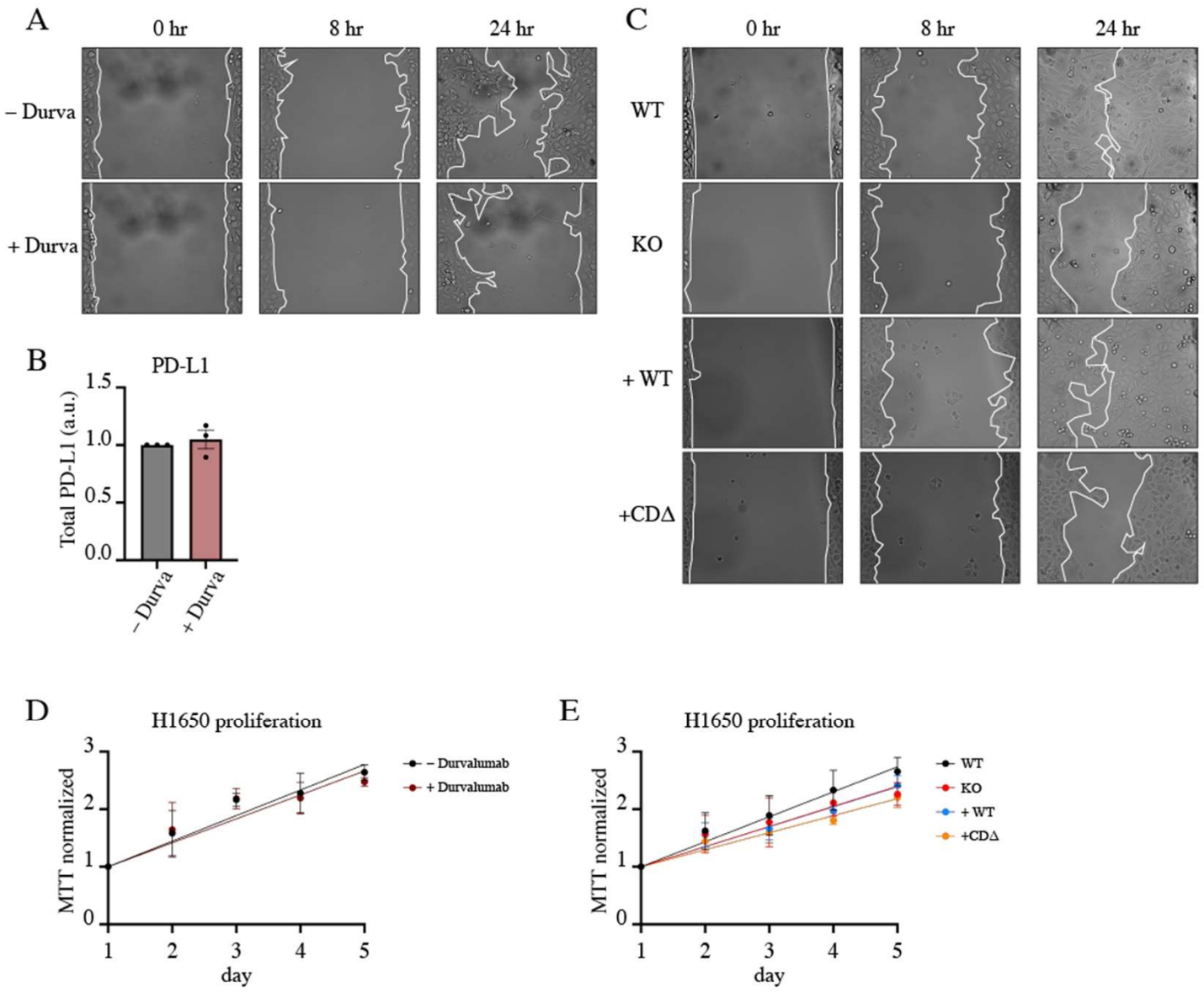

Figure Supplemental 5. PD-L1 controls cell migration in EGFR mutant cells

A. Timelapse images of scratch assay at 0, 8 and 24 hr in H1650 cells treated with Durvalumab (10μg/mL). Leading edge of the cells are marked in white. Cells were in serum-free media for the duration of the assay.
B. PD-L1 protein expression in H1650 treated with Durvalumab (10μg/mL) for 5 days. Each data point is an experiment. One sample t-test.
C. Timelapse images of scratch assay at 0, 8 and 24 hr in H1650 KO rescue cells. Leading edge of the cells are marked in white. Cells were in serum complete media for the duration of the assay.
D. Cell proliferation as measured by MTT assay in H1650 cells treated with Durvalumab (10μg/mL). N=2 Difference in slope values is calculated.
E. Cell proliferation as measured by MTT assay in H1650 KO rescue cells. N=3 Difference in slope values is calculated.

All error bars = SEM. * ≤ 0.05, ** ≤ 0.01, *** ≤0.001

Table S1. Proteins in PD-L1 proximity (overlapping list of N=5 experiments)

#	Uniprot	Gene name	Protein name
1	Q2M2I8	AAK1	AP2-associated protein kinase 1
2	P49588	AARS	Alanine--tRNA ligase, cytoplasmic
3	P33527	ABCC1	Multidrug resistance-associated protein 1
4	Q8N2K0	ABHD12	Monoacylglycerol lipase ABHD12
5	Q8IZP0	ABI1	Abl interactor 1
6	Q9NYB9	ABI2	Abl interactor 2
7	P53396	ACLY	ATP-citrate synthase
8	O60488	ACSL4	Long-chain-fatty-acid--CoA ligase 4
9	P12814	ACTN1	Alpha-actinin-1
10	O43707	ACTN4	Alpha-actinin-4
11	P61160	ACTR2	Actin-related protein 2
12	P61158	ACTR3	Actin-related protein 3
13	Q13443	ADAM9	Disintegrin and metalloproteinase domain-containing protein 9
14	P35611	ADD1	Alpha-adducin
15	Q9UEY8	ADD3	Gamma-adducin
16	P30520	ADSS	Adenylosuccinate synthetase isozyme 2
17	Q09666	AHNAK	Neuroblast differentiation-associated protein AHNAK
18	Q8IVF2	AHNAK2	Protein AHNAK2
19	Q9Y4K1	AIM1	Absent in melanoma 1 protein
20	Q96IF1	AJUBA	LIM domain-containing protein ajuba
21	Q9UKA4	AKAP11	A-kinase anchor protein 11
22	Q02952	AKAP12	A-kinase anchor protein 12
23	Q12802	AKAP13	A-kinase anchor protein 13
24	Q9Y2D5	AKAP2	A-kinase anchor protein 2
25	Q9Y2J4	AMOTL2	Angiomotin-like protein 2
26	Q8IWZ3	ANKHD1	Ankyrin repeat and KH domain-containing protein 1
27	O75179	ANKRD17	Ankyrin repeat domain-containing protein 17
28	Q9NQW6	ANLN	Actin-binding protein anillin
29	P50995	ANXA11	Annexin A11
30	P08133	ANXA6	Annexin A6
31	P20073	ANXA7	Annexin A7
32	Q8N6T3	ARFGAP1	ADP-ribosylation factor GTPase-activating protein 1
33	Q5T5U3	ARHGAP21	Rho GTPase-activating protein 21
34	Q52LW3	ARHGAP29	Rho GTPase-activating protein 29
35	O15013	ARHGEF10	Rho guanine nucleotide exchange factor 10
36	Q96PE2	ARHGEF17	Rho guanine nucleotide exchange factor 17
37	Q9ULH1	ASAP1	Arf-GAP with SH3 domain, ANK repeat and PH domain-containing protein 1
38	Q9NT62	ATG3	Ubiquitin-like-conjugating enzyme ATG3
39	P20020	ATP2B1	Plasma membrane calcium-transporting ATPase 1
40	P23634	ATP2B4	Plasma membrane calcium-transporting ATPase 4
41	Q99700	ATXN2	Ataxin-2
42	Q8WWM7	ATXN2L	Ataxin-2-like protein
43	O14965	AURKA	Aurora kinase A
44	P30530	AXL	Tyrosine-protein kinase receptor UFO
45	O95817	BAG3	BAG family molecular chaperone regulator 3
46	Q9UQB8	BAIAP2	Brain-specific angiogenesis inhibitor 1-associated protein 2
47	P80723	BASP1	Brain acid soluble protein 1

48	P56945	BCAR1	Breast cancer anti-estrogen resistance protein 1
49	P11274	BCR	Breakpoint cluster region protein
50	O60566	BUB1B	Mitotic checkpoint serine/threonine-protein kinase BUB1 beta
51	Q6ZUT6	C15orf52	Uncharacterized protein C15orf52
52	Q9HB71	CACYBP	Calcyclin-binding protein
53	P27708	CAD	CAD protein;Glutamine-dependent carbamoyl-phosphate synthase;Aspartate carbamoyltransferase;Dihydroorotase
54	Q05682	CALD1	Caldesmon
55	P40123	CAP2	Adenylyl cyclase-associated protein 2
56	P40121	CAPG	Macrophage-capping protein
57	P17655	CAPN2	Calpain-2 catalytic subunit
58	Q14444	CAPRIN1	Caprin-1
59	P47755	CAPZA2	F-actin-capping protein subunit alpha-2
60	O14936	CASK	Peripheral plasma membrane protein CASK
61	P20810	CAST	Calpastatin
62	Q03135	CAV1	Caveolin-1
63	Q9NZQ7	CD274	Programmed cell death 1 ligand 1
64	Q9Y5K6	CD2AP	CD2-associated protein
65	Q16543	CDC37	Hsp90 co-chaperone Cdc37;Hsp90 co-chaperone Cdc37, N-terminally processed
66	P60953	CDC42	Cell division control protein 42 homolog
67	Q5VT25	CDC42BPA	Serine/threonine-protein kinase MRCK alpha
68	Q9Y5S2	CDC42BPB	Serine/threonine-protein kinase MRCK beta
69	P19022	CDH2	Cadherin-2
70	Q9UKY7	CDV3	Protein CDV3 homolog
71	Q5SW79	CEP170	Centrosomal protein of 170 kDa
72	Q53EZ4	CEP55	Centrosomal protein of 55 kDa
73	Q8IW35	CEP97	Centrosomal protein of 97 kDa
74	Q9UHD1	CHORDC1	Cysteine and histidine-rich domain-containing protein 1
75	Q6FI81	CIAPIN1	Anamorsin
76	O14578	CIT	Citron Rho-interacting kinase
77	Q14008	CKAP5	Cytoskeleton-associated protein 5
78	Q7Z460	CLASP1	CLIP-associating protein 1
79	Q00610	CLTC	Clathrin heavy chain 1
80	Q99439	CNN2	Calponin-2
81	Q15417	CNN3	Calponin-3
82	A5YKK6	CNOT1	CCR4-NOT transcription complex subunit 1
83	P20908	COL5A1	Collagen alpha-1(V) chain
84	O75131	CPNE3	Copine-3
85	P46109	CRKL	Crk-like protein
86	Q6UVK1	CSPG4	Chondroitin sulfate proteoglycan 4
87	P21291	CSRP1	Cysteine and glycine-rich protein 1
88	P35221	CTNNA1	Catenin alpha-1
89	P35222	CTNNB1	Catenin beta-1
90	O60716	CTNND1	Catenin delta-1
91	Q14247	CTTN	Src substrate cortactin
92	Q7L576	CYFIP1	Cytoplasmic FMR1-interacting protein 1
93	Q16643	DBN1	Drebrin
94	Q9UJU6	DBNL	Drebrin-like protein
95	Q8N8Z6	DCBLD1	Discoidin, CUB and LCCL domain-containing protein 1

96	Q96PD2	DCBLD2	Discoidin, CUB and LCCL domain-containing protein 2
97	Q13561	DCTN2	Dynactin subunit 2
98	Q9UHI6	DDX20	Probable ATP-dependent RNA helicase DDX20
99	Q5VZ89	DENND4C	DENN domain-containing protein 4C
100	O60610	DIAPH1	Protein diaphanous homolog 1
101	Q12959	DLG1	Disks large homolog 1
102	Q99615	DNAJC7	DnaJ homolog subfamily C member 7
103	Q6XZF7	DNMBP	Dynamin-binding protein
104	Q96BY6	DOCK10	Dedicator of cytokinesis protein 10
105	Q96N67	DOCK7	Dedicator of cytokinesis protein 7
106	Q14126	DSG2	Desmoglein-2
107	Q03001	DST	Dystonin
108	P33316	DUT	Deoxyuridine 5'-triphosphate nucleotidohydrolase, mitochondrial
109	O75923	DYSF	Dysferlin
110	Q6P2E9	EDC4	Enhancer of mRNA-decapping protein 4
111	P00533	EGFR	Epidermal growth factor receptor
112	Q14152	EIF3A	Eukaryotic translation initiation factor 3 subunit A
113	Q13347	EIF3I	Eukaryotic translation initiation factor 3 subunit I
114	P23588	EIF4B	Eukaryotic translation initiation factor 4B
115	Q04637	EIF4G1	Eukaryotic translation initiation factor 4 gamma 1
116	Q9HC35	EML4	Echinoderm microtubule-associated protein-like 4
117	O43491	EPB41L2	Band 4.1-like protein 2
118	P29323	EPHB2	Ephrin type-B receptor 2
119	P07814	EPRS	Bifunctional glutamate/proline--tRNA ligase;Glutamate--tRNA ligase;Proline--tRNA ligase
120	Q9UBC2	EPS15L1	Epidermal growth factor receptor substrate 15-like 1
121	Q12929	EPS8	Epidermal growth factor receptor kinase substrate 8
122	Q9H6S3	EPS8L2	Epidermal growth factor receptor kinase substrate 8-like protein 2
123	P04626	ERBB2	Receptor tyrosine-protein kinase erbB-2
124	Q96RT1	ERBB2IP	Protein LAP2
125	Q2NKX8	ERCC6L	DNA excision repair protein ERCC-6-like
126	Q9BSJ8	ESYT1	Extended synaptotagmin-1
127	P15311	EZR	Ezrin
128	Q9BZQ8	FAM129A	Protein Niban
129	Q96TA1	FAM129B	Niban-like protein 1
130	Q6ZS17	FAM65A	Protein FAM65A
131	Q9H4H8	FAM83D	Protein FAM83D
132	O94887	FARP2	FERM, RhoGEF and pleckstrin domain-containing protein 2
133	Q9Y285	FARSA	Phenylalanine--tRNA ligase alpha subunit
134	P49327	FASN	Fatty acid synthase;[Acyl-carrier-protein] S-acetyltransferase;[Acyl-carrier-protein] S-malonyltransferase;3-oxoacyl-[acyl-carrier-protein] synthase;3-oxoacyl-[acyl-carrier-protein] reductase;3-hydroxyacyl-[acyl-carrier-protein] dehydratase;Enoyl-[acyl-carrier-protein] reductase;Oleoyl-[acyl-carrier-protein] hydrolase
135	Q8WUP2	FBLIM1	Filamin-binding LIM protein 1
136	Q96AC1	FERMT2	Fermitin family homolog 2
137	Q4L180	FILIP1L	Filamin A-interacting protein 1-like
138	Q5T1M5	FKBP15	FK506-binding protein 15
139	P21333	FLNA	Filamin-A
140	O75369	FLNB	Filamin-B

141	Q14315	FLNC	Filamin-C
142	O75955	FLOT1	Flotillin-1
143	Q9P2Q2	FRMD4A	FERM domain-containing protein 4A
144	O94915	FRYL	Protein furry homolog-like
145	P11413	G6PD	Glucose-6-phosphate 1-dehydrogenase
146	O14976	GAK	Cyclin-G-associated kinase
147	Q14C86	GAPVD1	GTPase-activating protein and VPS9 domain-containing protein 1
148	P22102	GART	Trifunctional purine biosynthetic protein adenosine-3;Phosphoribosylamine--glycine ligase;Phosphoribosylformylglycinamidine cyclo-ligase;Phosphoribosylglycinamide formyltransferase
149	Q04446	GBE1	1,4-alpha-glucan-branching enzyme
150	Q92538	GBF1	Golgi-specific brefeldin A-resistance guanine nucleotide exchange factor 1
151	Q8TEQ6	GEMIN5	Gem-associated protein 5
152	Q6Y7W6	GIGYF2	PERQ amino acid-rich with GYF domain-containing protein 2
153	O76003	GLRX3	Glutaredoxin-3
154	P29992	GNA11	Guanine nucleotide-binding protein subunit alpha-11
155	P04899	GNAI2	Guanine nucleotide-binding protein G(i) subunit alpha-2
156	P08754	GNAI3	Guanine nucleotide-binding protein G(k) subunit alpha
157	P50148	GNAQ	Guanine nucleotide-binding protein G(q) subunit alpha
158	Q7Z2K8	GPRIN1	G protein-regulated inducer of neurite outgrowth 1
159	P15170	GSPT1	Eukaryotic peptide chain release factor GTP-binding subunit ERF3A
160	P12081	HARS	Histidine--tRNA ligase, cytoplasmic
161	P51610	HCFC1	Host cell factor 1;HCF N-terminal chain 1;HCF N-terminal chain 2;HCF N-terminal chain 3;HCF N-terminal chain 4;HCF N-terminal chain 5;HCF N-terminal chain 6;HCF C-terminal chain 1;HCF C-terminal chain 2;HCF C-terminal chain 3;HCF C-terminal chain 4;HCF C-terminal chain 5;HCF C-terminal chain 6
162	Q9H583	HEATR1	HEAT repeat-containing protein 1;HEAT repeat-containing protein 1, N-terminally processed
163	Q9ULT8	HECTD1	E3 ubiquitin-protein ligase HECTD1
164	O14964	HGS	Hepatocyte growth factor-regulated tyrosine kinase substrate
165	P30443	HLA-A	HLA class I histocompatibility antigen, A-1 alpha chain
166	P01892	HLA-A	HLA class I histocompatibility antigen, A-2 alpha chain
167	P04439	HLA-A	HLA class I histocompatibility antigen, A-3 alpha chain
168	P10319	HLA-B	HLA class I histocompatibility antigen, B-58 alpha chain
169	P18465	HLA-B	HLA class I histocompatibility antigen, B-57 alpha chain
170	P30479	HLA-B	HLA class I histocompatibility antigen, B-41 alpha chain
171	P30483	HLA-B	HLA class I histocompatibility antigen, B-45 alpha chain
172	P10321	HLA-C	HLA class I histocompatibility antigen, Cw-7 alpha chain
173	Q29963	HLA-C	HLA class I histocompatibility antigen, Cw-6 alpha chain
174	P30508	HLA-C	HLA class I histocompatibility antigen, Cw-12 alpha chain
175	P30519	HMOX2	Heme oxygenase 2
176	Q9H910	HN1L	Hematological and neurological expressed 1-like protein
177	Q7Z6Z7	HUWE1	E3 ubiquitin-protein ligase HUWE1
178	P41252	IARS	Isoleucine--tRNA ligase, cytoplasmic
179	P12268	IMPDH2	Inosine-5'-monophosphate dehydrogenase 2
180	Q27J81	INF2	Inverted formin-2
181	O15357	INPPL1	Phosphatidylinositol 3,4,5-trisphosphate 5-phosphatase 2
182	P53990	IST1	IST1 homolog
183	P26006	ITGA3	Integrin alpha-3;Integrin alpha-3 heavy chain;Integrin alpha-3 light chain

184	P23229	ITGA6	Integrin alpha-6;Integrin alpha-6 heavy chain;Integrin alpha-6 light chain;Processed integrin alpha-6
185	P05556	ITGB1	Integrin beta-1
186	P16144	ITGB4	Integrin beta-4
187	Q14573	ITPR3	Inositol 1,4,5-trisphosphate receptor type 3
188	P23458	JAK1	Tyrosine-protein kinase JAK1
189	Q63ZY3	KANK2	KN motif and ankyrin repeat domain-containing protein 2
190	Q14145	KEAP1	Kelch-like ECH-associated protein 1
191	Q8TCG1	KIAA1524	Protein CIP2A
192	Q9ULH0	KIDINS220	Kinase D-interacting substrate of 220 kDa
193	P52732	KIF11	Kinesin-like protein KIF11
194	Q9H1H9	KIF13A	Kinesin-like protein KIF13A
195	Q15058	KIF14	Kinesin-like protein KIF14
196	O60333	KIF1B	Kinesin-like protein KIF1B
197	O95235	KIF20A	Kinesin-like protein KIF20A
198	O00139	KIF2A	Kinesin-like protein KIF2A
199	Q99661	KIF2C	Kinesin-like protein KIF2C
200	O95239	KIF4A	Chromosome-associated kinesin KIF4A
201	P33176	KIF5B	Kinesin-1 heavy chain
202	Q07866	KLC1	Kinesin light chain 1
203	Q9H0B6	KLC2	Kinesin light chain 2
204	O60684	KPNA6	Importin subunit alpha-7
205	Q14974	KPNB1	Importin subunit beta-1
206	Q9NS86	LANCL2	LanC-like protein 2
207	Q14847	LASP1	LIM and SH3 domain protein 1
208	P17931	LGALS3	Galectin-3
209	Q9UHB6	LIMA1	LIM domain and actin-binding protein 1
210	Q9UPQ0	LIMCH1	LIM and calponin homology domains-containing protein 1
211	Q9UGP4	LIMD1	LIM domain-containing protein 1
212	P20700	LMNB1	Lamin-B1
213	Q8WWI1	LMO7	LIM domain only protein 7
214	Q93052	LPP	Lipoma-preferred partner
215	Q32MZ4	LRRFIP1	Leucine-rich repeat flightless-interacting protein 1
216	Q86V48	LUZP1	Leucine zipper protein 1
217	Q9UPN3	MACF1	Microtubule-actin cross-linking factor 1, isoforms 1/2/3/5
218	P46821	MAP1B	Microtubule-associated protein 1B;MAP1B heavy chain;MAP1 light chain LC1
219	P27816	MAP4	Microtubule-associated protein 4
220	Q15691	MAPRE1	Microtubule-associated protein RP/EB family member 1
221	P43121	MCAM	Cell surface glycoprotein MUC18
222	P53582	METAP1	Methionine aminopeptidase 1
223	O60502	MGEA5	Protein O-GlcNAcase
224	P55196	MLLT4	Afadin
225	O75970	MPDZ	Multiple PDZ domain protein
226	P26038	MSN	Moesin
227	Q9Y4B5	MTCL1	Microtubule cross-linking factor 1
228	P35580	MYH10	Myosin-10
229	Q15746	MYLK	Myosin light chain kinase, smooth muscle;Myosin light chain kinase, smooth muscle, deglutamylated form
230	Q92614	MYO18A	Unconventional myosin-XVIIIa
231	Q9Y4I1	MYO5A	Unconventional myosin-Va

232	Q9UM54	MYO6	Unconventional myosin-VI
233	Q9NZM1	MYOF	Myoferlin
234	P43490	NAMPT	Nicotinamide phosphoribosyltransferase
235	Q6PIU2	NCEH1	Neutral cholesterol ester hydrolase 1
236	Q9Y2A7	NCKAP1	Nck-associated protein 1
237	O14777	NDC80	Kinetochore protein NDC80 homolog
238	Q9UGV2	NDRG3	Protein NDRG3
239	Q8NHV4	NEDD1	Protein NEDD1
240	Q8TD19	NEK9	Serine/threonine-protein kinase Nek9
241	Q00653	NFKB2	Nuclear factor NF-kappa-B p100 subunit;Nuclear factor NF-kappa-B p52 subunit
242	P30419	NMT1	Glycylpeptide N-tetradecanoyltransferase 1
243	Q04721	NOTCH2	Neurogenic locus notch homolog protein 2;Notch 2 extracellular truncation;Notch 2 intracellular domain
244	O14786	NRP1	Neuropilin-1
245	Q9UNZ2	NSFL1C	NSFL1 cofactor p47
246	Q9Y5Y2	NUBP2	Cytosolic Fe-S cluster assembly factor NUBP2
247	Q9BZD4	NUF2	Kinetochore protein Nuf2
248	P49790	NUP153	Nuclear pore complex protein Nup153
249	P22059	OSBP	Oxysterol-binding protein 1
250	Q96SU4	OSBPL9	Oxysterol-binding protein-related protein 9
251	Q96FW1	OTUB1	Ubiquitin thioesterase OTUB1
252	P07237	P4HB	Protein disulfide-isomerase
253	Q9UNF0	PACSIN2	Protein kinase C and casein kinase substrate in neurons protein 2
254	P22234	PAICS	Multifunctional protein ADE2;Phosphoribosylaminoimidazole-succinocarboxamide synthase;Phosphoribosylaminoimidazole carboxylase
255	Q13177	PAK2	Serine/threonine-protein kinase PAK 2;PAK-2p27;PAK-2p34
256	Q8WX93	PALLD	Palladin
257	Q8TEW0	PARD3	Partitioning defective 3 homolog
258	Q9UKK3	PARP4	Poly [ADP-ribose] polymerase 4
259	Q96IZ0	PAWR	PRKC apoptosis WT1 regulator protein
260	P22061	PCMT1	Protein-L-isoaspartate(D-aspartate) O-methyltransferase
261	O75340	PDCD6	Programmed cell death protein 6
262	Q8WUM4	PDCD6IP	Programmed cell death 6-interacting protein
263	O00151	PDLIM1	PDZ and LIM domain protein 1
264	P50479	PDLIM4	PDZ and LIM domain protein 4
265	Q96HC4	PDLIM5	PDZ and LIM domain protein 5
266	Q9UBV8	PEF1	Peflin
267	O15173	PGRMC2	Membrane-associated progesterone receptor component 2
268	Q86UU1	PHLDB1	Pleckstrin homology-like domain family B member 1
269	P42356	PI4KA	Phosphatidylinositol 4-kinase alpha
270	Q99959	PKP2	Plakophilin-2
271	Q99569	PKP4	Plakophilin-4
272	P19174	PLCG1	1-phosphatidylinositol 4,5-bisphosphate phosphodiesterase gamma-1
273	O60664	PLIN3	Perilipin-3
274	P13797	PLS3	Plastin-3
275	O15031	PLXNB2	Plexin-B2
276	P29590	PML	Protein PML
277	O14974	PPP1R12A	Protein phosphatase 1 regulatory subunit 12A
278	Q6NYC8	PPP1R18	Phostensin

279	P30153	PPP2R1A	Serine/threonine-protein phosphatase 2A 65 kDa regulatory subunit A alpha isoform
280	Q8TF05	PPP4R1	Serine/threonine-protein phosphatase 4 regulatory subunit 1
281	O75170	PPP6R2	Serine/threonine-protein phosphatase 6 regulatory subunit 2
282	P10644	PRKAR1A	cAMP-dependent protein kinase type I-alpha regulatory subunit;cAMP-dependent protein kinase type I-alpha regulatory subunit, N-terminally processed
283	P17252	PRKCA	Protein kinase C alpha type
284	Q9Y520	PRRC2C	Protein PRRC2C
285	P60900	PSMA6	Proteasome subunit alpha type-6
286	P62195	PSMC5	26S protease regulatory subunit 8
287	O00231	PSMD11	26S proteasome non-ATPase regulatory subunit 11
288	O00232	PSMD12	26S proteasome non-ATPase regulatory subunit 12
289	Q13200	PSMD2	26S proteasome non-ATPase regulatory subunit 2
290	Q13308	PTK7	Inactive tyrosine-protein kinase 7
291	Q06124	PTPN11	Tyrosine-protein phosphatase non-receptor type 11
292	Q05209	PTPN12	Tyrosine-protein phosphatase non-receptor type 12
293	Q15678	PTPN14	Tyrosine-protein phosphatase non-receptor type 14
294	P18433	PTPRA	Receptor-type tyrosine-protein phosphatase alpha
295	P10586	PTPRF	Receptor-type tyrosine-protein phosphatase F
296	Q15262	PTPRK	Receptor-type tyrosine-protein phosphatase kappa
297	Q6NZI2	PTRF	Polymerase I and transcript release factor
298	Q92692	PVRL2	Nectin-2
299	P49023	PXN	Paxillin
300	P61106	RAB14	Ras-related protein Rab-14
301	P61020	RAB5B	Ras-related protein Rab-5B
302	P51149	RAB7A	Ras-related protein Rab-7a
303	Q9Y3P9	RABGAP1	Rab GTPase-activating protein 1
304	P63000	RAC1	Ras-related C3 botulinum toxin substrate 1
305	P15153	RAC2	Ras-related C3 botulinum toxin substrate 2
306	P11234	RALB	Ras-related protein Ral-B
307	P49792	RANBP2	E3 SUMO-protein ligase RanBP2
308	P46060	RANGAP1	Ran GTPase-activating protein 1
309	Q70E73	RAPH1	Ras-associated and pleckstrin homology domains-containing protein 1
310	Q04206	RELA	Transcription factor p65
311	Q14699	RFTN1	Raftlin
312	P61586	RHOA	Transforming protein RhoA
313	Q13546	RIPK1	Receptor-interacting serine/threonine-protein kinase 1
314	Q13464	ROCK1	Rho-associated protein kinase 1
315	O75116	ROCK2	Rho-associated protein kinase 2
316	P27694	RPA1	Replication protein A 70 kDa DNA-binding subunit;Replication protein A 70 kDa DNA-binding subunit, N-terminally processed
317	P10301	RRAS	Ras-related protein R-Ras
318	P62070	RRAS2	Ras-related protein R-Ras2
319	P23921	RRM1	Ribonucleoside-diphosphate reductase large subunit
320	Q9Y3I0	RTCB	tRNA-splicing ligase RtcB homolog
321	Q9NQC3	RTN4	Reticulon-4
322	O95248	SBF1	Myotubularin-related protein 5
323	Q14160	SCRIB	Protein scribble homolog
324	O15027	SEC16A	Protein transport protein Sec16A

325	Q9Y6Y8	SEC23IP	SEC23-interacting protein
326	P53992	SEC24C	Protein transport protein Sec24C
327	P31947	SFN	14-3-3 protein sigma
328	Q86YV5	SGK223	Tyrosine-protein kinase SgK223
329	Q9P0V3	SH3BP4	SH3 domain-binding protein 4
330	Q6UWI4	SHISA2	Protein shisa-2 homolog
331	P78324	SIRPA	Tyrosine-protein phosphatase non-receptor type substrate 1
332	Q8IX90	SKA3	Spindle and kinetochore-associated protein 3
333	Q9P270	SLAIN2	SLAIN motif-containing protein 2
334	Q15796	SMAD2	Mothers against decapentaplegic homolog 2
335	O00161	SNAP23	Synaptosomal-associated protein 23
336	O95721	SNAP29	Synaptosomal-associated protein 29
337	Q13425	SNTB2	Beta-2-syntrophin
338	Q9Y5X1	SNX9	Sorting nexin-9
339	O94964	SOGA1	Protein SOGA1;N-terminal form;C-terminal 80 kDa form
340	O60271	SPAG9	C-Jun-amino-terminal kinase-interacting protein 4
341	Q5M775	SPECC1	Cytospin-B
342	Q69YQ0	SPECC1L	Cytospin-A
343	Q8N0X7	SPG20	Spartin
344	Q13813	SPTAN1	Spectrin alpha chain, non-erythrocytic 1
345	Q01082	SPTBN1	Spectrin beta chain, non-erythrocytic 1
346	Q13501	SQSTM1	Sequestosome-1
347	O75044	SRGAP2	SLIT-ROBO Rho GTPase-activating protein 2
348	O60232	SSSCA1	Sjoegren syndrome/scleroderma autoantigen 1
349	Q92783	STAM	Signal transducing adapter molecule 1
350	P40763	STAT3	Signal transducer and activator of transcription 3
351	P31948	STIP1	Stress-induced-phosphoprotein 1
352	O94804	STK10	Serine/threonine-protein kinase 10
353	O94901	SUN1	SUN domain-containing protein 1
354	O95425	SVIL	Supervillin
355	Q8WXH0	SYNE2	Nesprin-2
356	O15056	SYNJ2	Synaptojanin-2
357	Q9NYJ8	TAB2	TGF-beta-activated kinase 1 and MAP3K7-binding protein 2
358	O75410	TACC1	Transforming acidic coiled-coil-containing protein 1
359	Q9Y6A5	TACC3	Transforming acidic coiled-coil-containing protein 3
360	Q01995	TAGLN	Transgelin
361	Q9HCD6	TANC2	Protein TANC2
362	Q8TC07	TBC1D15	TBC1 domain family member 15
363	Q9BYX2	TBC1D2	TBC1 domain family member 2A
364	Q99426	TBCB	Tubulin-folding cofactor B
365	Q9UGI8	TES	Testin
366	Q9UDY2	TJP2	Tight junction protein ZO-2
367	P04183	TK1	Thymidine kinase, cytosolic
368	Q9Y4G6	TLN2	Talin-2
369	Q9NYL9	TMOD3	Tropomodulin-3
370	Q9C0C2	TNKS1BP1	182 kDa tankyrase-1-binding protein
371	Q92973	TNPO1	Transportin-1
372	Q9HBL0	TNS1	Tensin-1
373	Q68CZ2	TNS3	Tensin-3
374	Q12888	TP53BP1	Tumor suppressor p53-binding protein 1

375	Q13625	TP53BP2	Apoptosis-stimulating of p53 protein 2
376	P06753	TPM3	Tropomyosin alpha-3 chain
377	P13693	TPT1	Translationally-controlled tumor protein
378	Q12933	TRAF2	TNF receptor-associated factor 2
379	O75962	TRIO	Triple functional domain protein
380	Q15654	TRIP6	Thyroid receptor-interacting protein 6
381	Q99816	TSG101	Tumor susceptibility gene 101 protein
382	Q99614	TTC1	Tetratricopeptide repeat protein 1
383	P33981	TTK	Dual specificity protein kinase TTK
384	Q9BSJ2	TUBGCP2	Gamma-tubulin complex component 2
385	Q96CW5	TUBGCP3	Gamma-tubulin complex component 3
386	Q5T6F2	UBAP2	Ubiquitin-associated protein 2
387	Q14157	UBAP2L	Ubiquitin-associated protein 2-like
388	Q9C0C9	UBE2O	E2/E3 hybrid ubiquitin-protein ligase UBE2O
389	Q16851	UGP2	UTP--glucose-1-phosphate uridylyltransferase
390	P54578	USP14	Ubiquitin carboxyl-terminal hydrolase 14
391	Q9UPU5	USP24	Ubiquitin carboxyl-terminal hydrolase 24
392	P45974	USP5	Ubiquitin carboxyl-terminal hydrolase 5
393	P46939	UTRN	Utrophin
394	Q6EMK4	VASN	Vasorin
395	P50552	VASP	Vasodilator-stimulated phosphoprotein
396	P18206	VCL	Vinculin
397	Q96QK1	VPS35	Vacuolar protein sorting-associated protein 35
398	O75351	VPS4B	Vacuolar protein sorting-associated protein 4B
399	Q9Y6W5	WASF2	Wiskott-Aldrich syndrome protein family member 2
400	O75083	WDR1	WD repeat-containing protein 1
401	Q9H4A3	WNK1	Serine/threonine-protein kinase WNK1
402	P31946	YWHAB	14-3-3 protein beta/alpha;14-3-3 protein beta/alpha, N-terminally processed
403	P61981	YWHAG	14-3-3 protein gamma;14-3-3 protein gamma, N-terminally processed
404	Q9C0B5	ZDHHC5	Palmitoyltransferase ZDHHC5
405	O15231	ZNF185	Zinc finger protein 185
406	Q15942	ZYX	Zyxin

Table S2. Proteins identified in PD-L1 proximity map involved in EGFR biology

#	Uniprot	Gene name	Protein name
1	P00533	EGFR	Epidermal growth factor receptor
2	P04626	ERBB2	Receptor tyrosine-protein kinase erbB-2
3	P19174	PLCG1	1-phosphatidylinositol 4,5-bisphosphate phosphodiesterase gamma-1
4	P27708	CAD	CAD protein;Glutamine-dependent carbamoyl-phosphate synthase;Aspartate carbamoyltransferase;Dihydroorotase
5	Q05209	PTPN12	Tyrosine-protein phosphatase non-receptor type 12
6	Q06124	PTPN11	Tyrosine-protein phosphatase non-receptor type 11
7	Q9UQB8	BAIAP2	Brain-specific angiogenesis inhibitor 1-associated protein 2
8	O14964	HGS	Hepatocyte growth factor-regulated tyrosine kinase substrate
9	O75351	VPS4B	Vacuolar protein sorting-associated protein 4B
10	P53990	IST1	IST1 homolog
11	Q8WUM4	PDCD6IP	Programmed cell death 6-interacting protein
12	Q92783	STAM	Signal transducing adapter molecule 1
13	Q99816	TSG101	Tumor susceptibility gene 101 protein

Table S3. Proteins increased in H1650 with Durvalumab treatment

#	Fasta headers	Gene names
1	sp|P49588|SYAC_HUMAN Alanine--tRNA ligase, cytoplasmic OS=Homo sapiens (Human) OX=9606 GN=AARS1 PE=1 SV=2	AARS
2	sp|Q12979|ABR_HUMAN Active breakpoint cluster region-related protein OS=Homo sapiens (Human) OX=9606 GN=ABR PE=1 SV=2	ABR
3	sp|Q9H845|ACAD9_HUMAN Complex I assembly factor ACAD9, mitochondrial OS=Homo sapiens (Human) OX=9606 GN=ACAD9 PE=1 SV=1	ACAD9
4	sp|Q99798|ACON_HUMAN Aconitate hydratase, mitochondrial OS=Homo sapiens (Human) OX=9606 GN=ACO2 PE=1 SV=2	ACO2
5	sp|Q9NPJ3|ACO13_HUMAN Acyl-coenzyme A thioesterase 13 OS=Homo sapiens (Human) OX=9606 GN=ACOT13 PE=1 SV=1	ACOT13
6	sp|Q9Y305|ACOT9_HUMAN Acyl-coenzyme A thioesterase 9, mitochondrial OS=Homo sapiens (Human) OX=9606 GN=ACOT9 PE=1 SV=2	ACOT9
7	sp|O15254|ACOX3_HUMAN Peroxisomal acyl-coenzyme A oxidase 3 OS=Homo sapiens (Human) OX=9606 GN=ACOX3 PE=1 SV=2	ACOX3
8	sp|Q03154|ACY1_HUMAN Aminoacylase-1 OS=Homo sapiens (Human) OX=9606 GN=ACY1 PE=1 SV=1	ACY1
9	sp|O14672|ADA10_HUMAN Disintegrin and metalloproteinase domain-containing protein 10 OS=Homo sapiens (Human) OX=9606 GN=ADAM10 PE=1 SV=1	ADAM10
10	sp|P55263|ADK_HUMAN Adenosine kinase OS=Homo sapiens (Human) OX=9606 GN=ADK PE=1 SV=2	ADK
11	sp|Q9H2P0|ADNP_HUMAN Activity-dependent neuroprotector homeobox protein OS=Homo sapiens (Human) OX=9606 GN=ADNP PE=1 SV=1	ADNP
12	sp|Q16186|ADRM1_HUMAN Proteasomal ubiquitin receptor ADRM1 OS=Homo sapiens (Human) OX=9606 GN=ADRM1 PE=1 SV=2	ADRM1
13	sp|Q53H12|AGK_HUMAN Acylglycerol kinase, mitochondrial OS=Homo sapiens (Human) OX=9606 GN=AGK PE=1 SV=2	AGK
14	sp|Q8IVF2|AHNK2_HUMAN Protein AHNAK2 OS=Homo sapiens (Human) OX=9606 GN=AHNAK2 PE=1 SV=2	AHNAK2
15	sp|O95433|AHSA1_HUMAN Activator of 90 kDa heat shock protein ATPase homolog 1 OS=Homo sapiens (Human) OX=9606 GN=AHSA1 PE=1 SV=1	AHSA1
16	sp|Q12904|AIMP1_HUMAN Aminoacyl tRNA synthase complex-interacting multifunctional protein 1 OS=Homo sapiens (Human) OX=9606 GN=AIMP1 PE=1 SV=2	AIMP1
17	sp|Q13155|AIMP2_HUMAN Aminoacyl tRNA synthase complex-interacting multifunctional protein 2 OS=Homo sapiens (Human) OX=9606 GN=AIMP2 PE=1 SV=2	AIMP2
18	sp|Q02952|AKA12_HUMAN A-kinase anchor protein 12 OS=Homo sapiens (Human) OX=9606 GN=AKAP12 PE=1 SV=4	AKAP12
19	sp|P15121|ALDR_HUMAN Aldo-keto reductase family 1 member B1 OS=Homo sapiens (Human) OX=9606 GN=AKR1B1 PE=1 SV=3	AKR1B1
20	sp|P00352|AL1A1_HUMAN Retinal dehydrogenase 1 OS=Homo sapiens (Human) OX=9606 GN=ALDH1A1 PE=1 SV=2	ALDH1A1
21	sp|Q9P2R3|ANFY1_HUMAN Rabankyrin-5 OS=Homo sapiens (Human) OX=9606 GN=ANKFY1 PE=1 SV=2	ANKFY1
22	sp|Q8IWZ3|ANKH1_HUMAN Ankyrin repeat and KH domain-containing protein 1 OS=Homo sapiens (Human) OX=9606 GN=ANKHD1 PE=1 SV=1	ANKHD1
23	sp|O75179|ANR17_HUMAN Ankyrin repeat domain-containing protein 17 OS=Homo sapiens (Human) OX=9606 GN=ANKRD17 PE=1 SV=3	ANKRD17
24	sp|P15144|AMPN_HUMAN Aminopeptidase N OS=Homo sapiens (Human) OX=9606 GN=ANPEP PE=1 SV=4	ANPEP
25	sp|Q9BXS5|AP1M1_HUMAN AP-1 complex subunit mu-1 OS=Homo sapiens (Human) OX=9606 GN=AP1M1 PE=1 SV=3	AP1M1
26	sp|Q9HDC9|APMAP_HUMAN Adipocyte plasma membrane-associated protein OS=Homo sapiens (Human) OX=9606 GN=APMAP PE=1 SV=2	APMAP
27	sp|P05067|A4_HUMAN Amyloid-beta precursor protein OS=Homo sapiens (Human) OX=9606 GN=APP PE=1 SV=3	APP
28	sp|P18085|ARF4_HUMAN ADP-ribosylation factor 4 OS=Homo sapiens (Human) OX=9606 GN=ARF4 PE=1 SV=3	ARF4
29	sp|Q9Y6D6|BIG1_HUMAN Brefeldin A-inhibited guanine nucleotide-exchange protein 1 OS=Homo sapiens (Human) OX=9606 GN=ARFGEF1 PE=1 SV=2	ARFGEF1
30	sp|P40616|ARL1_HUMAN ADP-ribosylation factor-like protein 1 OS=Homo sapiens (Human) OX=9606 GN=ARL1 PE=1 SV=1	ARL1
31	sp|O15144|ARPC2_HUMAN Actin-related protein 2/3 complex subunit 2 OS=Homo sapiens (Human) OX=9606 GN=ARPC2 PE=1 SV=1	ARPC2
32	sp|P56211|ARP19_HUMAN cAMP-regulated phosphoprotein 19 OS=Homo sapiens (Human) OX=9606 GN=ARPP19 PE=1 SV=2	ARPP19
33	sp|P04424|ARLY_HUMAN Argininosuccinate lyase OS=Homo sapiens (Human) OX=9606 GN=ASL PE=1 SV=4	ASL
34	sp|Q12797|ASPH_HUMAN Aspartyl/asparaginyl beta-hydroxylase OS=Homo sapiens (Human) OX=9606 GN=ASPH PE=1 SV=3	ASPH
35	sp|Q9NT62|ATG3_HUMAN Ubiquitin-like-conjugating enzyme ATG3 OS=Homo sapiens (Human) OX=9606 GN=ATG3 PE=1 SV=1	ATG3
36	sp|P31939|PUR9_HUMAN Bifunctional purine biosynthesis protein ATIC OS=Homo sapiens (Human) OX=9606 GN=ATIC PE=1 SV=3	ATIC
37	sp|P05026|AT1B1_HUMAN Sodium/potassium-transporting ATPase subunit beta-1 OS=Homo sapiens (Human) OX=9606 GN=ATP1B1 PE=1 SV=1	ATP1B1
38	sp|P36542|ATPG_HUMAN ATP synthase subunit gamma, mitochondrial OS=Homo sapiens (Human) OX=9606 GN=ATP5F1C PE=1 SV=1	ATP5C1

39	sp|P61421|VA0D1_HUMAN V-type proton ATPase subunit d 1 OS=Homo sapiens (Human) OX=9606 GN=ATP6V0D1 PE=1 SV=1	ATP6V0D1
40	sp|Q96GX2|A7L3B_HUMAN Ataxin-7-like protein 3B OS=Homo sapiens (Human) OX=9606 GN=ATXN7L3B PE=1 SV=2	ATXN7L3B
41	sp|Q07812|BAX_HUMAN Apoptosis regulator BAX OS=Homo sapiens (Human) OX=9606 GN=BAX PE=1 SV=1	BAX
42	sp|P50895|BCAM_HUMAN Basal cell adhesion molecule OS=Homo sapiens (Human) OX=9606 GN=BCAM PE=1 SV=2	BCAM
43	sp|O75934|SPF27_HUMAN Pre-mRNA-splicing factor SPF27 OS=Homo sapiens (Human) OX=9606 GN=BCAS2 PE=1 SV=1	BCAS2
44	sp|Q14137|BOP1_HUMAN Ribosome biogenesis protein BOP1 OS=Homo sapiens (Human) OX=9606 GN=BOP1 PE=1 SV=2	BOP1
45	sp|Q9Y6E2|BZW2_HUMAN Basic leucine zipper and W2 domain-containing protein 2 OS=Homo sapiens (Human) OX=9606 GN=BZW2 PE=1 SV=1	BZW2
46	sp|Q9H0W9|CK054_HUMAN Ester hydrolase C11orf54 OS=Homo sapiens (Human) OX=9606 GN=C11orf54 PE=1 SV=1	C11orf54
47	sp|Q99622|C10_HUMAN Protein C10 OS=Homo sapiens (Human) OX=9606 GN=C12orf57 PE=1 SV=1	C12orf57
48	sp|Q9NS00|C1GLT_HUMAN Glycoprotein-N-acetylgalactosamine 3-beta-galactosyltransferase 1 OS=Homo sapiens (Human) OX=9606 GN=C1GALT1 PE=1 SV=1	C1GALT1
49	sp|A6NDU8|CE051_HUMAN UPF0600 protein C5orf51 OS=Homo sapiens (Human) OX=9606 GN=C5orf51 PE=1 SV=1	C5orf51
50	sp|P27708|PYR1_HUMAN CAD protein OS=Homo sapiens (Human) OX=9606 GN=CAD PE=1 SV=3	CAD
51	sp|Q13555|KCC2G_HUMAN Calcium/calmodulin-dependent protein kinase type II subunit gamma OS=Homo sapiens (Human) OX=9606 GN=CAMK2G PE=1 SV=4	CAMK2G
52	sp|P27824|CALX_HUMAN Calnexin OS=Homo sapiens (Human) OX=9606 GN=CANX PE=1 SV=2	CANX
53	sp|P07384|CAN1_HUMAN Calpain-1 catalytic subunit OS=Homo sapiens (Human) OX=9606 GN=CAPN1 PE=1 SV=1	CAPN1
54	sp|P17655|CAN2_HUMAN Calpain-2 catalytic subunit OS=Homo sapiens (Human) OX=9606 GN=CAPN2 PE=1 SV=6	CAPN2
55	sp|P04632|CPNS1_HUMAN Calpain small subunit 1 OS=Homo sapiens (Human) OX=9606 GN=CAPNS1 PE=1 SV=1	CAPNS1
56	sp|P31944|CASPE_HUMAN Caspase-14 OS=Homo sapiens (Human) OX=9606 GN=CASP14 PE=1 SV=2	CASP14
57	sp|P49662|CASP4_HUMAN Caspase-4 OS=Homo sapiens (Human) OX=9606 GN=CASP4 PE=1 SV=1	CASP4
58	sp|Q13951|PEBB_HUMAN Core-binding factor subunit beta OS=Homo sapiens (Human) OX=9606 GN=CBFB PE=1 SV=2	CBFB
59	sp|Q13185|CBX3_HUMAN Chromobox protein homolog 3 OS=Homo sapiens (Human) OX=9606 GN=CBX3 PE=1 SV=4	CBX3
60	sp|P49368|TCPG_HUMAN T-complex protein 1 subunit gamma OS=Homo sapiens (Human) OX=9606 GN=CCT3 PE=1 SV=4	CCT3
61	sp|P50990|TCPQ_HUMAN T-complex protein 1 subunit theta OS=Homo sapiens (Human) OX=9606 GN=CCT8 PE=1 SV=4	CCT8
62	sp|P48509|CD151_HUMAN CD151 antigen OS=Homo sapiens (Human) OX=9606 GN=CD151 PE=1 SV=3	CD151
63	sp|P60033|CD81_HUMAN CD81 antigen OS=Homo sapiens (Human) OX=9606 GN=CD81 PE=1 SV=1	CD81
64	sp|P30260|CDC27_HUMAN Cell division cycle protein 27 homolog OS=Homo sapiens (Human) OX=9606 GN=CDC27 PE=1 SV=2	CDC27
65	sp|Q6DT37|MRCKG_HUMAN Serine/threonine-protein kinase MRCK gamma OS=Homo sapiens (Human) OX=9606 GN=CDC42BPG PE=1 SV=2	CDC42BPG
66	sp|P12830|CADH1_HUMAN Cadherin-1 OS=Homo sapiens (Human) OX=9606 GN=CDH1 PE=1 SV=3	CDH1
67	sp|P50750|CDK9_HUMAN Cyclin-dependent kinase 9 OS=Homo sapiens (Human) OX=9606 GN=CDK9 PE=1 SV=3	CDK9
68	sp|O95674|CDS2_HUMAN Phosphatidate cytidylyltransferase 2 OS=Homo sapiens (Human) OX=9606 GN=CDS2 PE=1 SV=1	CDS2
69	sp|Q92879|CELF1_HUMAN CUGBP Elav-like family member 1 OS=Homo sapiens (Human) OX=9606 GN=CELF1 PE=1 SV=2	CELF1
70	sp|O00299|CLIC1_HUMAN Chloride intracellular channel protein 1 OS=Homo sapiens (Human) OX=9606 GN=CLIC1 PE=1 SV=4	CLIC1
71	sp|O95833|CLIC3_HUMAN Chloride intracellular channel protein 3 OS=Homo sapiens (Human) OX=9606 GN=CLIC3 PE=1 SV=2	CLIC3
72	sp|Q9Y696|CLIC4_HUMAN Chloride intracellular channel protein 4 OS=Homo sapiens (Human) OX=9606 GN=CLIC4 PE=1 SV=4	CLIC4
73	sp|P30622|CLIP1_HUMAN CAP-Gly domain-containing linker protein 1 OS=Homo sapiens (Human) OX=9606 GN=CLIP1 PE=1 SV=2	CLIP1
74	sp|Q00610|CLH1_HUMAN Clathrin heavy chain 1 OS=Homo sapiens (Human) OX=9606 GN=CLTC PE=1 SV=5	CLTC
75	sp|Q96DG6|CMBL_HUMAN Carboxymethylenebutenolidase homolog OS=Homo sapiens (Human) OX=9606 GN=CMBL PE=1 SV=1	CMBL
76	sp|A5YKK6|CNOT1_HUMAN CCR4-NOT transcription complex subunit 1 OS=Homo sapiens (Human) OX=9606 GN=CNOT1 PE=1 SV=2	CNOT1
77	sp|Q5JTJ3|COA6_HUMAN Cytochrome c oxidase assembly factor 6 homolog OS=Homo sapiens (Human) OX=9606 GN=COA6 PE=1 SV=1	COA6
78	sp|Q8NBJ5|GT251_HUMAN Procollagen galactosyltransferase 1 OS=Homo sapiens (Human) OX=9606 GN=COLGALT1 PE=1 SV=1	COLGALT1
79	sp|P53618|COPB_HUMAN Coatomer subunit beta OS=Homo sapiens (Human) OX=9606 GN=COPB1 PE=1 SV=3	COPB1
80	sp|Q9Y678|COPG1_HUMAN Coatomer subunit gamma-1 OS=Homo sapiens (Human) OX=9606 GN=COPG1 PE=1 SV=1	COPG1
81	sp|Q9UNS2|CSN3_HUMAN COP9 signalosome complex subunit 3 OS=Homo sapiens (Human) OX=9606 GN=COPS3 PE=1 SV=3	COPS3

82	sp|Q9H9Q2|CSN7B_HUMAN COP9 signalosome complex subunit 7b OS=Homo sapiens (Human) OX=9606 GN=COPS7B PE=1 SV=1	COPS7B
83	sp|Q9ULV4|COR1C_HUMAN Coronin-1C OS=Homo sapiens (Human) OX=9606 GN=CORO1C PE=1 SV=1	CORO1C
84	sp|P14406|CX7A2_HUMAN Cytochrome c oxidase subunit 7A2, mitochondrial OS=Homo sapiens (Human) OX=9606 GN=COX7A2 PE=1 SV=1	COX7A2
85	sp|Q9UI42|CBPA4_HUMAN Carboxypeptidase A4 OS=Homo sapiens (Human) OX=9606 GN=CPA4 PE=1 SV=2	CPA4
86	sp|P36551|HEM6_HUMAN Oxygen-dependent coproporphyrinogen-III oxidase, mitochondrial OS=Homo sapiens (Human) OX=9606 GN=CPOX PE=1 SV=3	CPOX
87	sp|P50416|CPT1A_HUMAN Carnitine O-palmitoyltransferase 1, liver isoform OS=Homo sapiens (Human) OX=9606 GN=CPT1A PE=1 SV=2	CPT1A
88	sp|P23786|CPT2_HUMAN Carnitine O-palmitoyltransferase 2, mitochondrial OS=Homo sapiens (Human) OX=9606 GN=CPT2 PE=1 SV=2	CPT2
89	sp|Q5TZA2|CROCC_HUMAN Rootletin OS=Homo sapiens (Human) OX=9606 GN=CROCC PE=1 SV=1	CROCC
90	sp|O75718|CRTAP_HUMAN Cartilage-associated protein OS=Homo sapiens (Human) OX=9606 GN=CRTAP PE=1 SV=1	CRTAP
91	sp|Q08257|QOR_HUMAN Quinone oxidoreductase OS=Homo sapiens (Human) OX=9606 GN=CRYZ PE=1 SV=1	CRYZ
92	sp|P35222|CTNB1_HUMAN Catenin beta-1 OS=Homo sapiens (Human) OX=9606 GN=CTNNB1 PE=1 SV=1	CTNNB1
93	sp|P17812|PYRG1_HUMAN CTP synthase 1 OS=Homo sapiens (Human) OX=9606 GN=CTPS1 PE=1 SV=2	CTPS1
94	sp|Q69YN2|C19L1_HUMAN CWF19-like protein 1 OS=Homo sapiens (Human) OX=9606 GN=CWF19L1 PE=1 SV=2	CWF19L1
95	sp|P00387|NB5R3_HUMAN NADH-cytochrome b5 reductase 3 OS=Homo sapiens (Human) OX=9606 GN=CYB5R3 PE=1 SV=3	CYB5R3
96	sp|Q7L576|CYFP1_HUMAN Cytoplasmic FMR1-interacting protein 1 OS=Homo sapiens (Human) OX=9606 GN=CYFIP1 PE=1 SV=1	CYFIP1
97	sp|O00622|CCN1_HUMAN CCN family member 1 OS=Homo sapiens (Human) OX=9606 GN=CCN1 PE=1 SV=1	CYR61
98	sp|Q96GG9|DCNL1_HUMAN DCN1-like protein 1 OS=Homo sapiens (Human) OX=9606 GN=DCUN1D1 PE=1 SV=1	DCUN1D1
99	sp|O95865|DDAH2_HUMAN N(G),N(G)-dimethylarginine dimethylaminohydrolase 2 OS=Homo sapiens (Human) OX=9606 GN=DDAH2 PE=1 SV=1	DDAH2
100	sp|Q16531|DDB1_HUMAN DNA damage-binding protein 1 OS=Homo sapiens (Human) OX=9606 GN=DDB1 PE=1 SV=1	DDB1
101	sp|Q9NR30|DDX21_HUMAN Nucleolar RNA helicase 2 OS=Homo sapiens (Human) OX=9606 GN=DDX21 PE=1 SV=5	DDX21
102	sp|Q13838|DX39B_HUMAN Spliceosome RNA helicase DDX39B OS=Homo sapiens (Human) OX=9606 GN=DDX39B PE=1 SV=1	DDX39B
103	sp|P26196|DDX6_HUMAN Probable ATP-dependent RNA helicase DDX6 OS=Homo sapiens (Human) OX=9606 GN=DDX6 PE=1 SV=2	DDX6
104	sp|Q16698|DECR_HUMAN 2,4-dienoyl-CoA reductase, mitochondrial OS=Homo sapiens (Human) OX=9606 GN=DECR1 PE=1 SV=1	DECR1
105	sp|P23743|DGKA_HUMAN Diacylglycerol kinase alpha OS=Homo sapiens (Human) OX=9606 GN=DGKA PE=1 SV=3	DGKA
106	sp|P49366|DHYS_HUMAN Deoxyhypusine synthase OS=Homo sapiens (Human) OX=9606 GN=DHPS PE=1 SV=1	DHPS
107	sp|Q08211|DHX9_HUMAN ATP-dependent RNA helicase A OS=Homo sapiens (Human) OX=9606 GN=DHX9 PE=1 SV=4	DHX9
108	sp|Q9P265|DIP2B_HUMAN Disco-interacting protein 2 homolog B OS=Homo sapiens (Human) OX=9606 GN=DIP2B PE=1 SV=3	DIP2B
109	sp|P10515|ODP2_HUMAN Dihydrolipoyllysine-residue acetyltransferase component of pyruvate dehydrogenase complex, mitochondrial OS=Homo sapiens (Human) OX=9606 GN=DLAT PE=1 SV=3	DLAT
110	sp|Q9Y2H0|DLGP4_HUMAN Disks large-associated protein 4 OS=Homo sapiens (Human) OX=9606 GN=DLGAP4 PE=1 SV=3	DLGAP4
111	sp|Q96EY1|DNJA3_HUMAN DnaJ homolog subfamily A member 3, mitochondrial OS=Homo sapiens (Human) OX=9606 GN=DNAJA3 PE=1 SV=2	DNAJA3
112	sp|Q99543|DNJC2_HUMAN DnaJ homolog subfamily C member 2 OS=Homo sapiens (Human) OX=9606 GN=DNAJC2 PE=1 SV=4	DNAJC2
113	sp|Q13217|DNJC3_HUMAN DnaJ homolog subfamily C member 3 OS=Homo sapiens (Human) OX=9606 GN=DNAJC3 PE=1 SV=1	DNAJC3
114	sp|Q9P2X0|DPM3_HUMAN Dolichol-phosphate mannosyltransferase subunit 3 OS=Homo sapiens (Human) OX=9606 GN=DPM3 PE=1 SV=2	DPM3
115	sp|O14972|VP26C_HUMAN Vacuolar protein sorting-associated protein 26C OS=Homo sapiens (Human) OX=9606 GN=VPS26C PE=1 SV=1	DSCR3
116	sp|Q14204|DYHC1_HUMAN Cytoplasmic dynein 1 heavy chain 1 OS=Homo sapiens (Human) OX=9606 GN=DYNC1H1 PE=1 SV=5	DYNC1H1
117	sp|Q6P2E9|EDC4_HUMAN Enhancer of mRNA-decapping protein 4 OS=Homo sapiens (Human) OX=9606 GN=EDC4 PE=1 SV=1	EDC4
118	sp|Q05639|EF1A2_HUMAN Elongation factor 1-alpha 2 OS=Homo sapiens (Human) OX=9606 GN=EEF1A2 PE=1 SV=1	EEF1A2
119	sp|P24534|EF1B_HUMAN Elongation factor 1-beta OS=Homo sapiens (Human) OX=9606 GN=EEF1B2 PE=1 SV=3	EEF1B2
120	sp|Q96C19|EFHD2_HUMAN EF-hand domain-containing protein D2 OS=Homo sapiens (Human) OX=9606 GN=EFHD2 PE=1 SV=1	EFHD2
121	sp|P00533|EGFR_HUMAN Epidermal growth factor receptor OS=Homo sapiens (Human) OX=9606 GN=EGFR PE=1 SV=2	EGFR
122	sp|Q8NDI1|EHBP1_HUMAN EH domain-binding protein 1 OS=Homo sapiens (Human) OX=9606 GN=EHBP1 PE=1 SV=3	EHBP1

123	sp|Q9H4M9|EHD1_HUMAN EH domain-containing protein 1 OS=Homo sapiens (Human) OX=9606 GN=EHD1 PE=1 SV=2	EHD1
124	sp|Q9NZN4|EHD2_HUMAN EH domain-containing protein 2 OS=Homo sapiens (Human) OX=9606 GN=EHD2 PE=1 SV=2	EHD2
125	sp|Q9H223|EHD4_HUMAN EH domain-containing protein 4 OS=Homo sapiens (Human) OX=9606 GN=EHD4 PE=1 SV=1	EHD4
126	sp|Q9BY44|EIF2A_HUMAN Eukaryotic translation initiation factor 2A OS=Homo sapiens (Human) OX=9606 GN=EIF2A PE=1 SV=3	EIF2A
127	sp|P19525|E2AK2_HUMAN Interferon-induced, double-stranded RNA-activated protein kinase OS=Homo sapiens (Human) OX=9606 GN=EIF2AK2 PE=1 SV=2	EIF2AK2
128	sp|P55884|EIF3B_HUMAN Eukaryotic translation initiation factor 3 subunit B OS=Homo sapiens (Human) OX=9606 GN=EIF3B PE=1 SV=3	EIF3B
129	sp|P60228|EIF3E_HUMAN Eukaryotic translation initiation factor 3 subunit E OS=Homo sapiens (Human) OX=9606 GN=EIF3E PE=1 SV=1	EIF3E
130	sp|O75822|EIF3J_HUMAN Eukaryotic translation initiation factor 3 subunit J OS=Homo sapiens (Human) OX=9606 GN=EIF3J PE=1 SV=2	EIF3J
131	sp|Q14240|IF4A2_HUMAN Eukaryotic initiation factor 4A-II OS=Homo sapiens (Human) OX=9606 GN=EIF4A2 PE=1 SV=2	EIF4A2
132	sp|Q04637|IF4G1_HUMAN Eukaryotic translation initiation factor 4 gamma 1 OS=Homo sapiens (Human) OX=9606 GN=EIF4G1 PE=1 SV=4	EIF4G1
133	sp|Q9H4G0|E41L1_HUMAN Band 4.1-like protein 1 OS=Homo sapiens (Human) OX=9606 GN=EPB41L1 PE=1 SV=2	EPB41L1
134	sp|Q9H6S3|ES8L2_HUMAN Epidermal growth factor receptor kinase substrate 8-like protein 2 OS=Homo sapiens (Human) OX=9606 GN=EPS8L2 PE=1 SV=2	EPS8L2
135	sp|Q9NZ08|ERAP1_HUMAN Endoplasmic reticulum aminopeptidase 1 OS=Homo sapiens (Human) OX=9606 GN=ERAP1 PE=1 SV=3	ERAP1
136	sp|Q96HE7|ERO1A_HUMAN ERO1-like protein alpha OS=Homo sapiens (Human) OX=9606 GN=ERO1A PE=1 SV=2	ERO1L
137	sp|Q9H098|F107B_HUMAN Protein FAM107B OS=Homo sapiens (Human) OX=9606 GN=FAM107B PE=1 SV=1	FAM107B
138	sp|Q8NC44|RETR2_HUMAN Reticulophagy regulator 2 OS=Homo sapiens (Human) OX=9606 GN=RETREG2 PE=1 SV=3	FAM134A
139	sp|Q96C01|F136A_HUMAN Protein FAM136A OS=Homo sapiens (Human) OX=9606 GN=FAM136A PE=1 SV=1	FAM136A
140	sp|Q9BRX8|PXL2A_HUMAN Peroxiredoxin-like 2A OS=Homo sapiens (Human) OX=9606 GN=PRXL2A PE=1 SV=3	FAM213A
141	sp|Q9NUQ9|CYRIB_HUMAN CYFIP-related Rac1 interactor B OS=Homo sapiens (Human) OX=9606 GN=CYRIB PE=1 SV=1	FAM49B
142	sp|O95684|CEP43_HUMAN Centrosomal protein 43 OS=Homo sapiens (Human) OX=9606 GN=CEP43 PE=1 SV=1	FGFR1OP
143	sp|P07954|FUMH_HUMAN Fumarate hydratase, mitochondrial OS=Homo sapiens (Human) OX=9606 GN=FH PE=1 SV=3	FH
144	sp|Q96AY3|FKB10_HUMAN Peptidyl-prolyl cis-trans isomerase FKBP10 OS=Homo sapiens (Human) OX=9606 GN=FKBP10 PE=1 SV=1	FKBP10
145	sp|Q5T0N5|FBP1L_HUMAN Formin-binding protein 1-like OS=Homo sapiens (Human) OX=9606 GN=FNBP1L PE=1 SV=3	FNBP1L
146	sp|Q53EP0|FND3B_HUMAN Fibronectin type III domain-containing protein 3B OS=Homo sapiens (Human) OX=9606 GN=FNDC3B PE=1 SV=2	FNDC3B
147	sp|Q9C0B1|FTO_HUMAN Alpha-ketoglutarate-dependent dioxygenase FTO OS=Homo sapiens (Human) OX=9606 GN=FTO PE=1 SV=3	FTO
148	sp|Q8IY81|SPB1_HUMAN pre-rRNA 2-O-ribose RNA methyltransferase FTSJ3 OS=Homo sapiens (Human) OX=9606 GN=FTSJ3 PE=1 SV=2	FTSJ3
149	sp|Q96I24|FUBP3_HUMAN Far upstream element-binding protein 3 OS=Homo sapiens (Human) OX=9606 GN=FUBP3 PE=1 SV=2	FUBP3
150	sp|P51114|FXR1_HUMAN Fragile X mental retardation syndrome-related protein 1 OS=Homo sapiens (Human) OX=9606 GN=FXR1 PE=1 SV=3	FXR1
151	sp|Q9UN86|G3BP2_HUMAN Ras GTPase-activating protein-binding protein 2 OS=Homo sapiens (Human) OX=9606 GN=G3BP2 PE=1 SV=2	G3BP2
152	sp|P10253|LYAG_HUMAN Lysosomal alpha-glucosidase OS=Homo sapiens (Human) OX=9606 GN=GAA PE=1 SV=4	GAA
153	sp|Q14376|GALE_HUMAN UDP-glucose 4-epimerase OS=Homo sapiens (Human) OX=9606 GN=GALE PE=1 SV=2	GALE
154	sp|Q86SF2|GALT7_HUMAN N-acetylgalactosaminyltransferase 7 OS=Homo sapiens (Human) OX=9606 GN=GALNT7 PE=1 SV=1	GALNT7
155	sp|P22102|PUR2_HUMAN Trifunctional purine biosynthetic protein adenosine-3 OS=Homo sapiens (Human) OX=9606 GN=GART PE=1 SV=1	GART
156	sp|P48507|GSH0_HUMAN Glutamate--cysteine ligase regulatory subunit OS=Homo sapiens (Human) OX=9606 GN=GCLM PE=1 SV=1	GCLM
157	sp|Q8TEQ6|GEMI5_HUMAN Gem-associated protein 5 OS=Homo sapiens (Human) OX=9606 GN=GEMIN5 PE=1 SV=3	GEMIN5
158	sp|Q06210|GFPT1_HUMAN Glutamine--fructose-6-phosphate aminotransferase [isomerizing] 1 OS=Homo sapiens (Human) OX=9606 GN=GFPT1 PE=1 SV=3	GFPT1
159	sp|Q9UJY5|GGA1_HUMAN ADP-ribosylation factor-binding protein GGA1 OS=Homo sapiens (Human) OX=9606 GN=GGA1 PE=1 SV=1	GGA1
160	sp|P49915|GUAA_HUMAN GMP synthase [glutamine-hydrolyzing] OS=Homo sapiens (Human) OX=9606 GN=GMPS PE=1 SV=1	GMPS
161	sp|Q14344|GNA13_HUMAN Guanine nucleotide-binding protein subunit alpha-13 OS=Homo sapiens (Human) OX=9606 GN=GNA13 PE=1 SV=2	GNA13

162	sp|P04899|GNAI2_HUMAN Guanine nucleotide-binding protein G(i) subunit alpha-2 OS=Homo sapiens (Human) OX=9606 GN=GNAI2 PE=1 SV=3	GNAI2
163	sp|P62873|GBB1_HUMAN Guanine nucleotide-binding protein G(I)/G(S)/G(T) subunit beta-1 OS=Homo sapiens (Human) OX=9606 GN=GNB1 PE=1 SV=3	GNB1
164	sp|P63244|RACK1_HUMAN Receptor of activated protein C kinase 1 OS=Homo sapiens (Human) OX=9606 GN=RACK1 PE=1 SV=3	GNB2L1
165	sp|P46926|GNPI1_HUMAN Glucosamine-6-phosphate isomerase 1 OS=Homo sapiens (Human) OX=9606 GN=GNPDA1 PE=1 SV=1	GNPDA1
166	sp|P17174|AATC_HUMAN Aspartate aminotransferase, cytoplasmic OS=Homo sapiens (Human) OX=9606 GN=GOT1 PE=1 SV=3	GOT1
167	sp|P00505|AATM_HUMAN Aspartate aminotransferase, mitochondrial OS=Homo sapiens (Human) OX=9606 GN=GOT2 PE=1 SV=3	GOT2
168	sp|Q13098|CSN1_HUMAN COP9 signalosome complex subunit 1 OS=Homo sapiens (Human) OX=9606 GN=GPS1 PE=1 SV=4	GPS1
169	sp|Q12849|GRSF1_HUMAN G-rich sequence factor 1 OS=Homo sapiens (Human) OX=9606 GN=GRSF1 PE=1 SV=3	GRSF1
170	sp|P48637|GSHB_HUMAN Glutathione synthetase OS=Homo sapiens (Human) OX=9606 GN=GSS PE=1 SV=1	GSS
171	sp|P52655|TF2AA_HUMAN Transcription initiation factor IIA subunit 1 OS=Homo sapiens (Human) OX=9606 GN=GTF2A1 PE=1 SV=1	GTF2A1
172	sp|Q9Y5Q8|TF3C5_HUMAN General transcription factor 3C polypeptide 5 OS=Homo sapiens (Human) OX=9606 GN=GTF3C5 PE=1 SV=2	GTF3C5
173	sp|P13807|GYS1_HUMAN Glycogen [starch] synthase, muscle OS=Homo sapiens (Human) OX=9606 GN=GYS1 PE=1 SV=2	GYS1
174	sp|P07686|HEXB_HUMAN Beta-hexosaminidase subunit beta OS=Homo sapiens (Human) OX=9606 GN=HEXB PE=1 SV=3	HEXB
175	sp|Q6NVY1|HIBCH_HUMAN 3-hydroxyisobutyryl-CoA hydrolase, mitochondrial OS=Homo sapiens (Human) OX=9606 GN=HIBCH PE=1 SV=2	HIBCH
176	sp|P19367|HXK1_HUMAN Hexokinase-1 OS=Homo sapiens (Human) OX=9606 GN=HK1 PE=1 SV=3	HK1
177	sp|P52789|HXK2_HUMAN Hexokinase-2 OS=Homo sapiens (Human) OX=9606 GN=HK2 PE=1 SV=2	HK2
178	sp|P10321|HLAC_HUMAN HLA class I histocompatibility antigen, C alpha chain OS=Homo sapiens (Human) OX=9606 GN=HLA-C PE=1 SV=3	HLA-C
179	sp|Q01581|HMCS1_HUMAN Hydroxymethylglutaryl-CoA synthase, cytoplasmic OS=Homo sapiens (Human) OX=9606 GN=HMGCS1 PE=1 SV=2	HMGCS1
180	sp|P51991|ROA3_HUMAN Heterogeneous nuclear ribonucleoprotein A3 OS=Homo sapiens (Human) OX=9606 GN=HNRNPA3 PE=1 SV=2	HNRNPA3
181	sp|P55795|HNRH2_HUMAN Heterogeneous nuclear ribonucleoprotein H2 OS=Homo sapiens (Human) OX=9606 GN=HNRNPH2 PE=1 SV=1	HNRNPH2
182	sp|P61978|HNRPK_HUMAN Heterogeneous nuclear ribonucleoprotein K OS=Homo sapiens (Human) OX=9606 GN=HNRNPK PE=1 SV=1	HNRNPK
183	sp|P00492|HPRT_HUMAN Hypoxanthine-guanine phosphoribosyltransferase OS=Homo sapiens (Human) OX=9606 GN=HPRT1 PE=1 SV=2	HPRT1
184	sp|P34932|HSP74_HUMAN Heat shock 70 kDa protein 4 OS=Homo sapiens (Human) OX=9606 GN=HSPA4 PE=1 SV=4	HSPA4
185	sp|Q92598|HS105_HUMAN Heat shock protein 105 kDa OS=Homo sapiens (Human) OX=9606 GN=HSPH1 PE=1 SV=1	HSPH1
186	sp|P41252|SYIC_HUMAN Isoleucine--tRNA ligase, cytoplasmic OS=Homo sapiens (Human) OX=9606 GN=IARS1 PE=1 SV=2	IARS
187	sp|P05362|ICAM1_HUMAN Intercellular adhesion molecule 1 OS=Homo sapiens (Human) OX=9606 GN=ICAM1 PE=1 SV=2	ICAM1
188	sp|Q16666|IF16_HUMAN Gamma-interferon-inducible protein 16 OS=Homo sapiens (Human) OX=9606 GN=IFI16 PE=1 SV=3	IFI16
189	sp|P09914|IFIT1_HUMAN Interferon-induced protein with tetratricopeptide repeats 1 OS=Homo sapiens (Human) OX=9606 GN=IFIT1 PE=1 SV=2	IFIT1
190	sp|P09913|IFIT2_HUMAN Interferon-induced protein with tetratricopeptide repeats 2 OS=Homo sapiens (Human) OX=9606 GN=IFIT2 PE=1 SV=1	IFIT2
191	sp|O14879|IFIT3_HUMAN Interferon-induced protein with tetratricopeptide repeats 3 OS=Homo sapiens (Human) OX=9606 GN=IFIT3 PE=1 SV=1	IFIT3
192	sp|Q12906|ILF3_HUMAN Interleukin enhancer-binding factor 3 OS=Homo sapiens (Human) OX=9606 GN=ILF3 PE=1 SV=3	ILF3
193	sp|Q13418|ILK_HUMAN Integrin-linked protein kinase OS=Homo sapiens (Human) OX=9606 GN=ILK PE=1 SV=2	ILK
194	sp|Q9NX62|IMPA3_HUMAN Golgi-resident adenosine 3,5-bisphosphate 3-phosphatase OS=Homo sapiens (Human) OX=9606 GN=BPNT2 PE=1 SV=1	IMPAD1
195	sp|P46940|IQGA1_HUMAN Ras GTPase-activating-like protein IQGAP1 OS=Homo sapiens (Human) OX=9606 GN=IQGAP1 PE=1 SV=1	IQGAP1
196	sp|Q8WZA9|IRGQ_HUMAN Immunity-related GTPase family Q protein OS=Homo sapiens (Human) OX=9606 GN=IRGQ PE=1 SV=1	IRGQ
197	sp|P08648|ITA5_HUMAN Integrin alpha-5 OS=Homo sapiens (Human) OX=9606 GN=ITGA5 PE=1 SV=2	ITGA5
198	sp|P23229|ITA6_HUMAN Integrin alpha-6 OS=Homo sapiens (Human) OX=9606 GN=ITGA6 PE=1 SV=5	ITGA6
199	sp|P16144|ITB4_HUMAN Integrin beta-4 OS=Homo sapiens (Human) OX=9606 GN=ITGB4 PE=1 SV=5	ITGB4
200	sp|Q8N5M9|JAGN1_HUMAN Protein jagunal homolog 1 OS=Homo sapiens (Human) OX=9606 GN=JAGN1 PE=1 SV=1	JAGN1

201	sp|Q6NYC1|JMJD6_HUMAN Bifunctional arginine demethylase and lysyl-hydroxylase JMJD6 OS=Homo sapiens (Human) OX=9606 GN=JMJD6 PE=1 SV=1	JMJD6
202	sp|Q9P0J7|KCMF1_HUMAN E3 ubiquitin-protein ligase KCMF1 OS=Homo sapiens (Human) OX=9606 GN=KCMF1 PE=1 SV=2	KCMF1
203	sp|Q9P260|RELCH_HUMAN RAB11-binding protein RELCH OS=Homo sapiens (Human) OX=9606 GN=RELCH PE=1 SV=2	KIAA1468
204	sp|Q07866|KLC1_HUMAN Kinesin light chain 1 OS=Homo sapiens (Human) OX=9606 GN=KLC1 PE=1 SV=2	KLC1
205	sp|P52292|IMA1_HUMAN Importin subunit alpha-1 OS=Homo sapiens (Human) OX=9606 GN=KPNA2 PE=1 SV=1	KPNA2
206	sp|Q14974|IMB1_HUMAN Importin subunit beta-1 OS=Homo sapiens (Human) OX=9606 GN=KPNB1 PE=1 SV=2	KPNB1
207	sp|P13473|LAMP2_HUMAN Lysosome-associated membrane glycoprotein 2 OS=Homo sapiens (Human) OX=9606 GN=LAMP2 PE=1 SV=2	LAMP2
208	sp|Q6IAA8|LTOR1_HUMAN Ragulator complex protein LAMTOR1 OS=Homo sapiens (Human) OX=9606 GN=LAMTOR1 PE=1 SV=2	LAMTOR1
209	sp|P18858|DNLI1_HUMAN DNA ligase 1 OS=Homo sapiens (Human) OX=9606 GN=LIG1 PE=1 SV=1	LIG1
210	sp|P48059|LIMS1_HUMAN LIM and senescent cell antigen-like-containing domain protein 1 OS=Homo sapiens (Human) OX=9606 GN=LIMS1 PE=1 SV=4	LIMS1
211	sp|Q12907|LMAN2_HUMAN Vesicular integral-membrane protein VIP36 OS=Homo sapiens (Human) OX=9606 GN=LMAN2 PE=1 SV=1	LMAN2
212	sp|Q8NF37|PCAT1_HUMAN Lysophosphatidylcholine acyltransferase 1 OS=Homo sapiens (Human) OX=9606 GN=LPCAT1 PE=1 SV=2	LPCAT1
213	sp|Q6P1A2|MBOA5_HUMAN Lysophospholipid acyltransferase 5 OS=Homo sapiens (Human) OX=9606 GN=LPCAT3 PE=1 SV=1	LPCAT3
214	sp|Q9BQK8|LPIN3_HUMAN Phosphatidate phosphatase LPIN3 OS=Homo sapiens (Human) OX=9606 GN=LPIN3 PE=1 SV=3	LPIN3
215	sp|P50851|LRBA_HUMAN Lipopolysaccharide-responsive and beige-like anchor protein OS=Homo sapiens (Human) OX=9606 GN=LRBA PE=1 SV=4	LRBA
216	sp|P42704|LPPRC_HUMAN Leucine-rich PPR motif-containing protein, mitochondrial OS=Homo sapiens (Human) OX=9606 GN=LRPPRC PE=1 SV=3	LRPPRC
217	sp|Q9H0U3|MAGT1_HUMAN Magnesium transporter protein 1 OS=Homo sapiens (Human) OX=9606 GN=MAGT1 PE=1 SV=1	MAGT1
218	sp|O43318|M3K7_HUMAN Mitogen-activated protein kinase kinase kinase 7 OS=Homo sapiens (Human) OX=9606 GN=MAP3K7 PE=1 SV=1	MAP3K7
219	sp|P43121|MUC18_HUMAN Cell surface glycoprotein MUC18 OS=Homo sapiens (Human) OX=9606 GN=MCAM PE=1 SV=2	MCAM
220	sp|Q8NI22|MCFD2_HUMAN Multiple coagulation factor deficiency protein 2 OS=Homo sapiens (Human) OX=9606 GN=MCFD2 PE=1 SV=1	MCFD2
221	sp|P50579|MAP2_HUMAN Methionine aminopeptidase 2 OS=Homo sapiens (Human) OX=9606 GN=METAP2 PE=1 SV=1	METAP2
222	sp|Q9UNW1|MINP1_HUMAN Multiple inositol polyphosphate phosphatase 1 OS=Homo sapiens (Human) OX=9606 GN=MINPP1 PE=1 SV=1	MINPP1
223	sp|Q14165|MLEC_HUMAN Malectin OS=Homo sapiens (Human) OX=9606 GN=MLEC PE=1 SV=1	MLEC
224	sp|P08473|NEP_HUMAN Neprilysin OS=Homo sapiens (Human) OX=9606 GN=MME PE=1 SV=2	MME
225	sp|O96007|MOC2B_HUMAN Molybdopterin synthase catalytic subunit OS=Homo sapiens (Human) OX=9606 GN=MOCS2 PE=1 SV=1	MOCS2
226	sp|Q9HCE1|MOV10_HUMAN Helicase MOV-10 OS=Homo sapiens (Human) OX=9606 GN=MOV10 PE=1 SV=2	MOV10
227	sp|O75352|MPU1_HUMAN Mannose-P-dolichol utilization defect 1 protein OS=Homo sapiens (Human) OX=9606 GN=MPDU1 PE=1 SV=2	MPDU1
228	sp|Q8N3R9|MPP5_HUMAN MAGUK p55 subfamily member 5 OS=Homo sapiens (Human) OX=9606 GN=MPP5 PE=1 SV=3	MPP5
229	sp|Q9NWU5|RM22_HUMAN 39S ribosomal protein L22, mitochondrial OS=Homo sapiens (Human) OX=9606 GN=MRPL22 PE=1 SV=1	MRPL22
230	sp|Q9BZE1|RM37_HUMAN 39S ribosomal protein L37, mitochondrial OS=Homo sapiens (Human) OX=9606 GN=MRPL37 PE=1 SV=2	MRPL37
231	sp|Q9Y676|RT18B_HUMAN 28S ribosomal protein S18b, mitochondrial OS=Homo sapiens (Human) OX=9606 GN=MRPS18B PE=1 SV=1	MRPS18B
232	sp|P82673|RT35_HUMAN 28S ribosomal protein S35, mitochondrial OS=Homo sapiens (Human) OX=9606 GN=MRPS35 PE=1 SV=1	MRPS35
233	sp|P00403|COX2_HUMAN Cytochrome c oxidase subunit 2 OS=Homo sapiens (Human) OX=9606 GN=MT-CO2 PE=1 SV=1	MT-CO2
234	sp|O94776|MTA2_HUMAN Metastasis-associated protein MTA2 OS=Homo sapiens (Human) OX=9606 GN=MTA2 PE=1 SV=1	MTA2
235	sp|P42345|MTOR_HUMAN Serine/threonine-protein kinase mTOR OS=Homo sapiens (Human) OX=9606 GN=MTOR PE=1 SV=1	MTOR
236	sp|Q14764|MVP_HUMAN Major vault protein OS=Homo sapiens (Human) OX=9606 GN=MVP PE=1 SV=4	MVP
237	sp|P20591|MX1_HUMAN Interferon-induced GTP-binding protein Mx1 OS=Homo sapiens (Human) OX=9606 GN=MX1 PE=1 SV=4	MX1
238	sp|Q96S97|MYADM_HUMAN Myeloid-associated differentiation marker OS=Homo sapiens (Human) OX=9606 GN=MYADM PE=1 SV=2	MYADM
239	sp|Q7Z406|MYH14_HUMAN Myosin-14 OS=Homo sapiens (Human) OX=9606 GN=MYH14 PE=1 SV=2	MYH14

240	sp|P05976|MYL1_HUMAN Myosin light chain 1/3, skeletal muscle isoform OS=Homo sapiens (Human) OX=9606 GN=MYL1 PE=1 SV=3;sp|P08590|MYL3_HUMAN Myosin light chain 3 OS=Homo sapiens (Human) OX=9606 GN=MYL3 PE=1 SV=3	MYL1;MYL3
241	sp|P19105|ML12A_HUMAN Myosin regulatory light chain 12A OS=Homo sapiens (Human) OX=9606 GN=MYL12A PE=1 SV=2;sp|O14950|ML12B_HUMAN Myosin regulatory light chain 12B OS=Homo sapiens (Human) OX=9606 GN=MYL12B PE=1 SV=2	MYL12A;MYL12B
242	sp|O43795|MYO1B_HUMAN Unconventional myosin-Ib OS=Homo sapiens (Human) OX=9606 GN=MYO1B PE=1 SV=3	MYO1B
243	sp|O00159|MYO1C_HUMAN Unconventional myosin-Ic OS=Homo sapiens (Human) OX=9606 GN=MYO1C PE=1 SV=4	MYO1C
244	sp|Q13564|ULA1_HUMAN NEDD8-activating enzyme E1 regulatory subunit OS=Homo sapiens (Human) OX=9606 GN=NAE1 PE=1 SV=1	NAE1
245	sp|P43490|NAMPT_HUMAN Nicotinamide phosphoribosyltransferase OS=Homo sapiens (Human) OX=9606 GN=NAMPT PE=1 SV=1	NAMPT
246	sp|P54920|SNAA_HUMAN Alpha-soluble NSF attachment protein OS=Homo sapiens (Human) OX=9606 GN=NAPA PE=1 SV=3	NAPA
247	sp|O43776|SYNC_HUMAN Asparagine--tRNA ligase, cytoplasmic OS=Homo sapiens (Human) OX=9606 GN=NARS1 PE=1 SV=1	NARS
248	sp|Q09161|NCBP1_HUMAN Nuclear cap-binding protein subunit 1 OS=Homo sapiens (Human) OX=9606 GN=NCBP1 PE=1 SV=1	NCBP1
249	sp|Q6ZVX7|FBX50_HUMAN F-box only protein 50 OS=Homo sapiens (Human) OX=9606 GN=NCCRP1 PE=1 SV=1	NCCRP1
250	sp|Q6PIU2|NCEH1_HUMAN Neutral cholesterol ester hydrolase 1 OS=Homo sapiens (Human) OX=9606 GN=NCEH1 PE=1 SV=3	NCEH1
251	sp|Q9P0J0|NDUAD_HUMAN NADH dehydrogenase [ubiquinone] 1 alpha subcomplex subunit 13 OS=Homo sapiens (Human) OX=9606 GN=NDUFA13 PE=1 SV=3	NDUFA13
252	sp|Q9P032|NDUF4_HUMAN NADH dehydrogenase [ubiquinone] 1 alpha subcomplex assembly factor 4 OS=Homo sapiens (Human) OX=9606 GN=NDUFAF4 PE=1 SV=1	NDUFAF4
253	sp|O75438|NDUB1_HUMAN NADH dehydrogenase [ubiquinone] 1 beta subcomplex subunit 1 OS=Homo sapiens (Human) OX=9606 GN=NDUFB1 PE=1 SV=1	NDUFB1
254	sp|P28331|NDUS1_HUMAN NADH-ubiquinone oxidoreductase 75 kDa subunit, mitochondrial OS=Homo sapiens (Human) OX=9606 GN=NDUFS1 PE=1 SV=3	NDUFS1
255	sp|Q9NVZ3|NECP2_HUMAN Adaptin ear-binding coat-associated protein 2 OS=Homo sapiens (Human) OX=9606 GN=NECAP2 PE=1 SV=1	NECAP2
256	sp|Q96PU5|NED4L_HUMAN E3 ubiquitin-protein ligase NEDD4-like OS=Homo sapiens (Human) OX=9606 GN=NEDD4L PE=1 SV=2	NEDD4L
257	sp|O60524|NEMF_HUMAN Nuclear export mediator factor NEMF OS=Homo sapiens (Human) OX=9606 GN=NEMF PE=1 SV=4	NEMF
258	sp|Q9BYT8|NEUL_HUMAN Neurolysin, mitochondrial OS=Homo sapiens (Human) OX=9606 GN=NLN PE=1 SV=1	NLN
259	sp|P15531|NDKA_HUMAN Nucleoside diphosphate kinase A OS=Homo sapiens (Human) OX=9606 GN=NME1 PE=1 SV=1	NME1
260	sp|Q13423|NNTM_HUMAN NAD(P) transhydrogenase, mitochondrial OS=Homo sapiens (Human) OX=9606 GN=NNT PE=1 SV=3	NNT
261	sp|Q9H6R4|NOL6_HUMAN Nucleolar protein 6 OS=Homo sapiens (Human) OX=9606 GN=NOL6 PE=1 SV=2	NOL6
262	sp|Q8NDH3|PEPL1_HUMAN Probable aminopeptidase NPEPL1 OS=Homo sapiens (Human) OX=9606 GN=NPEPL1 PE=1 SV=3	NPEPL1
263	sp|P46459|NSF_HUMAN Vesicle-fusing ATPase OS=Homo sapiens (Human) OX=9606 GN=NSF PE=1 SV=3	NSF
264	sp|Q08J23|NSUN2_HUMAN RNA cytosine C(5)-methyltransferase NSUN2 OS=Homo sapiens (Human) OX=9606 GN=NSUN2 PE=1 SV=2	NSUN2
265	sp|Q9Y266|NUDC_HUMAN Nuclear migration protein nudC OS=Homo sapiens (Human) OX=9606 GN=NUDC PE=1 SV=1	NUDC
266	sp|Q14980|NUMA1_HUMAN Nuclear mitotic apparatus protein 1 OS=Homo sapiens (Human) OX=9606 GN=NUMA1 PE=1 SV=2	NUMA1
267	sp|P49790|NU153_HUMAN Nuclear pore complex protein Nup153 OS=Homo sapiens (Human) OX=9606 GN=NUP153 PE=1 SV=2	NUP153
268	sp|Q9BW27|NUP85_HUMAN Nuclear pore complex protein Nup85 OS=Homo sapiens (Human) OX=9606 GN=NUP85 PE=1 SV=1	NUP85
269	sp|Q8N1F7|NUP93_HUMAN Nuclear pore complex protein Nup93 OS=Homo sapiens (Human) OX=9606 GN=NUP93 PE=1 SV=2	NUP93
270	sp|Q9BVL2|NUP58_HUMAN Nucleoporin p58/p45 OS=Homo sapiens (Human) OX=9606 GN=NUP58 PE=1 SV=1	NUPL1
271	sp|Q9Y6K5|OAS3_HUMAN 2-5-oligoadenylate synthase 3 OS=Homo sapiens (Human) OX=9606 GN=OAS3 PE=1 SV=3	OAS3
272	sp|Q02218|ODO1_HUMAN 2-oxoglutarate dehydrogenase, mitochondrial OS=Homo sapiens (Human) OX=9606 GN=OGDH PE=1 SV=3	OGDH
273	sp|Q9H4L5|OSBL3_HUMAN Oxysterol-binding protein-related protein 3 OS=Homo sapiens (Human) OX=9606 GN=OSBPL3 PE=1 SV=1	OSBPL3
274	sp|O15460|P4HA2_HUMAN Prolyl 4-hydroxylase subunit alpha-2 OS=Homo sapiens (Human) OX=9606 GN=P4HA2 PE=1 SV=1	P4HA2
275	sp|P68402|PA1B2_HUMAN Platelet-activating factor acetylhydrolase IB subunit alpha2 OS=Homo sapiens (Human) OX=9606 GN=PAFAH1B2 PE=1 SV=1	PAFAH1B2
276	sp|Q460N5|PAR14_HUMAN Protein mono-ADP-ribosyltransferase PARP14 OS=Homo sapiens (Human) OX=9606 GN=PARP14 PE=1 SV=3	PARP14

277	sp|Q96KB5|TOPK_HUMAN Lymphokine-activated killer T-cell-originated protein kinase OS=Homo sapiens (Human) OX=9606 GN=PBK PE=1 SV=3	PBK
278	sp|P11498|PYC_HUMAN Pyruvate carboxylase, mitochondrial OS=Homo sapiens (Human) OX=9606 GN=PC PE=1 SV=2	PC
279	sp|Q16822|PCKGM_HUMAN Phosphoenolpyruvate carboxykinase [GTP], mitochondrial OS=Homo sapiens (Human) OX=9606 GN=PCK2 PE=1 SV=4	PCK2
280	sp|Q8NBM8|PCYXL_HUMAN Prenylcysteine oxidase-like OS=Homo sapiens (Human) OX=9606 GN=PCYOX1L PE=1 SV=2	PCYOX1L
281	sp|Q9H2J4|PDCL3_HUMAN Phosducin-like protein 3 OS=Homo sapiens (Human) OX=9606 GN=PDCL3 PE=1 SV=1	PDCL3
282	sp|P11177|ODPB_HUMAN Pyruvate dehydrogenase E1 component subunit beta, mitochondrial OS=Homo sapiens (Human) OX=9606 GN=PDHB PE=1 SV=3	PDHB
283	sp|Q96HC4|PDLI5_HUMAN PDZ and LIM domain protein 5 OS=Homo sapiens (Human) OX=9606 GN=PDLIM5 PE=1 SV=5	PDLIM5
284	sp|Q8NCN5|PDPR_HUMAN Pyruvate dehydrogenase phosphatase regulatory subunit, mitochondrial OS=Homo sapiens (Human) OX=9606 GN=PDPR PE=1 SV=2	PDPR
285	sp|Q29RF7|PDS5A_HUMAN Sister chromatid cohesion protein PDS5 homolog A OS=Homo sapiens (Human) OX=9606 GN=PDS5A PE=1 SV=1	PDS5A
286	sp|Q9NTI5|PDS5B_HUMAN Sister chromatid cohesion protein PDS5 homolog B OS=Homo sapiens (Human) OX=9606 GN=PDS5B PE=1 SV=1	PDS5B
287	sp|Q6P996|PDXD1_HUMAN Pyridoxal-dependent decarboxylase domain-containing protein 1 OS=Homo sapiens (Human) OX=9606 GN=PDXDC1 PE=1 SV=2	PDXDC1
288	sp|Q15121|PEA15_HUMAN Astrocytic phosphoprotein PEA-15 OS=Homo sapiens (Human) OX=9606 GN=PEA15 PE=1 SV=2	PEA15
289	sp|P30086|PEBP1_HUMAN Phosphatidylethanolamine-binding protein 1 OS=Homo sapiens (Human) OX=9606 GN=PEBP1 PE=1 SV=3	PEBP1
290	sp|Q86TG7|PEG10_HUMAN Retrotransposon-derived protein PEG10 OS=Homo sapiens (Human) OX=9606 GN=PEG10 PE=1 SV=2	PEG10
291	sp|Q8IZL8|PELP1_HUMAN Proline-, glutamic acid- and leucine-rich protein 1 OS=Homo sapiens (Human) OX=9606 GN=PELP1 PE=1 SV=2	PELP1
292	sp|O96011|PX11B_HUMAN Peroxisomal membrane protein 11B OS=Homo sapiens (Human) OX=9606 GN=PEX11B PE=1 SV=1	PEX11B
293	sp|P17858|PFKAL_HUMAN ATP-dependent 6-phosphofructokinase, liver type OS=Homo sapiens (Human) OX=9606 GN=PFKL PE=1 SV=6	PFKL
294	sp|P52209|6PGD_HUMAN 6-phosphogluconate dehydrogenase, decarboxylating OS=Homo sapiens (Human) OX=9606 GN=PGD PE=1 SV=3	PGD
295	sp|Q8IZ21|PHAR4_HUMAN Phosphatase and actin regulator 4 OS=Homo sapiens (Human) OX=9606 GN=PHACTR4 PE=1 SV=1	PHACTR4
296	sp|Q9H490|PIGU_HUMAN Phosphatidylinositol glycan anchor biosynthesis class U protein OS=Homo sapiens (Human) OX=9606 GN=PIGU PE=1 SV=3	PIGU
297	sp|Q13526|PIN1_HUMAN Peptidyl-prolyl cis-trans isomerase NIMA-interacting 1 OS=Homo sapiens (Human) OX=9606 GN=PIN1 PE=1 SV=1	PIN1
298	sp|Q16513|PKN2_HUMAN Serine/threonine-protein kinase N2 OS=Homo sapiens (Human) OX=9606 GN=PKN2 PE=1 SV=1	PKN2
299	sp|Q99959|PKP2_HUMAN Plakophilin-2 OS=Homo sapiens (Human) OX=9606 GN=PKP2 PE=1 SV=2	PKP2
300	sp|P13797|PLST_HUMAN Plastin-3 OS=Homo sapiens (Human) OX=9606 GN=PLS3 PE=1 SV=4	PLS3
301	sp|Q10713|MPPA_HUMAN Mitochondrial-processing peptidase subunit alpha OS=Homo sapiens (Human) OX=9606 GN=PMPCA PE=1 SV=2	PMPCA
302	sp|Q9NRX1|PNO1_HUMAN RNA-binding protein PNO1 OS=Homo sapiens (Human) OX=9606 GN=PNO1 PE=1 SV=1	PNO1
303	sp|P28340|DPOD1_HUMAN DNA polymerase delta catalytic subunit OS=Homo sapiens (Human) OX=9606 GN=POLD1 PE=1 SV=2	POLD1
304	sp|P52434|RPAB3_HUMAN DNA-directed RNA polymerases I, II, and III subunit RPABC3 OS=Homo sapiens (Human) OX=9606 GN=POLR2H PE=1 SV=4	POLR2H
305	sp|Q15165|PON2_HUMAN Serum paraoxonase/arylesterase 2 OS=Homo sapiens (Human) OX=9606 GN=PON2 PE=1 SV=4	PON2
306	sp|P45877|PPIC_HUMAN Peptidyl-prolyl cis-trans isomerase C OS=Homo sapiens (Human) OX=9606 GN=PPIC PE=1 SV=1	PPIC
307	sp|O43447|PPIH_HUMAN Peptidyl-prolyl cis-trans isomerase H OS=Homo sapiens (Human) OX=9606 GN=PPIH PE=1 SV=1	PPIH
308	sp|P49593|PPM1F_HUMAN Protein phosphatase 1F OS=Homo sapiens (Human) OX=9606 GN=PPM1F PE=1 SV=3	PPM1F
309	sp|P62136|PP1A_HUMAN Serine/threonine-protein phosphatase PP1-alpha catalytic subunit OS=Homo sapiens (Human) OX=9606 GN=PPP1CA PE=1 SV=1	PPP1CA
310	sp|Q12972|PP1R8_HUMAN Nuclear inhibitor of protein phosphatase 1 OS=Homo sapiens (Human) OX=9606 GN=PPP1R8 PE=1 SV=2	PPP1R8
311	sp|Q08209|PP2BA_HUMAN Serine/threonine-protein phosphatase 2B catalytic subunit alpha isoform OS=Homo sapiens (Human) OX=9606 GN=PPP3CA PE=1 SV=1	PPP3CA
312	sp|P30044|PRDX5_HUMAN Peroxiredoxin-5, mitochondrial OS=Homo sapiens (Human) OX=9606 GN=PRDX5 PE=1 SV=4	PRDX5
313	sp|P17612|KAPCA_HUMAN cAMP-dependent protein kinase catalytic subunit alpha OS=Homo sapiens (Human) OX=9606 GN=PRKACA PE=1 SV=2	PRKACA

314	sp|P22694|KAPCB_HUMAN cAMP-dependent protein kinase catalytic subunit beta OS=Homo sapiens (Human) OX=9606 GN=PRKACB PE=1 SV=2	PRKACB
315	sp|Q969G5|CAVN3_HUMAN Caveolae-associated protein 3 OS=Homo sapiens (Human) OX=9606 GN=CAVIN3 PE=1 SV=3	PRKCDBP
316	sp|P41743|KPCI_HUMAN Protein kinase C iota type OS=Homo sapiens (Human) OX=9606 GN=PRKCI PE=1 SV=2	PRKCI
317	sp|O75569|PRKRA_HUMAN Interferon-inducible double-stranded RNA-dependent protein kinase activator A OS=Homo sapiens (Human) OX=9606 GN=PRKRA PE=1 SV=1	PRKRA
318	sp|O14744|ANM5_HUMAN Protein arginine N-methyltransferase 5 OS=Homo sapiens (Human) OX=9606 GN=PRMT5 PE=1 SV=4	PRMT5
319	sp|Q6P2Q9|PRP8_HUMAN Pre-mRNA-processing-splicing factor 8 OS=Homo sapiens (Human) OX=9606 GN=PRPF8 PE=1 SV=2	PRPF8
320	sp|P60900|PSA6_HUMAN Proteasome subunit alpha type-6 OS=Homo sapiens (Human) OX=9606 GN=PSMA6 PE=1 SV=1	PSMA6
321	sp|Q99460|PSMD1_HUMAN 26S proteasome non-ATPase regulatory subunit 1 OS=Homo sapiens (Human) OX=9606 GN=PSMD1 PE=1 SV=2	PSMD1
322	sp|O95456|PSMG1_HUMAN Proteasome assembly chaperone 1 OS=Homo sapiens (Human) OX=9606 GN=PSMG1 PE=1 SV=1	PSMG1
323	sp|Q15185|TEBP_HUMAN Prostaglandin E synthase 3 OS=Homo sapiens (Human) OX=9606 GN=PTGES3 PE=1 SV=1	PTGES3
324	sp|Q13308|PTK7_HUMAN Inactive tyrosine-protein kinase 7 OS=Homo sapiens (Human) OX=9606 GN=PTK7 PE=1 SV=2	PTK7
325	sp|Q9UHX1|PUF60_HUMAN Poly(U)-binding-splicing factor PUF60 OS=Homo sapiens (Human) OX=9606 GN=PUF60 PE=1 SV=1	PUF60
326	sp|Q9Y606|TRUA_HUMAN tRNA pseudouridine synthase A OS=Homo sapiens (Human) OX=9606 GN=PUS1 PE=1 SV=3	PUS1
327	sp|Q9ULZ3|ASC_HUMAN Apoptosis-associated speck-like protein containing a CARD OS=Homo sapiens (Human) OX=9606 GN=PYCARD PE=1 SV=2	PYCARD
328	sp|P11216|PYGB_HUMAN Glycogen phosphorylase, brain form OS=Homo sapiens (Human) OX=9606 GN=PYGB PE=1 SV=5	PYGB
329	sp|P06737|PYGL_HUMAN Glycogen phosphorylase, liver form OS=Homo sapiens (Human) OX=9606 GN=PYGL PE=1 SV=4	PYGL
330	sp|Q6ZRP7|QSOX2_HUMAN Sulfhydryl oxidase 2 OS=Homo sapiens (Human) OX=9606 GN=QSOX2 PE=1 SV=3	QSOX2
331	sp|P61026|RAB10_HUMAN Ras-related protein Rab-10 OS=Homo sapiens (Human) OX=9606 GN=RAB10 PE=1 SV=1	RAB10
332	sp|Q92696|PGTA_HUMAN Geranylgeranyl transferase type-2 subunit alpha OS=Homo sapiens (Human) OX=9606 GN=RABGGTA PE=1 SV=2	RABGGTA
333	sp|Q3YEC7|RABL6_HUMAN Rab-like protein 6 OS=Homo sapiens (Human) OX=9606 GN=RABL6 PE=1 SV=2	RABL6
334	sp|Q9H0H5|RGAP1_HUMAN Rac GTPase-activating protein 1 OS=Homo sapiens (Human) OX=9606 GN=RACGAP1 PE=1 SV=1	RACGAP1
335	sp|P46060|RAGP1_HUMAN Ran GTPase-activating protein 1 OS=Homo sapiens (Human) OX=9606 GN=RANGAP1 PE=1 SV=1	RANGAP1
336	sp|P52306|GDS1_HUMAN Rap1 GTPase-GDP dissociation stimulator 1 OS=Homo sapiens (Human) OX=9606 GN=RAP1GDS1 PE=1 SV=3	RAP1GDS1
337	sp|P18754|RCC1_HUMAN Regulator of chromosome condensation OS=Homo sapiens (Human) OX=9606 GN=RCC1 PE=1 SV=1	RCC1
338	sp|Q14257|RCN2_HUMAN Reticulocalbin-2 OS=Homo sapiens (Human) OX=9606 GN=RCN2 PE=1 SV=1	RCN2
339	sp|Q96D15|RCN3_HUMAN Reticulocalbin-3 OS=Homo sapiens (Human) OX=9606 GN=RCN3 PE=1 SV=1	RCN3
340	sp|Q8TC12|RDH11_HUMAN Retinol dehydrogenase 11 OS=Homo sapiens (Human) OX=9606 GN=RDH11 PE=1 SV=2	RDH11
341	sp|P35251|RFC1_HUMAN Replication factor C subunit 1 OS=Homo sapiens (Human) OX=9606 GN=RFC1 PE=1 SV=4	RFC1
342	sp|Q6NTF9|RHBD2_HUMAN Rhomboid domain-containing protein 2 OS=Homo sapiens (Human) OX=9606 GN=RHBDD2 PE=1 SV=2	RHBDD2
343	sp|P61586|RHOA_HUMAN Transforming protein RhoA OS=Homo sapiens (Human) OX=9606 GN=RHOA PE=1 SV=1	RHOA
344	sp|Q96DB5|RMD1_HUMAN Regulator of microtubule dynamics protein 1 OS=Homo sapiens (Human) OX=9606 GN=RMDN1 PE=1 SV=1	RMDN1
345	sp|Q9H4A4|AMPB_HUMAN Aminopeptidase B OS=Homo sapiens (Human) OX=9606 GN=RNPEP PE=1 SV=2	RNPEP
346	sp|P46776|RL27A_HUMAN 60S ribosomal protein L27a OS=Homo sapiens (Human) OX=9606 GN=RPL27A PE=1 SV=2	RPL27A
347	sp|Q02878|RL6_HUMAN 60S ribosomal protein L6 OS=Homo sapiens (Human) OX=9606 GN=RPL6 PE=1 SV=3	RPL6
348	sp|P04843|RPN1_HUMAN Dolichyl-diphosphooligosaccharide--protein glycosyltransferase subunit 1 OS=Homo sapiens (Human) OX=9606 GN=RPN1 PE=1 SV=1	RPN1
349	sp|P15880|RS2_HUMAN 40S ribosomal protein S2 OS=Homo sapiens (Human) OX=9606 GN=RPS2 PE=1 SV=2	RPS2
350	sp|P62847|RS24_HUMAN 40S ribosomal protein S24 OS=Homo sapiens (Human) OX=9606 GN=RPS24 PE=1 SV=1	RPS24
351	sp|P10301|RRAS_HUMAN Ras-related protein R-Ras OS=Homo sapiens (Human) OX=9606 GN=RRAS PE=1 SV=1	RRAS
352	sp|O95197|RTN3_HUMAN Reticulon-3 OS=Homo sapiens (Human) OX=9606 GN=RTN3 PE=1 SV=2	RTN3
353	sp|P05109|S10A8_HUMAN Protein S100-A8 OS=Homo sapiens (Human) OX=9606 GN=S100A8 PE=1 SV=1	S100A8
354	sp|Q9UBE0|SAE1_HUMAN SUMO-activating enzyme subunit 1 OS=Homo sapiens (Human) OX=9606 GN=SAE1 PE=1 SV=1	SAE1

355	sp|Q5K651|SAMD9_HUMAN Sterile alpha motif domain-containing protein 9 OS=Homo sapiens (Human) OX=9606 GN=SAMD9 PE=1 SV=1	SAMD9
356	sp|Q8IVG5|SAM9L_HUMAN Sterile alpha motif domain-containing protein 9-like OS=Homo sapiens (Human) OX=9606 GN=SAMD9L PE=1 SV=2	SAMD9L
357	sp|O00422|SAP18_HUMAN Histone deacetylase complex subunit SAP18 OS=Homo sapiens (Human) OX=9606 GN=SAP18 PE=1 SV=1	SAP18
358	sp|P49591|SYSC_HUMAN Serine--tRNA ligase, cytoplasmic OS=Homo sapiens (Human) OX=9606 GN=SARS1 PE=1 SV=3	SARS
359	sp|Q15020|SART3_HUMAN Squamous cell carcinoma antigen recognized by T-cells 3 OS=Homo sapiens (Human) OX=9606 GN=SART3 PE=1 SV=1	SART3
360	sp|Q9HB40|RISC_HUMAN Retinoid-inducible serine carboxypeptidase OS=Homo sapiens (Human) OX=9606 GN=SCPEP1 PE=1 SV=1	SCPEP1
361	sp|P18827|SDC1_HUMAN Syndecan-1 OS=Homo sapiens (Human) OX=9606 GN=SDC1 PE=1 SV=3	SDC1
362	sp|P31431|SDC4_HUMAN Syndecan-4 OS=Homo sapiens (Human) OX=9606 GN=SDC4 PE=1 SV=2	SDC4
363	sp|Q9BRK5|CAB45_HUMAN 45 kDa calcium-binding protein OS=Homo sapiens (Human) OX=9606 GN=SDF4 PE=1 SV=1	SDF4
364	sp|P21912|SDHB_HUMAN Succinate dehydrogenase [ubiquinone] iron-sulfur subunit, mitochondrial OS=Homo sapiens (Human) OX=9606 GN=SDHB PE=1 SV=3	SDHB
365	sp|Q99643|C560_HUMAN Succinate dehydrogenase cytochrome b560 subunit, mitochondrial OS=Homo sapiens (Human) OX=9606 GN=SDHC PE=1 SV=1	SDHC
366	sp|P55735|SEC13_HUMAN Protein SEC13 homolog OS=Homo sapiens (Human) OX=9606 GN=SEC13 PE=1 SV=3	SEC13
367	sp|O15027|SC16A_HUMAN Protein transport protein Sec16A OS=Homo sapiens (Human) OX=9606 GN=SEC16A PE=1 SV=4	SEC16A
368	sp|O95487|SC24B_HUMAN Protein transport protein Sec24B OS=Homo sapiens (Human) OX=9606 GN=SEC24B PE=1 SV=2	SEC24B
369	sp|P60059|SC61G_HUMAN Protein transport protein Sec61 subunit gamma OS=Homo sapiens (Human) OX=9606 GN=SEC61G PE=1 SV=1	SEC61G
370	sp|Q6UXD5|SE6L2_HUMAN Seizure 6-like protein 2 OS=Homo sapiens (Human) OX=9606 GN=SEZ6L2 PE=1 SV=2	SEZ6L2
371	sp|Q15393|SF3B3_HUMAN Splicing factor 3B subunit 3 OS=Homo sapiens (Human) OX=9606 GN=SF3B3 PE=1 SV=4	SF3B3
372	sp|Q9BWM7|SFXN3_HUMAN Sideroflexin-3 OS=Homo sapiens (Human) OX=9606 GN=SFXN3 PE=1 SV=3	SFXN3
373	sp|Q9NR46|SHLB2_HUMAN Endophilin-B2 OS=Homo sapiens (Human) OX=9606 GN=SH3GLB2 PE=1 SV=1	SH3GLB2
374	sp|P29353|SHC1_HUMAN SHC-transforming protein 1 OS=Homo sapiens (Human) OX=9606 GN=SHC1 PE=1 SV=4	SHC1
375	sp|O15427|MOT4_HUMAN Monocarboxylate transporter 4 OS=Homo sapiens (Human) OX=9606 GN=SLC16A3 PE=1 SV=1	SLC16A3
376	sp|Q9UBX3|DIC_HUMAN Mitochondrial dicarboxylate carrier OS=Homo sapiens (Human) OX=9606 GN=SLC25A10 PE=1 SV=2	SLC25A10
377	sp|Q9UJS0|CMC2_HUMAN Calcium-binding mitochondrial carrier protein Aralar2 OS=Homo sapiens (Human) OX=9606 GN=SLC25A13 PE=1 SV=2	SLC25A13
378	sp|Q6NUK1|SCMC1_HUMAN Calcium-binding mitochondrial carrier protein SCaMC-1 OS=Homo sapiens (Human) OX=9606 GN=SLC25A24 PE=1 SV=2	SLC25A24
379	sp|P05141|ADT2_HUMAN ADP/ATP translocase 2 OS=Homo sapiens (Human) OX=9606 GN=SLC25A5 PE=1 SV=7	SLC25A5
380	sp|Q15796|SMAD2_HUMAN Mothers against decapentaplegic homolog 2 OS=Homo sapiens (Human) OX=9606 GN=SMAD2 PE=1 SV=1	SMAD2
381	sp|Q12824|SNF5_HUMAN SWI/SNF-related matrix-associated actin-dependent regulator of chromatin subfamily B member 1 OS=Homo sapiens (Human) OX=9606 GN=SMARCB1 PE=1 SV=2	SMARCB1
382	sp|O95347|SMC2_HUMAN Structural maintenance of chromosomes protein 2 OS=Homo sapiens (Human) OX=9606 GN=SMC2 PE=1 SV=2	SMC2
383	sp|Q6GMV2|SMYD5_HUMAN SET and MYND domain-containing protein 5 OS=Homo sapiens (Human) OX=9606 GN=SMYD5 PE=1 SV=2	SMYD5
384	sp|O75643|U520_HUMAN U5 small nuclear ribonucleoprotein 200 kDa helicase OS=Homo sapiens (Human) OX=9606 GN=SNRNP200 PE=1 SV=2	SNRNP200
385	sp|Q96L92|SNX27_HUMAN Sorting nexin-27 OS=Homo sapiens (Human) OX=9606 GN=SNX27 PE=1 SV=2	SNX27
386	sp|O95219|SNX4_HUMAN Sorting nexin-4 OS=Homo sapiens (Human) OX=9606 GN=SNX4 PE=1 SV=1	SNX4
387	sp|Q9NUQ6|SPS2L_HUMAN SPATS2-like protein OS=Homo sapiens (Human) OX=9606 GN=SPATS2L PE=1 SV=2	SPATS2L
388	sp|Q8NBT2|SPC24_HUMAN Kinetochore protein Spc24 OS=Homo sapiens (Human) OX=9606 GN=SPC24 PE=1 SV=2	SPC24
389	sp|O15269|SPTC1_HUMAN Serine palmitoyltransferase 1 OS=Homo sapiens (Human) OX=9606 GN=SPTLC1 PE=1 SV=1	SPTLC1
390	sp|O15270|SPTC2_HUMAN Serine palmitoyltransferase 2 OS=Homo sapiens (Human) OX=9606 GN=SPTLC2 PE=1 SV=1	SPTLC2
391	sp|P12931|SRC_HUMAN Proto-oncogene tyrosine-protein kinase Src OS=Homo sapiens (Human) OX=9606 GN=SRC PE=1 SV=3	SRC
392	sp|O76094|SRP72_HUMAN Signal recognition particle subunit SRP72 OS=Homo sapiens (Human) OX=9606 GN=SRP72 PE=1 SV=3	SRP72
393	sp|Q16629|SRSF7_HUMAN Serine/arginine-rich splicing factor 7 OS=Homo sapiens (Human) OX=9606 GN=SRSF7 PE=1 SV=1	SRSF7
394	sp|P05455|LA_HUMAN Lupus La protein OS=Homo sapiens (Human) OX=9606 GN=SSB PE=1 SV=2	SSB
395	sp|Q8N3U4|STAG2_HUMAN Cohesin subunit SA-2 OS=Homo sapiens (Human) OX=9606 GN=STAG2 PE=1 SV=3	STAG2
396	sp|P42224|STAT1_HUMAN Signal transducer and activator of transcription 1-alpha/beta OS=Homo sapiens (Human) OX=9606 GN=STAT1 PE=1 SV=2	STAT1

397	sp|O95793|STAU1_HUMAN Double-stranded RNA-binding protein Staufen homolog 1 OS=Homo sapiens (Human) OX=9606 GN=STAU1 PE=1 SV=2	STAU1
398	sp|Q9UEW8|STK39_HUMAN STE20/SPS1-related proline-alanine-rich protein kinase OS=Homo sapiens (Human) OX=9606 GN=STK39 PE=1 SV=3	STK39
399	sp|Q8TCJ2|STT3B_HUMAN Dolichyl-diphosphooligosaccharide--protein glycosyltransferase subunit STT3B OS=Homo sapiens (Human) OX=9606 GN=STT3B PE=1 SV=1	STT3B
400	sp|Q9UNE7|CHIP_HUMAN E3 ubiquitin-protein ligase CHIP OS=Homo sapiens (Human) OX=9606 GN=STUB1 PE=1 SV=2	STUB1
401	sp|P53597|SUCA_HUMAN Succinate--CoA ligase [ADP/GDP-forming] subunit alpha, mitochondrial OS=Homo sapiens (Human) OX=9606 GN=SUCLG1 PE=1 SV=4	SUCLG1
402	sp|P55854|SUMO3_HUMAN Small ubiquitin-related modifier 3 OS=Homo sapiens (Human) OX=9606 GN=SUMO3 PE=1 SV=2	SUMO3
403	sp|O95425|SVIL_HUMAN Supervillin OS=Homo sapiens (Human) OX=9606 GN=SVIL PE=1 SV=2	SVIL
404	sp|P37837|TALDO_HUMAN Transaldolase OS=Homo sapiens (Human) OX=9606 GN=TALDO1 PE=1 SV=2	TALDO1
405	sp|Q03518|TAP1_HUMAN Antigen peptide transporter 1 OS=Homo sapiens (Human) OX=9606 GN=TAP1 PE=1 SV=2	TAP1
406	sp|Q8TC07|TBC15_HUMAN TBC1 domain family member 15 OS=Homo sapiens (Human) OX=9606 GN=TBC1D15 PE=1 SV=2	TBC1D15
407	sp|Q14241|ELOA1_HUMAN Elongin-A OS=Homo sapiens (Human) OX=9606 GN=ELOA PE=1 SV=2	TCEB3
408	sp|P17987|TCPA_HUMAN T-complex protein 1 subunit alpha OS=Homo sapiens (Human) OX=9606 GN=TCP1 PE=1 SV=1	TCP1
409	sp|Q9Y6I9|TX264_HUMAN Testis-expressed protein 264 OS=Homo sapiens (Human) OX=9606 GN=TEX264 PE=1 SV=1	TEX264
410	sp|Q92734|TFG_HUMAN Protein TFG OS=Homo sapiens (Human) OX=9606 GN=TFG PE=1 SV=2	TFG
411	sp|P02786|TFR1_HUMAN Transferrin receptor protein 1 OS=Homo sapiens (Human) OX=9606 GN=TFRC PE=1 SV=2	TFRC
412	sp|P21980|TGM2_HUMAN Protein-glutamine gamma-glutamyltransferase 2 OS=Homo sapiens (Human) OX=9606 GN=TGM2 PE=1 SV=2	TGM2
413	sp|Q96CP7|TLCD1_HUMAN TLC domain-containing protein 1 OS=Homo sapiens (Human) OX=9606 GN=TLCD1 PE=1 SV=1	TLCD1
414	sp|Q99805|TM9S2_HUMAN Transmembrane 9 superfamily member 2 OS=Homo sapiens (Human) OX=9606 GN=TM9SF2 PE=1 SV=1	TM9SF2
415	sp|Q9HD45|TM9S3_HUMAN Transmembrane 9 superfamily member 3 OS=Homo sapiens (Human) OX=9606 GN=TM9SF3 PE=1 SV=2	TM9SF3
416	sp|Q9HC07|TM165_HUMAN Transmembrane protein 165 OS=Homo sapiens (Human) OX=9606 GN=TMEM165 PE=1 SV=1	TMEM165
417	sp|Q8N2U0|TM256_HUMAN Transmembrane protein 256 OS=Homo sapiens (Human) OX=9606 GN=TMEM256 PE=3 SV=1	TMEM256
418	sp|P57088|TMM33_HUMAN Transmembrane protein 33 OS=Homo sapiens (Human) OX=9606 GN=TMEM33 PE=1 SV=2	TMEM33
419	sp|Q9Y320|TMX2_HUMAN Thioredoxin-related transmembrane protein 2 OS=Homo sapiens (Human) OX=9606 GN=TMX2 PE=1 SV=1	TMX2
420	sp|Q9C0C2|TB182_HUMAN 182 kDa tankyrase-1-binding protein OS=Homo sapiens (Human) OX=9606 GN=TNKS1BP1 PE=1 SV=4	TNKS1BP1
421	sp|Q92973|TNPO1_HUMAN Transportin-1 OS=Homo sapiens (Human) OX=9606 GN=TNPO1 PE=1 SV=2	TNPO1
422	sp|Q68CZ2|TENS3_HUMAN Tensin-3 OS=Homo sapiens (Human) OX=9606 GN=TNS3 PE=1 SV=2	TNS3
423	sp|O94826|TOM70_HUMAN Mitochondrial import receptor subunit TOM70 OS=Homo sapiens (Human) OX=9606 GN=TOMM70 PE=1 SV=1	TOMM70A
424	sp|P62995|TRA2B_HUMAN Transformer-2 protein homolog beta OS=Homo sapiens (Human) OX=9606 GN=TRA2B PE=1 SV=1	TRA2B
425	sp|Q15629|TRAM1_HUMAN Translocating chain-associated membrane protein 1 OS=Homo sapiens (Human) OX=9606 GN=TRAM1 PE=1 SV=3	TRAM1
426	sp|P36406|TRI23_HUMAN E3 ubiquitin-protein ligase TRIM23 OS=Homo sapiens (Human) OX=9606 GN=TRIM23 PE=1 SV=1	TRIM23
427	sp|Q14258|TRI25_HUMAN E3 ubiquitin/ISG15 ligase TRIM25 OS=Homo sapiens (Human) OX=9606 GN=TRIM25 PE=1 SV=2	TRIM25
428	sp|Q15645|PCH2_HUMAN Pachytene checkpoint protein 2 homolog OS=Homo sapiens (Human) OX=9606 GN=TRIP13 PE=1 SV=2	TRIP13
429	sp|O75157|T22D2_HUMAN TSC22 domain family protein 2 OS=Homo sapiens (Human) OX=9606 GN=TSC22D2 PE=1 SV=3	TSC22D2
430	sp|Q9BSV6|SEN34_HUMAN tRNA-splicing endonuclease subunit Sen34 OS=Homo sapiens (Human) OX=9606 GN=TSEN34 PE=1 SV=1	TSEN34
431	sp|Q71U36|TBA1A_HUMAN Tubulin alpha-1A chain OS=Homo sapiens (Human) OX=9606 GN=TUBA1A PE=1 SV=1;sp|P0DPH8|TBA3D_HUMAN Tubulin alpha-3D chain OS=Homo sapiens (Human) OX=9606 GN=TUBA3D PE=1 SV=1;sp|P0DPH7|TBA3C_HUMAN Tubulin alpha-3C chain OS=Homo sapiens (	TUBA1A
432	sp|P68366|TBA4A_HUMAN Tubulin alpha-4A chain OS=Homo sapiens (Human) OX=9606 GN=TUBA4A PE=1 SV=1	TUBA4A
433	sp|Q9BUF5|TBB6_HUMAN Tubulin beta-6 chain OS=Homo sapiens (Human) OX=9606 GN=TUBB6 PE=1 SV=1	TUBB6
434	sp|P23258|TBG1_HUMAN Tubulin gamma-1 chain OS=Homo sapiens (Human) OX=9606 GN=TUBG1 PE=1 SV=2;sp|Q9NRH3|TBG2_HUMAN Tubulin gamma-2 chain OS=Homo sapiens (Human) OX=9606 GN=TUBG2 PE=2 SV=1	TUBG1;TUBG2

435	sp|O14530|TXND9_HUMAN Thioredoxin domain-containing protein 9 OS=Homo sapiens (Human) OX=9606 GN=TXNDC9 PE=1 SV=2	TXNDC9
436	sp|Q9BZF9|UACA_HUMAN Uveal autoantigen with coiled-coil domains and ankyrin repeats OS=Homo sapiens (Human) OX=9606 GN=UACA PE=1 SV=2	UACA
437	sp|Q16222|UAP1_HUMAN UDP-N-acetylhexosamine pyrophosphorylase OS=Homo sapiens (Human) OX=9606 GN=UAP1 PE=1 SV=3	UAP1
438	sp|Q8TBC4|UBA3_HUMAN NEDD8-activating enzyme E1 catalytic subunit OS=Homo sapiens (Human) OX=9606 GN=UBA3 PE=1 SV=2	UBA3
439	sp|A0AVT1|UBA6_HUMAN Ubiquitin-like modifier-activating enzyme 6 OS=Homo sapiens (Human) OX=9606 GN=UBA6 PE=1 SV=1	UBA6
440	sp|Q5T6F2|UBAP2_HUMAN Ubiquitin-associated protein 2 OS=Homo sapiens (Human) OX=9606 GN=UBAP2 PE=1 SV=1	UBAP2
441	sp|Q96LR5|UB2E2_HUMAN Ubiquitin-conjugating enzyme E2 E2 OS=Homo sapiens (Human) OX=9606 GN=UBE2E2 PE=1 SV=1;sp|Q969T4|UB2E3_HUMAN Ubiquitin-conjugating enzyme E2 E3 OS=Homo sapiens (Human) OX=9606 GN=UBE2E3 PE=1 SV=1	UBE2E2;UBE2E3
442	sp|O14933|UB2L6_HUMAN Ubiquitin/ISG15-conjugating enzyme E2 L6 OS=Homo sapiens (Human) OX=9606 GN=UBE2L6 PE=1 SV=4	UBE2L6
443	sp|Q8WVY7|UBCP1_HUMAN Ubiquitin-like domain-containing CTD phosphatase 1 OS=Homo sapiens (Human) OX=9606 GN=UBLCP1 PE=1 SV=2	UBLCP1
444	sp|P17480|UBF1_HUMAN Nucleolar transcription factor 1 OS=Homo sapiens (Human) OX=9606 GN=UBTF PE=1 SV=1	UBTF
445	sp|Q92890|UFD1_HUMAN Ubiquitin recognition factor in ER-associated degradation protein 1 OS=Homo sapiens (Human) OX=9606 GN=UFD1 PE=1 SV=3	UFD1L
446	sp|Q9NUQ7|UFSP2_HUMAN Ufm1-specific protease 2 OS=Homo sapiens (Human) OX=9606 GN=UFSP2 PE=1 SV=3	UFSP2
447	sp|P11172|UMPS_HUMAN Uridine 5-monophosphate synthase OS=Homo sapiens (Human) OX=9606 GN=UMPS PE=1 SV=1	UMPS
448	sp|Q70J99|UN13D_HUMAN Protein unc-13 homolog D OS=Homo sapiens (Human) OX=9606 GN=UNC13D PE=1 SV=1	UNC13D
449	sp|Q16831|UPP1_HUMAN Uridine phosphorylase 1 OS=Homo sapiens (Human) OX=9606 GN=UPP1 PE=1 SV=1	UPP1
450	sp|Q9UDW1|QCR9_HUMAN Cytochrome b-c1 complex subunit 9 OS=Homo sapiens (Human) OX=9606 GN=UQCR10 PE=1 SV=3	UQCR10
451	sp|P14927|QCR7_HUMAN Cytochrome b-c1 complex subunit 7 OS=Homo sapiens (Human) OX=9606 GN=UQCRB PE=1 SV=2	UQCRB
452	sp|P31930|QCR1_HUMAN Cytochrome b-c1 complex subunit 1, mitochondrial OS=Homo sapiens (Human) OX=9606 GN=UQCRC1 PE=1 SV=3	UQCRC1
453	sp|P61758|PFD3_HUMAN Prefoldin subunit 3 OS=Homo sapiens (Human) OX=9606 GN=VBP1 PE=1 SV=4	VBP1
454	sp|Q3ZAQ7|VMA21_HUMAN Vacuolar ATPase assembly integral membrane protein VMA21 OS=Homo sapiens (Human) OX=9606 GN=VMA21 PE=1 SV=1	VMA21
455	sp|Q9UBQ0|VPS29_HUMAN Vacuolar protein sorting-associated protein 29 OS=Homo sapiens (Human) OX=9606 GN=VPS29 PE=1 SV=1	VPS29
456	sp|Q9H9H4|VP37B_HUMAN Vacuolar protein sorting-associated protein 37B OS=Homo sapiens (Human) OX=9606 GN=VPS37B PE=1 SV=1	VPS37B
457	sp|Q9NRW7|VPS45_HUMAN Vacuolar protein sorting-associated protein 45 OS=Homo sapiens (Human) OX=9606 GN=VPS45 PE=1 SV=1	VPS45
458	sp|Q9UN37|VPS4A_HUMAN Vacuolar protein sorting-associated protein 4A OS=Homo sapiens (Human) OX=9606 GN=VPS4A PE=1 SV=1	VPS4A
459	sp|Q8NI36|WDR36_HUMAN WD repeat-containing protein 36 OS=Homo sapiens (Human) OX=9606 GN=WDR36 PE=1 SV=1	WDR36
460	sp|Q9GZS3|WDR61_HUMAN WD repeat-containing protein 61 OS=Homo sapiens (Human) OX=9606 GN=WDR61 PE=1 SV=1	WDR61
461	sp|Q9NQW7|XPP1_HUMAN Xaa-Pro aminopeptidase 1 OS=Homo sapiens (Human) OX=9606 GN=XPNPEP1 PE=1 SV=3	XPNPEP1
462	sp|Q9NQH7|XPP3_HUMAN Xaa-Pro aminopeptidase 3 OS=Homo sapiens (Human) OX=9606 GN=XPNPEP3 PE=1 SV=1	XPNPEP3
463	sp|O14980|XPO1_HUMAN Exportin-1 OS=Homo sapiens (Human) OX=9606 GN=XPO1 PE=1 SV=1	XPO1
464	sp|P67809|YBOX1_HUMAN Y-box-binding protein 1 OS=Homo sapiens (Human) OX=9606 GN=YBX1 PE=1 SV=3	YBX1
465	sp|Q5BJH7|YIF1B_HUMAN Protein YIF1B OS=Homo sapiens (Human) OX=9606 GN=YIF1B PE=1 SV=1	YIF1B
466	sp|Q9GZM5|YIPF3_HUMAN Protein YIPF3 OS=Homo sapiens (Human) OX=9606 GN=YIPF3 PE=1 SV=1	YIPF3
467	sp|P49750|YLPM1_HUMAN YLP motif-containing protein 1 OS=Homo sapiens (Human) OX=9606 GN=YLPM1 PE=1 SV=4	YLPM1
468	sp|Q9Y5A9|YTHD2_HUMAN YTH domain-containing family protein 2 OS=Homo sapiens (Human) OX=9606 GN=YTHDF2 PE=1 SV=2	YTHDF2
469	sp|Q7Z739|YTHD3_HUMAN YTH domain-containing family protein 3 OS=Homo sapiens (Human) OX=9606 GN=YTHDF3 PE=1 SV=1	YTHDF3
470	sp|P62258|1433E_HUMAN 14-3-3 protein epsilon OS=Homo sapiens (Human) OX=9606 GN=YWHAE PE=1 SV=1	YWHAE
471	sp|Q14966|ZN638_HUMAN Zinc finger protein 638 OS=Homo sapiens (Human) OX=9606 GN=ZNF638 PE=1 SV=2	ZNF638
472	sp|O43264|ZW10_HUMAN Centromere/kinetochore protein zw10 homolog OS=Homo sapiens (Human) OX=9606 GN=ZW10 PE=1 SV=3	ZW10

Table S4. RT-PCR primer sets

name	sequence (5'-3')
PDL1Human_fw	TGGCATTTGCTGAACGCATTT
PDL1Human_rev	TGCAGCCAGGTCTAATTGTTTT
human_gapdh_fw	CTTCAACAGCGACACCCACTCCTC
human_gapdh_rev	GTCCACCACCCTGTTGCTGTAG
hCMTM6 fw	TTTCCACACATGACAGGACTTC
hCMTM6 rev	GGCTTCAGCCCTAGTGGTAT
hFOS_fw	GCAAGGTGGAACAGTTATCTCCA
hFOS_rev	AGTGTATCAGTCAGCTCCCTCCTC
hMCL1_fw	CGTTGTCTCGAGTGATGATCCA
hMCL1_rev	CAAGTGTTTAGCCACAAAGGCA
hMMP3_fw	ATGGCATTCAGTCCCTCTATGG
hMMP3_rev	AAGCAGGATCACAGTTGGCTG
hVCL_fw	GCCAGGAATGACTAAGATGGCC
hVCL_rev	TTCACGGTGTTCATCGAGTTCA
hDKK1_fw	GAAAACGCTGCATGCGTC
hDKK1_rev	GGTTTCCTCAATTTCTCCTCGG
EGFR_fw	AGGCACGAGTAACAAGCTCAC
EGFR_rev	ATGAGGACATAACCAGCCACC